이학박사학위논문

신경 손상과 SOD1-G93A 형질전환 마우스 모델에서 재조합 AAV 를 이용한 HGF 유전자의 전달이 근육과 신경계에 미치는 영향

Effects of AAV-Mediated Delivery of HGF Gene on the Muscular and Nerve Systems in the Nerve Crush and SOD1-G93A Transgenic Mouse Models

2019 년 8 월

서울대학교 대학원

자연과학대학원 생명과학부

이 상 환

신경 손상과 SOD1-G93A 형질전환 마우스 모델에서 재조합 AAV 를 이용한 HGF 유전자의 전달이 근육과 신경계에 미치는 영향

Effects of AAV-mediated delivery of HGF gene on the muscular and nerve systems in the nerve crush and SOD1-G93A transgenic mouse models

지도교수 김 진 홍

이 논문을 이학박사학위논문으로 제출함

2019 년 8 월

서울대학교 대학원 자연과학대학 생명과학부

이 상 환

이상환의 박사학위논문을 인준함

2019 년 8 월

위 원 장 _____(인)

부 위 원 장 _____(인)

위 원 _____(인)

위 원 _____(인)

위 원 _____(인)

ABSTRACT

Sang Hwan Lee

School of Biological Sciences

The Graduate School

Seoul National University

Amyotrophic lateral sclerosis (ALS) is a fatal neuromuscular disease resulting from motor neuron degeneration that causes muscle weakness, paralysis, and eventually respiratory failure. A variety of chemicals, recombinant proteins, and gene therapies have been explored to develop treatment methods for ALS. To date, only two small molecules—riluzole and edaravone—have been approved by the FDA. However, the therapeutic effects of these are relatively low, and there is still a high unmet need for a medical solution to this devastating disease.

In this study, I investigated whether delivery of hepatocyte growth factor (HGF) could generate beneficial effects in two mouse models with neuromuscular problems: the sciatic nerve crush and SOD1-G93A transgenic (TG) mouse models. HGF is a versatile neurotrophic factor known to mediate a variety of cellular activities, such as facilitating cell proliferation, angiogenesis, and neurogenesis. To induce the long-term expression of HGF proteins, I used a recombinant adeno-associated virus encoding the HGF gene (rAAV-HGF). Based on the expression levels and distribution of HGF proteins, AAV serotype 6 was chosen for intramuscular (IM) injection, while AAV serotype 1 was shown to be appropriate for intrathecal (IT) injection.

The effects of rAAV-HGF were initially tested in the nerve crush mouse model. When intramuscularly delivered, rAAV6-HGF reduced the degree of mechanical allodynia, increased the cross-sectional area (CSA) of muscle fibers in the tibialis anterior (TA), and enhanced motor functions. When intramuscularly delivered in the SOD1-G93A TG mouse model, the most commonly used mouse model for ALS, rAAV6-HGF alleviated disease symptoms. When intrathecally injected with rAAV1-HGF, mouse hindlimb strength and rotarod performance both improved, while histological analyses showed that the length of regenerated axons increased and the structure of the neuromuscular junction (NMJ) restored in the crush model. It was also observed that rAAV1-HGF could not only improve motor performance, but also increase the survival rate of SOD1-G93A TG mice. Moreover, the number and diameter of the spinal motor neurons (SMNs) were increased, and the shape of the NMJs restored.

Data from *in vitro* motor cortical culture experiments indicated that treatment with recombinant HGF proteins (rHGF) increased the axon length of corticospinal motor neurons (CSMNs). When cultures were treated with an ERK inhibitor, the effects of HGF on axon elongation, protein aggregation, and oxidative stress were suppressed, indicating that ERK phosphorylation played an important role(s) in protecting the motor neurons.

Taken together, it appears that the HGF gene could be a good starting point for developing therapeutic agents for ALS, and that the rAAV vector in particular could be a useful gene delivery vehicle.

Keywords: Amyotrophic lateral sclerosis (ALS), Adeno-associated virus (AAV), Hepatocyte growth factor (HGF), Corticospinal motor neuron (CSMN), Oxidative stress

Student number: 2015-22640

Contents

LIST OF TABLES

LIST OF FIGURES

ABBREVIATIONS

ALS	amyotrophic lateral sclerosis
CSA	cross-sectional area
CSMN	corticospinal motor neuron
ELISA	enzyme-linked immunosorbent assay
GC	gastrocnemius
HGF	hepatocyte growth factor
ICC	immunocytochemistry
IHC	immunohistochemistry
IM	intramuscular
IT	intrathecal
LSC	lumbar spinal cord
NAC	N-acetyl-L-cysteine
NMJ	neuromuscular junction
rAAV	recombinant adeno-associated virus
ROS	reactive oxygen species
SMN	spinal motor neuron
TA	tibialis anterior
TG	transgenic

Chapter I

Introduction

1. Amyotrophic lateral sclerosis (ALS)

ALS is a destructive neuromuscular disease in which the motor neurons in the central nervous system (CNS) selectively perish [1-3]. ALS is known to occur when protein aggregates like inclusion bodies accumulate in the cytoplasm of the lower motor neurons (LMNs) in the spinal cord, and the upper motor neurons (UMNs) in the motor cortex [4]. Although there are no definite criteria for diagnosing ALS, most patients experience progressive degeneration of the skeletal muscles [2], and eventually die of respiratory failure [5]. ALS patients usually die within 2-5 years of disease onset.

ALS is divided into familial ALS (fALS) and sporadic ALS (sALS). fALS accounts for 10% of total ALS cases [6], and mutations in copper (Cu)/zinc (Zn) superoxide dismutase (SOD1), TAR DNA-binding protein (TARDBP), and fused in sarcoma (FUS) have been shown to be important in the pathogenesis of ALS [7, 8]. Recent studies have also shown that the repetition of GGGGCC, a hexanucleotide in the noncoding region on chromosome 9, is important for the pathophysiology of ALS [9]. The remaining 90% of total ALS cases are classified as sALS, the cause of which is unknown. It is thought that the causal genes of fALS and single nucleotide polymorphism (SNP) are involved in the development of ALS [10, 11].

There are several models for explaining the onset and progression of ALS, as shown in **Figure I-1** [12]. The dying-forward hypothesis proposes that UMNs containing corticospinal motor neurons (CSMNs) are damaged first. In this model, the excitotoxic process mediated by UMNs leads to degeneration of the LMNs and skeletal muscles. In contrast, the dying-back hypothesis suggests that the skeletal muscle is the primary disease

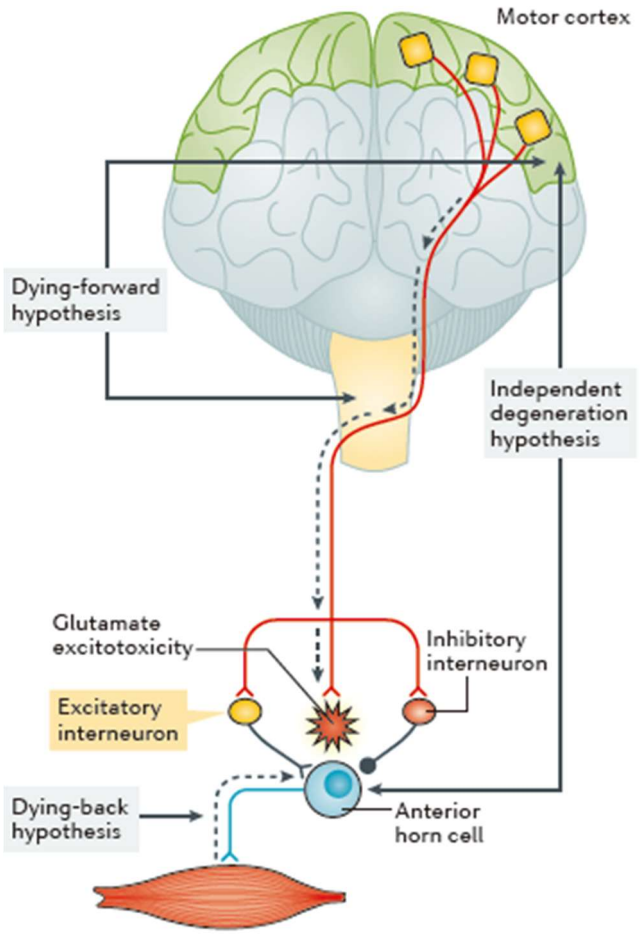

Figure I-1. Three hypothetical models for the onset and progression of ALS (Taken from Geevasinga *et al.*, 2016.)

The onset and progression of ALS can be explained by 3 hypothetical models. According to the dying-forward hypothesis and the dying-back hypothesis, either the motor cortex or skeletal muscles are the primary sites of the disease onset, while the independent degeneration hypothesis suggests that both sites degenerate simultaneously.

onset site. In this case, a NMJ that sends contractile signals to the motor neurons sends pathological signals, leading to degeneration of the anterior horn cells. Lastly, the independent degeneration hypothesis proposes that degeneration of the UMNs and LMNs occurs simultaneously and independently.

In addition to the motor neurons, glial cells consisting of astrocytes, oligodendrocytes, and microglia play an important role(s) in the onset of ALS (**Figure I-2**) [3]. Abnormalities in the quality control of proteins—in protein folding, for example— are one of the best-known mechanisms. Improper protein folding takes place in the endoplasmic reticulum when mutations occur in SOD1, which removes superoxide radicals, or in proteins such as FUS and TARDBP, which regulate transcription by binding to RNA. When abnormally folded proteins are not properly removed by proteasomes, lysosomes, and authophagosomes, protein aggregates that cause cytotoxicity are produced. Such cytotoxicity can also occur when microglia are hyperactivated or the absorption of glutamate is inhibited in astrocytes. It has also been reported that several metabolic processes are impaired when monocarboxylate transporter 1 (MCT1), an oligodendrocyte transporter, does not function properly. When MCT1 is not properly activated, the motor neurons die because the energy essential for motor neuron survival is not appropriately supplied. In addition, problems in alternative splicing, microRNA (miRNA) biosynthesis, RNA-binding protein, and protein translation can adversely affect the environments of the motor neurons.

In summary, the pathology of ALS is not well understood due to its complexity and diversity. Therefore, the treatment methods for ALS are extremely limited. A variety of

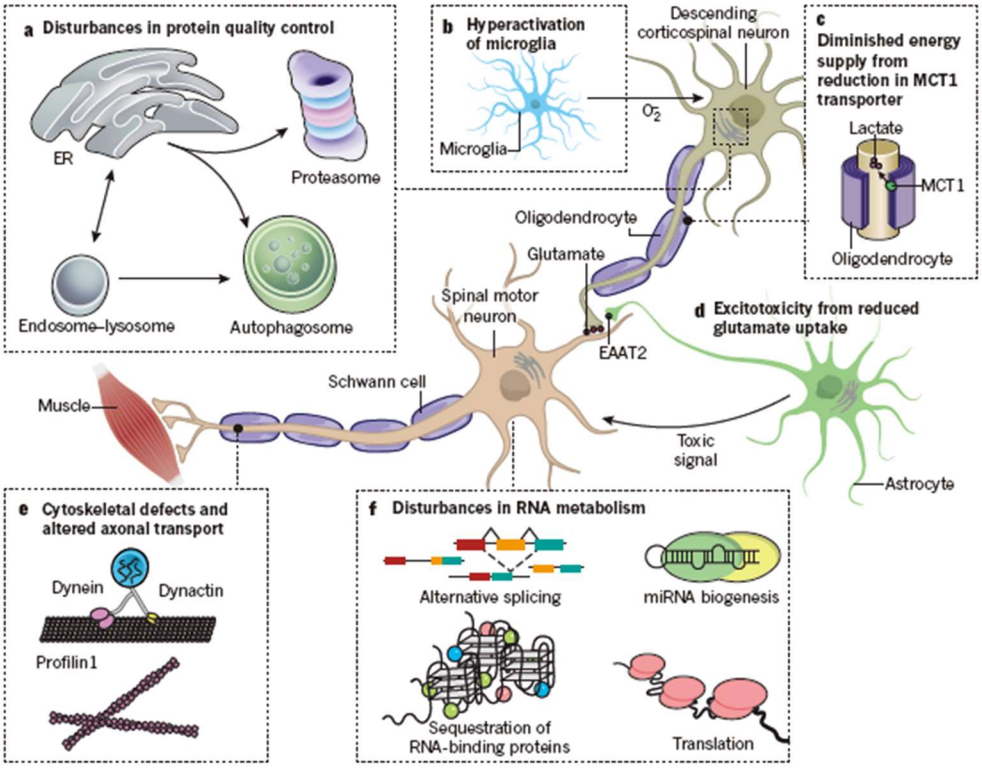

Figure I-2. Mechanism of ALS onset revealed by fALS. (Taken from Taylor *et al.*, 2016.)

There are six well-known mechanisms for the onset of ALS. Cytotoxicity is induced when protein quality control in the endoplasmic reticulum is impaired, or microglia is hyperactivated. When the activity of EAAT2, the transporter of astrocytes, is inhibited, glutamate uptake in astrocytes decreases and excitotoxicity is induced. In addition, abnormalities in cytoskeletal proteins or RNA metabolism play important roles in ALS pathogenesis.

chemicals, recombinant proteins, and gene therapies have been explored to develop treatment methods for ALS. However to date, only two small molecules—riluzole and edaravone—have been approved by the FDA [13-15]. Their therapeutic effects are relatively low: riluzole delays the time to tracheostomy by 2 to 3 months, and edaravone improves the ALSFRS-R score by 33%. Since it is particularly difficult to determine the exact cause of the disease, the treatment of ALS still need methodologies that can show overall improvements in the motor cortex and spinal cord.

2. Hepatocyte growth factor (HGF)

First discovered by the Nakamura group as a mitogen for hepatocytes in 1984 [16], HGF has been shown to play multiple roles. For example, HGF can promote various bioactivities, including cell proliferation, morphogenesis, anti-fibrosis, anti-inflammation, and angiogenesis [17-22]. Once expressed as an inactive precursor in a single chain, HGF is converted to an active heterodimer with α and β chains by the action of extracellular proteases (**Figure I-3**) [23]. The α chain of the activated HGF proteins has a hairpin loop (HL) domain and four kringle (K1-K4) domains, and the β chain has a serine protease homology (SPH) domain. The HL and the second kringle domain of the α chain have been reported to promote the binding of HGF to heparin or heparan sulfate [24].

Met, a receptor for HGF, is a heterodimer composed of an extracellular α subunit and a transmembrane β subunit. Both subunits are linked by a disulfide bond, which forms the

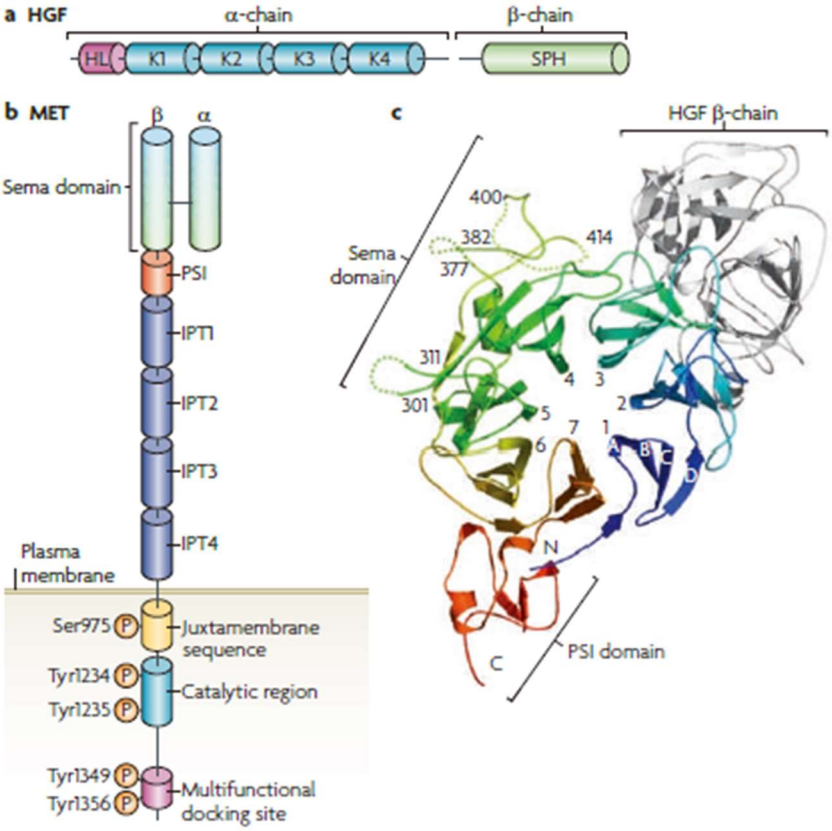

Figure I-3. The structure of HGF and the Met receptor. (Taken from Trusolino *et al.*, 2010.)

Produced as an inactive precursor, HGF protein forms a heterodimer by the action of extracellular proteases. Met, a receptor for HGF, has a heterodimer structure in which two subunits are linked via a disulfide bond. When the SPH domain of HGF binds to the Sema domain of the Met protein, the intracellular domain of the receptor is phosphorylated consecutively, activating the downstream signaling pathways.

Sema domain necessary for receptor dimerization and activation [25]. The extracellular segment of the β subunit has a PSI domain and four IPT (IPT1-4) domains, which increase the affinity and binding accuracy of the ligand-binding site and induce proper functioning of the receptor [26, 27]. The α chain of HGF recognizes the IPT3 and IPT4 domains of Met, and the SPH domain in the β chain of HGF binds to the Sema domain of Met [28].

The intracellular segment of Met consists of a juxtamembrane sequence, a catalytic region, and a multifunctional docking site. When HGF binds to the Met receptor, various intracellular signaling pathways including PI3K, JNK, p38, and/or ERK are activated depending on cell type [23, 29, 30]. When Tyr1234 and Tyr1235 residues of the catalytic region of Met are autophosphorylated after the binding of HGF, Tyr1349 and Tyr1356 residues of a multifunctional docking site are phosphorylated, resulting in several signaling transduction pathways [31, 32]. In contrast, the kinase activity of Met is downregulated when the Ser975 residue of a juxtamembrane sequence is phosphorylated [33]. As a potent trophic factor, HGF has been shown to regulate a variety of biological programs by promoting mitogenic, motogenic, and morphogenic activities in a variety of cell types [34].

Studies have shown that HGF or Met can play a positive role(s) in the treatment of ALS. The protein levels of HGF and Met increase in the ventral horn of sALS patients in the early stages, while patients with motor neurons defective in HGF or Met are more susceptible to the disease progression of ALS, being atrophied rapidly [35]. In SOD1-G93A TG mice, an animal model for ALS, RNA levels of HGF and Met were higher than the non-TG control, presumably to respond to or compensate for pathological conditions [36]. In the SOD1-G93A

TG mouse model, disease progression was delayed when HGF or Met expression was additionally introduced by generating double TG mice, or when recombinant HGF was intrathecally delivered, indicating that the delivery of the HGF gene could be applied in various neuromuscular diseases, including ALS.

3. Adeno-associated virus (AAV)

In this study, AAV was used as an alternative method to deliver the HGF gene [37, 38]. AAV is classified as a non-enveloped virus with a genome made up of single-stranded DNA (ssDNA) [37]. The genome of AAV consists of two open reading frames (ORFs) between palindromic inverted terminal repeat (ITR) sequences. When used in gene therapy, a transgene cassette containing the desired gene can be inserted between the ITR sequences. Recombinant AAV (rAAV) can be produced by transferring the *cap* and *rep* genes required for viral production *in trans*.

Although its insertion capacity is relatively small, the rAAV vector has many advantages over other gene therapy vectors. AAV is not known to cause any diseases, and immune responses by AAV have been reported to be relatively low [39]. Moreover, rAAV vectors can drive long-term expression *in vivo* and deliver the transgene to a variety of cell types, including non-dividing cells, through capsid pseudotyping [37]. It is also known that engineering of the capsid domain can alter tropism and cell-type specificity [40]. Since the first application of rAAV serotype 2 to clinical trials for cystic fibrosis, rAAV has been applied to a variety of CNS disorders such as metachromatic leukodystrophy, mucopolysaccharidosis,

Canavan disease, and late infantile neuronal ceroid lipofuscinosis [41, 42]. In addition, rAAV has been used in several preclinical animal models, suggesting the possibility of its application to various neurodegenerative diseases such as Alzheimer's disease, Parkinson's disease, giant axonal neuropathy, Huntington's disease, and spinal muscular atrophy [42].

The gene therapy approach is particularly appealing when it comes to HGF. It is an unstable protein with a half-life of less than 5 minutes, making recombinant protein strategy inefficient. Engineering HGF to a stable form is not desirable, as durable HGF many induce angiogenesis in a systemic manner and increase the possibility of carcinogenesis [43]. HL and Kringle domains in the N-terminal of HGF have a high affinity to heparin sulfate proteoglycans abundant at the cell surface and in the extracellular matrix [44]. Such biochemical properties of HGF lower the possibility of the systemic distribution of HGF proteins. Indeed, our group has not found any changes in the serum level of HGF in either human studies or animal experiments involving plasmid or AAV [45-52]. For HGF, therefore, the gene therapy approach means a strictly localized drug delivery, indicating a minimal possibility of off-target problems.

4. Overview of thesis research

In this study, I investigated whether AAV vectors expressing HGF could produce therapeutic effects in the sciatic nerve crush and SOD1-G93A TG mouse models, which are commonly used as neuromuscular disease models. To maximize the efficacy of HGF, rAAV-

HGF was constructed using a gDNA-cDNA-hybrid construct capable of simultaneously expressing two isoforms of human HGF (hHGF) —HGF723 (dHGF) and HGF728 (cHGF) [45, 53].

The two animal models used in this study are similar in that in both, the skeletal muscles are damaged and injury signals are transmitted to the spinal cord. As such, two methods were used for gene transfer: intramuscular (IM) injection and intrathecal (IT) injection. First, we conducted a study to select AAV serotypes that can efficiently transfer genes to the muscle and spinal cord. AAV serotypes 1 and 6 were chosen for IT and IM injection, respectively. After examining the kinetics of gene expression, the effects of AAV-HGF on both animal models were investigated as described above. In the sciatic nerve crush model, I analyzed the CSA of the TA, the functions of sensory and motor neurons, and the degree of the regeneration of injured nerves. In the SOD1-G93A TG mouse model, I analyzed the mass of the skeletal muscles, NMJ, motor performance, and survival rates.

In summary, the core of this thesis research was to investigate the histological, biochemical, and behavioral effects of HGF on the nerves and muscles, and to investigate underlying mechanisms when HGF is delivered either to the muscle or spinal cord using the AAV vector.

Chapter II

Materials and Methods

1. Animals

C57BL/6 mice were purchased from Orient Bio Inc. (Gyeonggi-do, Korea). B6SJL-TG(SOD1-G93A)1Gur/J mice (MGI ID: 2183719) were purchased from The Jackson Laboratory [54-56]. Mice were fed *ad libitum* and entrained to a standard light-dark cycle. All experimental protocols adhered to the regulations of the Seoul National University Institutional Animal Care and Use Committee (IACUC).

2. Adeno-associated virus

In this study, a gDNA-cDNA-hybrid sequence that could express HGF723 (dHGF) and HGF728 (cHGF) was generated using human genomic DNA, as previously described [45, 53]. This hybrid sequence has cDNA sequences of 18 exons of the HGF gene, containing a part of intron 4 between exon 4 and exon 5. Since the length of intron 4 is too long to produce viral vectors, 4,329 base pairs of intron 4 were deleted using site-directed mutagenesis by polymerase chain reaction (PCR). In order to generate pAAV-HGf, this chimeric sequence was then inserted between the ITR sequences of pAAV-MCS, a plasmid containing multiple cloning sites purchased from Agilent Technologies. To produce rAAV2-HGF, equal amounts of three plasmids (*rep*/*cap*-expressing plasmid, pAAV-HGF, and helper plasmid) were co-transfected into $1x10^6$ HEK293T cells using AAV Helper-Free System (Agilent Technologies). $1.23x10^8$ GC (genome copies) of rAAV2-HGF were then transduced into $1.6x10^5$ C2C12 cells. Forty-eight hours later, the supernatant was collected followed by ELISA specific to human HGF (hHGF). At the same time, total RNAs were isolated and subjected to RT-PCR

using Expand High Fidelity PCR System (Sigma). Primers used for PCR were as follows: 5'-CAAATGTCAGCCCTGGAGTTCCATGA-3' (forward); 5'-CTGGATTGCTTGTGAAACACCAGGGT-3' (reverse). PCR products were then run on NuPAGE 4-12% Bis-Tris Protein Gels (Thermofisher). rAAV2-MCS and rAAV6-MCS lacking the HGF sequence (rAAV2-C) were used as negative controls. For animal studies, rAAV with a titer higher than $1x10^8$ GC/ml was produced by a contract manufacturing company called CdmoGen (Chungbuk, Korea).

3. Sciatic nerve crush

The sciatic nerves of C57BL/6 mice were exposed, and nerve crush injury was induced using fine hemostatic forceps (FST), as previously described [53, 57]. Mice were exposed to isoflurane at 4-5% until anesthesia was induced, with concentration reduced to 1.5% during surgery. Behavioral tests were performed once a week for 4 weeks. For histological analysis, the sciatic nerves and TA were collected 5 days after surgery. The nerve pinch test was performed 7 days after the injury. The sciatic nerve was exposed and pinched using hemostatic forceps until mice showed a reflex response at the leg or muscles of the back contracted, from the distal end to the crush site. The distance from the crush site to the reflex site was measured.

4. Behavioral tests

To test the degree of mechanical allodynia, the von Frey filament test was performed as previously described [58]. After 3 hours of adaption on top of the mesh floor, von Frey filaments of a consistent thickness (0.16 g) were used to stimulate the hind paws of the mice, and withdrawal frequency was measured. Motor functions were evaluated using the rotarod test, wire hanging test, and grip strength test. For the rotarod test, latency to fall from the rotating rod was recorded. The speed of the rod was either constant (28 rpm) or accelerated from 4 rpm to 40 rpm for 5 minutes, as previously described [59-61]. For the wire hanging test, mice were placed upside down under wire mesh. Latency to fall was recorded. Maximum latency was set to 1 minute. Grip strengths of the forelimb and hindlimb were measured with a grip strength meter (Nidec-Shimpo). In SOD1-G93A TG mice, the neurological score was measured to assess disease progression, as previously described [62-64]. Mice were pre-trained for a week for each behavioral test. Each test was performed 3 times and values were averaged.

5. Primary motor cortical culture

Cerebral motor cortices of mice were isolated, and cells were incubated as described previously [65]. Six-well cell culture plates (SPL) pre-coated with 0.1 mg/ml of PDL (Sigma) were incubated overnight at 37°C, followed by two washings with distilled water (Sigma). Motor cortices of non-TG or TG mice at P3 were collected using fine forceps (FST) into dissociation solution (DS) containing magnesium chloride (Sigma), Hepes (Gibco), sodium sulfate (Sigma), potassium sulfate (Sigma), kyneuric acid (Sigma), glucose (Sigma), APV

(Sigma), penicillin/streptomycin (P/S) (Gibco), and B27 (Gibco). Cells were then dissociated in a papain solution (Worthington Biochem) for 15 minutes, and incubated in inhibitor solution containing ovomucoid (Sigma) for 1 minute. After being washed with Opti-MEM (Gibco) solution containing APV (Sigma) and B27, $3.2x10^5$ cells were seeded with serum-free media (SFM) containing BSA, L-glutamine (Sigma), P/S, glucose, and B27 in neurobasal media (Gibco). Cells were then treated with inhibitors for Met (PHA665752), ERK (U0126), PI3K (LY294002), p38 (SB203580), and JNK (SP600125). Thirty minutes later, cells were cultured in the presence of 100 ng/ml of rHGF (R&D Systems). 3 days later, cells were subjected to immunocytochemistry (ICC) assay.

6. Western blot

Total proteins were isolated using RIPA Buffer (Cell Signaling Technology) and Protease/Phosphatase Inhibitor Cocktail (Cell Signaling Technology), followed by polyacrylamide gel electrophoresis on NuPAGE 4-12% Bis-Tris Protein Gels (Thermofisher) using 10-20 μg of protein. Gels were transferred to the PVDF membrane (GE Healthcare) and blocked with 0.1% TBST solution containing 5% skim milk (Difco) for 1 hour. Membranes were incubated with 0.1% TBST solution containing 5% BSA and primary antibodies for 1 hour, then treated with 0.1% TBST solution containing 5% skim milk for 1 hour. HRP conjugated anti-rabbit or anti-mouse IgG (Sigma) was used as a secondary antibody. Membranes were incubated with Immobilin Western Chemiluminescent HRP Substrate (Millipore) for 1 minute and developed on X-ray film (AGFA).

7. Immunohistochemistry (IHC)

The sciatic nerves, LSCs, and TA muscles were fixed in 4% paraformaldehyde (Sigma) at 4°C overnight. After being washed three times with 0.1M PBS, the tissues were immersed in 0.1M PBS containing 30% sucrose (Sigma) at 4°C overnight, followed by cryopreservation in OCT compound (Sakura Tissue Tek). Samples were then cryosectioned using Cryostat (Leica). After 1 hour incubation in blocking solution containing 2% BSA, 5% normal donkey serum (Jackson ImmunoResearch), and 0.1% Triton X-100 (Samchun), samples were treated with blocking solution containing primary antibodies for 1 hour, and then with blocking solution containing secondary antibodies for 1 hour. IgG Alexa Fluor (Invitrogen) was used as a secondary antibody. After mounting tissue sections on microscope slides (Fisher Scientific) with DAPI (Vectashield), immunofluorescence was observed using LSM 700 confocal laser scanning microscopy (Carl Zeiss).

8. Immunocytochemistry (ICC)

Cells were fixed in 4% paraformaldehyde for 10 minutes at room temperature. After being washed three times with PBS, cells were immersed in 0.1M PBS containing 2% Triton X-100 for 5 minutes at 4°C, followed by one hour incubation in blocking solution with 2% normal donkey serum and 1% BSA. Cells were then treated with blocking solution containing primary antibodies for 1 hour, followed by another 1-hour incubation in blocking solution

with secondary antibodies. IgG Alexa Fluor was used as a secondary antibody. After mounting cells on microscope slides with DAPI, immunofluorescence was observed using LSM 700 confocal laser scanning microscopy. The axon length of CSMNs was measured using Fiji software (NIH).

9. Quantitative real time PCR (q-RTPCR)

The transgene copy number of SOD1-G93A TG mice was measured using q-RTPCR, as described previously [66]. For transgene (hSOD1), the primers used for PCR were as follows; 5'-CATCAGCCCTAATCCATCTGA-3' (forward); 5'-CGCGACTAACAATCAAAGTGA-3' (reverse). For reference gene (IL2), the primers used for PCR were as follows; 5'-CTAGGCCACAGAATTGAAAGATCT-3' (forward); 5'-GTAGGTGGAAATTCTAGCATCATCC-3' (reverse). After 40 cycles of qPCR using TB Green (Takara), the difference of threshold cycle (ΔCT) was calculated, and mice with values between 6.6 and 7.2 were used.

10. Cell viability assay

$1.6x10^5$ cells were seeded on PDL-coated 48-well cell culture plates (SPL) and incubated for 3 days. After being washed two times with warm PBS, cells were incubated with SFM containing 10% WST1 (AbFrontier) for 1 hour at 37°C. Absorbance was measured at 440 nm using a Magellan microplate reader (Tecan).

11. Enzyme-linked immunosorbent assay (ELISA)

To measure the HGF protein level *in vitro,* $1.6x10^5$ C2C12 cells were transduced with $5x10^{13}$ GC of rAAV2-HGF. Forty-eight hours later, supernatants were collected followed by ELISA specific to human HGF (R&D Systems). To measure the *in vivo* expression of HGF, C57BL/6 P60 mice were intrathecally injected with $5x10^9$ GC of rAAV1-HGF. The LSCs were collected 1, 2, 4, 8, 12, and 16 weeks after injection. Total proteins were then extracted using RIPA Buffer and Protease/Phosphatase Inhibitor Cocktail, followed by ELISA for hHGF. Absorbance was measured at 450 nm, and wavelength correction was made at 540 nm using a Magellan microplate reader.

12. Reactive oxygen species (ROS) detection assay

$6.4x10^4$ cells were seeded on PDL-coated 96-well cell culture plates (Nunc) and incubated for 3 days. ROS levels were measured using a ROS Detection Assay Kit (Abcam). Cells were incubated with detection solution for 1 hour at 37°C. Pyocianin was used as a ROS inducer, while N-acetyl-L-cysteine was used as a ROS scavenger. Absorbance was measured using a Magellan microplate reader.

13. Microarray assay

Motor cortical cells were treated with 100 ng/ml of rHGF, and total RNAs were isolated followed by Microarray analysis using Affymetrix Genechip (Thermofisher). After data extraction, RMA (robust multi-array average) normalization was performed, followed by DEG (differentially expressed gene) analysis. Out of selected DEGs, functional annotation was performed based on GO (gene ontologies) hierarchy and KEGG/BioCarta pathways. Selected genes were clustered according to the classification from the previous report [3].

14. H&E staining and morphometric analysis

To investigate histological changes, $3.12x10^8$ GC of rAAV6-C or rAAV6-HGF were injected into the TA. Fourteen days later, the TA was collected and fixed in 10% neutral-buffered formalin. After being embedded in paraffin, samples were longitudinally cut into 6-μm sections. Samples were then stained with hematoxylin-eosin (H&E), followed by morphometric analysis. To measure the CSA of the TA, the freehand selection tool in Fiji software (NIH) was used. For each mouse, at least 300 muscle fibers were assessed, and values were averaged.

15. Statistical analysis

All values are presented as mean ± standard error mean (SEM). Differences between two values were analyzed by Student's t-tests. Differences between three or more values were analyzed by one-way ANOVA followed by Tukey's post-hoc test. For values

containing temporal factors, two-way ANOVA was performed followed by Tukey or Sidak's post-hoc test.

Antigen	Host	Supplier	Cat. No.	Dilutions
p-Met (Y1234/1235)	Rabbit	CST	#3077	1:500
Met	Rabbit	Sigma	SAB4300599	1:2000
p-ERK (T202/Y204)	Mouse	CST	#9106	1:500
ERK	Rabbit	CST	#9102	1:500
p-PI3K p85 (Y458)/p55 (Y199)	Rabbit	CST	#4228	1:500
PI3K	Rabbit	CST	#4292	1:500
p-RSK	Rabbit	CST	#9346	1:500
RSK	Rabbit	CST	#9333	1:500
TUBB3	Mouse	Biolegend	801202	1:1000

Table 1. List of antibodies used for Western blot analysis.

Antigen	Host	Supplier	Cat. No.	Dilutions
p-S6 (S235/236)	Rabbit	CST	#2211	1:500
S6	Rabbit	CST	#2217	1:1000
p-STAT3 (Y705)	Rabbit	CST	#9145	1:500
STAT3	Rabbit	CST	#4904	1:500
p-cJUN (S73)	Rabbit	CST	#3270	1:500
cJun	Rabbit	CST	#9165	1:500
p-GSK-3β (S9)	Rabbit	CST	#9336	1:500
GSK-3β	Rabbit	CST	#9315	1:500
IKBα	Rabbit	CST	#9242	1:500
p-p38 (T180/Y182)	Rabbit	CST	#4511	1:500
p38	Rabbit	CST	#9212	1:500

Table 1. List of antibodies used for Western blot analysis (continued).

Antigen	Host	Supplier	Cat. No.	Dilutions
GFP	mouse	Merck	MAB3580	1:250
STMN2	rabbit	Novus	NBP1-49461	1:250
TUBB3	mouse	Biolegend	801202	1:500
UCHL1	rabbit	Proteintech	14730-1-ap	1:500
α-Bungarotoxin, Alexa Fluor™ 555 conjugate	N/A	Thermofisher	B35451	1:500
NeuN	mouse	Merck	MAB377	1:500
ChAT	goat	Merck	mab144p	1:200
Ctip2	rat	abcam	ab18465	1:250
hSOD1	mouse	R&D systems	MAB3418	25 µg/ml
p-Met (Y1234/1235)	rabbit	CST	#3077	1:250

Table 2. List of antibodies used for immunostaining.

Gene	Primer sequence Forward 5' → 3'	Primer sequence Reverse 5' → 3'
Mouse IL2	CTAGGCCACAGAATTGAAA GATCT	GTAGGTGGAAATTCTAGCAT CATCC
Human SOD1	CATCAGCCCTAATCCATCTG A	CGCGACTAACAATCAAAGT GA

Table 3. List of primers used for murine IL2 and human SOD1 to determine the copy number of mhSOD1.

Gene	Primer sequence Forward 5’ → 3’	Primer sequence Reverse 5’ → 3’
MuRF1	TGCCTGGAGATGTTTACCAAGC	AAACGACCTCCAGACATGGACA
Atrogin-1	AAGGCTGTTGGAGCTGATAGCA	CACCCACATGTTAATGTTGCCC
FOXO1	TTCAATTCGCCACAATCTGTCC	GGGTGATTTTCCGCTCTTGC
FOXO3	CTGGGGGAACCTGTCCTATG	TCATTCTGAACGCGCATGAAG
Pri-miR-206	ACCCAGTGCCCTGTGTTCCCA	AGCGCCTCTTCTCGGTTTCCCT
HDAC4	CACACCTCTTGGAGGGTACAA	AGCCCATCAGCTGTTTTGTC
MyoD	CCACTCCGGGACATAGACTT	AAAAGCGCAGGTCTGGTGAG
Myogenin	GAGACATCCCCCTATTTCTACCA	GCTCAGTCCGCTCATAGCC

GAPDH	CTGGAAAGCTGTGGCGTGAT	CCAGGCGGCACGTCAGATCC

Table 4. List of primers used in this study for q-RTPCR analysis.

Chapter III

Effects of intrathecally delivered rAAV-HGF in the nerve crush and SOD1-G93A TG mouse models

1. Background

ALS is a fatal neurodegenerative disease that kills the motor neurons of the CNS, which consists of the motor cortex and spinal cord [1-3]. It affects corticospinal motor neurons or upper motor neurons of the motor cortex, and spinal motor neurons or lower motor neurons of the spinal cord [4]. As the disease progresses, skeletal muscle wastes away, eventually causing respiratory failure [2, 5]. Only 10% of ALS is classified as familial ALS, the cause of which has been identified [6]. While SOD1 is one of the major known causative genes, further studies have shown that mutations in RNA-binding proteins FUS and TARDBP, or the repetition of the hexanucleotide sequence on the 72nd open reading frame of chromosome 9 are important in the pathogenesis of ALS [7-9]. The remaining 90% consists of sporadic ALS, the causes of which remain largely unknown.

The disease mechanisms of ALS are extremely diverse [3]. Among others, impairment of protein quality control is one of the best-known mechanisms. For example, when mutated SOD1 proteins are not properly folded in the endoplasmic reticulum, protein aggregates that cause cytotoxicity are generated. Abnormalities in proteins related to the cytoskeleton and RNA metabolism are also for mechanisms of ALS. In addition to the neuronal cells, the CNS also contains a variety of glial cells that maintain the nervous system with their unique functions. Relevant studies have shown that the improper operation of astrocytes, oligodendrocytes, and microglia are particularly important in the progression of ALS. For example, when microglia responsible for immune responses in the CNS are hyperactivated, ROS causing oxidative stress is generated, resulting in cytotoxicity. In addition,

when the activity of the MCT transporter of oligodendrocytes is downregulated, energy supply to the motor neurons is diminished. Lastly, when the EAAT2 transporter of astrocytes becomes abnormal, excess amounts of glutamate transmit continuous excitatory signals to the motor neurons.

ALS patients suffer from various symptoms related to the skeletal muscles responsible for voluntary movements. As muscles are atrophied, it becomes difficult to walk and maintain proper posture. As the disease progresses, tongue muscles are atrophied, making it difficult to pronounce and swallow. Only riluzole and edaravone are approved by the FDA for the treatment of ALS [13-15]. Riluzole is a competitive inhibitor of the ATP binding site of the sodium channel, preventing glutamate release in the synapses. Edaravone has been reported to relieve oxidative stress. Nevertheless, both drugs can only slightly alleviate the symptoms of ALS, without resolving the fundamental causes.

In an effort to develop effective treatment methods for neurodegenerative diseases like ALS, I focused on the trophic capabilities of HGF in this study. Initially known to promote the proliferation of hepatocytes, HGF has been shown to perform various bioactivities such as facilitating angiogenesis, neurogenesis, cell proliferation, and cell migration [16-22]. Expressed as an inactive single peptide, HGF is cleaved into two chains by the serine proteases in the extracellular matrix, becoming an active heterodimer [23]. Met, a receptor protein of HGF, has been known to be expressed both in the CNS and PNS. For example, the Met protein is found in endothelial cells, muscle cells, neuronal cells, and Schwann cells, which are all important in the pathology of various neuromuscular diseases

[67]. When HGF binds to the Met receptor, a number of signal transduction pathways, including those of MAPK, STAT3, and PI3K-Akt cascade, are activated [23, 29, 30]. Therefore, I focused on HGF as a pleiotropic growth factor capable of affecting several different cell types involved in the pathology of ALS.

As an alternative means of delivering the HGF gene, recombinant AAV vector encoding the human HGF gene (rAAV-HGF) was utilized in this study. rAAV vectors encoding insulin-like growth factor-1 (IGF-1), vesicular endothelial growth factor (VEGF), or granulocyte colony-stimulating factor (G-CSF) have been reported to delay disease progression when injected into SOD1-G93A TG mice [68-70]. I investigated whether HGF could also produce beneficial effects in such disease models when delivered via the rAAV vector. Since it has been shown that the expression of two isoforms of human HGF, HGF728 (cHGF) and HGF723 (dHGF), could boost the therapeutic effects in various disease models, rAAV-HGF that could simultaneously express two isoforms of HGF was generated [45, 46, 48, 71]. Effects of IT delivery of rAAV-HGF were first tested in the sciatic nerve crush and SOD1-G93A TG mouse models.

To further investigate the effect of HGF in the motor neurons, the motor cortices of SOD1-G93A TG mice were isolated and cultured *in vitro*, generating primary motor cortical culture [65]. Since this culture system consists of CSMNs as well as glial cells, it can better mimic *in vivo* conditions than a primary culture containing a single cell type. To understand the molecular mechanisms underlying the protective and regenerative effects of rAAV-HGF in

neurodegenerative disease models, I tested whether neuroprotective effects are reproducible in this culture system.

2. Results

2.1. Construction of rAAV vectors expressing human HGF

In this study, it was tested whether HGF could protect the neurons and the skeletal muscles when delivered with rAAV vector. AAV used in this study was designed to express two isoforms of human HGF—HGF723 (or dHGF) and HGF728 (or cHGF)—as in the case of our bodies [53]. In order to simultaneously express two isoforms, I used the gDNA-cDNA-hybrid sequence similar to that described by Cho et al. (**Figure III-1**). This chimeric sequence was inserted into pAAV-MCS containing multiple cloning sites, resulting in pAAV-HGF.

To produce rAAV vectors, equal amounts of three plasmids (pAAV-HGF, *rep/cap*-expressing plasmid, and helper plasmid) were co-transfected into $1x10^6$ HEK293T cells, initially producing AAV serotype 2 [72]. Seventy-two hours later, the supernatant was collected and viral titer was determined as described previously [73]. To determine whether rAAV vectors could indeed produce RNAs of two HGF isoforms, $1.6x10^5$ C2C12 cells were transduced with $1.23x10^8$ GC of rAAV2-HGF, and total RNAs were isolated 48 hours later followed by RT-PCR. A control virus—rAAV2-C lacking the HGF sequence—did not produce any HGF RNA, whereas two HGF RNA species, each for HGF723 and HGF728, were readily detectable in cells transduced with rAAV2-HGF **(Figure III-2)**.

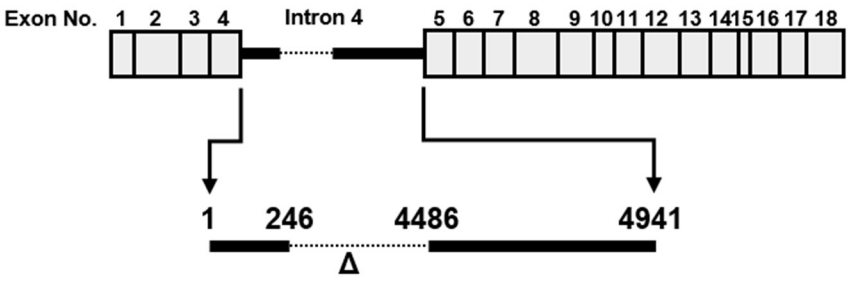

Figure III-1. A gDNA-cDNA-hybrid sequence expressing two isoforms of human HGF.

To co-express two isoforms of HGF, HGF723 (or dHGF) and HGF728 (or cHGF), a gDNA-cDNA-hybrid sequence was generated. In this chimeric sequence, a part of intron 4 of the HGF gene was inserted between cDNA sequences of exon 4 and exon 5, allowing alternative splicing. Since the length of intron 4 is relatively long, sequences between 246 and 4486 were deleted (Δ). The numbers represented indicate relative positions of intron 4, and '1' corresponds to the first nucleotide of intron 4.

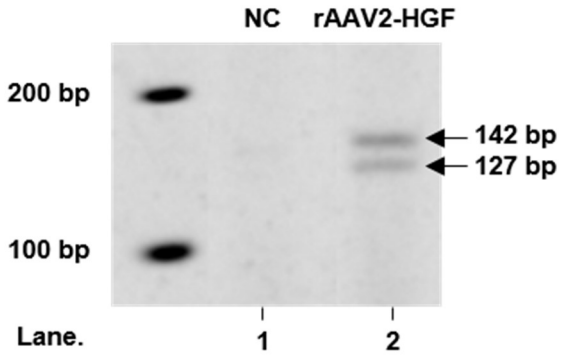

Figure III-2. Acrylamide gel analysis after transduction of HGF-expressing rAAV vector.

$1.6x10^5$ C2C12 cells were transduced with $1.23x10^8$ GC of rAAV2, and 48 hours later, total RNAs were isolated followed by RT-PCR and acrylamide gel analysis. rAAV2-C lacking the HGF sequence was used as a negative control (NC). The upper arrow indicates the amplicon size of cHGF (142 bp), while the lower arrow shows the amplicon size of dHGF (127 bp).

To test whether HGF proteins were indeed produced from rAAV vectors, $8x10^4$ C2C12 cells were transduced with $5x10^{13}$ GC of rAAV2-HGF, and total proteins were isolated 48 hours later followed by ELISA specific to human HGF proteins. rAAV2-HGF produced 159.13 ± 23.92 ng/mg of HGF, while no HGF was detectable in cells transduced with a control vector. **(Figure III-3)**.

2.2. Comparison of different AAV serotypes for IT delivery

To select an appropriate AAV serotype that could be used for gene transfer to the spinal cord, four serotypes of rAAV were prepared as described above, and $4.12x10^8$ GC of each AAV were injected into the LSC. Four weeks later, total proteins were extracted from the LSC, and the expression level of HGF was compared using ELISA. As summarized in **Figure III-4**, mice injected with rAAV1-HGF produced the highest level of HGF protein (621.89 ± 112.98 pg/mg), and other serotypes generated 7- to 17-fold lower amounts, 86.25 ± 7.59 pg/mg for rAAV6, 35.54 ± 4.87 pg/mg for rAAV2, and 80.15 ± 17.94 pg/mg for rAAV5 **(Figure III-4)**.

To determine the tissue distribution of transgene expression from different AAV vectors inside the LSC, different subtypes of AAV expressing GFP were used because it was technically difficult to analyze human HGF by IHC. Four weeks after IT injection of AAV vectors, tissue samples were taken and GFP-expressing cells were measured by IHC. rAAV1-GFP transduced the largest area of the ventral horn, while rAAV2 or rAAV6 expressed GFP

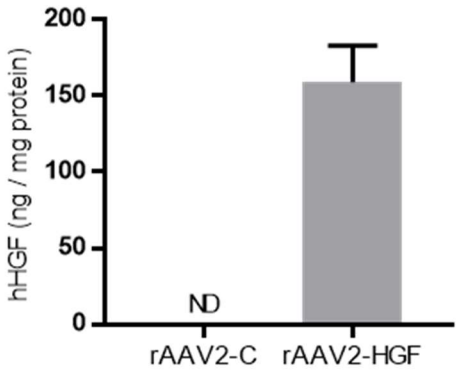

Figure III-3. ELISA for hHGF after transduction of HGF-expressing rAAV vector.

$8x10^4$ C2C12 cells were transduced with $5x10^{13}$ GC of rAAV2, and 48 hours later, supernatant was collected followed by ELISA for hHGF. rAAV2-C lacking the HGF sequence was used as a negative control. ND indicates that values were not detectable or lower than the minimum detectable dose. Values are represented as mean ± SEM.

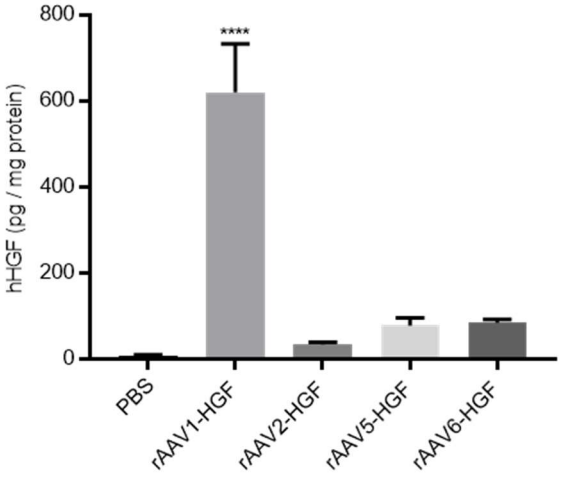

Figure III-4. ELISA for hHGF after IT injection of rAAV-HGF.

$4.12x10^8$ GC of rAAV1, 2, 5, or 6-HGF were intrathecally injected into C57BL/6 mice at postnatal day 60 (P60). The LSCs were collected and total proteins were isolated 4 weeks after injection, followed by ELISA specific to human HGF (hHGF). For statistical analysis, one-way ANOVA was performed, followed by Tukey's post-hoc test. $^{****}p < 0.0001$ for rAAV1 vs. other serotypes. Values are represented as mean ± SEM.

primarily on the surface of white matter **(Figure III-5)**. Taken together, AAV1 appeared to be the most effective serotype for IT gene delivery.

2.3. Kinetics of HGF expression from rAAV1-HGF

To determine how the HGF expression level changed over time, $5x10^9$ GC of rAAV1-HGF were injected into the LSC of 2-month-old C57BL/6 mice, and total proteins were isolated, followed by ELISA. One week after injection, 1.98 ± 0.95 ng/mg of hHGF were detectable, and the level was the highest after two weeks (2.44 ± 1.37 ng/mg), thereafter gradually decreasing over time until 16 weeks after injection (0.95 ± 0.58 ng/mg) **(Figure III-6)**. A control virus lacking the HGF sequence did not produce any HGF protein. While hHGF was not detectable in the motor cortex and serum, 170.17 ± 155.95 ng/mg were observed in the TA **(Figure III-7)**.

To investigate whether the HGF proteins expressed from rAAV1-HGF could increase the phosphorylation of Met, a receptor for HGF, $5x10^9$ GC of rAAV1-HGF were intrathecally injected into C57BL/6 mice at P60, Met phosphorylation levels were measured 7 days later using IHC. As shown in **Figure III-8**, SMNs were labeled with NeuN (red) and ChAT (green). In mice injected with rAAV1-C, 37.32 ± 0.02% of SMNs were co-stained with p-Met. The number of p-Met-positive SMNs was increased to 58.09 ± 0.01% in the rAAV1-HGF group **(Figure III-9)**. These results indicated that HGF proteins expressed from rAAV1-HGF could indeed augment the phosphorylation of Met.

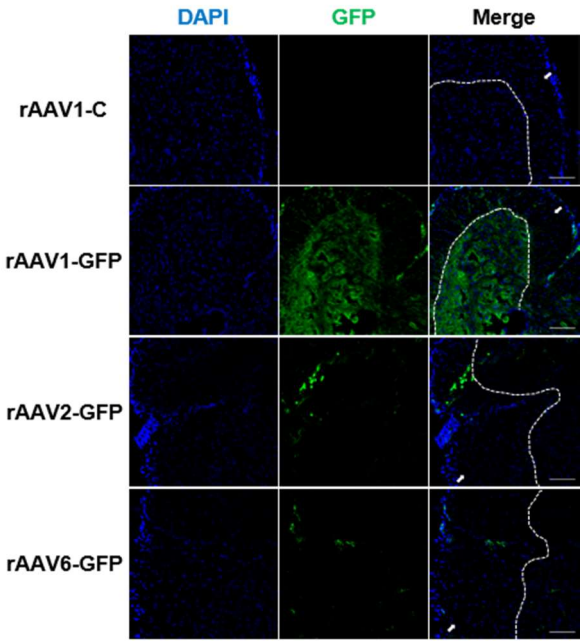

Figure III-5. IHC assay after IT injection of rAAV-GFP.

$1.4x10^9$ GC of four serotypes were intrathecally injected into 2-month-old C57BL/6 mice. The LSCs were collected 4 weeks after injection. Tissues were fixed, followed by IHC assay using an antibody specific to GFP (green). The boundary between white and grey matter is distinguished by dotted lines, and white matter is indicated by white arrows. Scale bar = 100 μm.

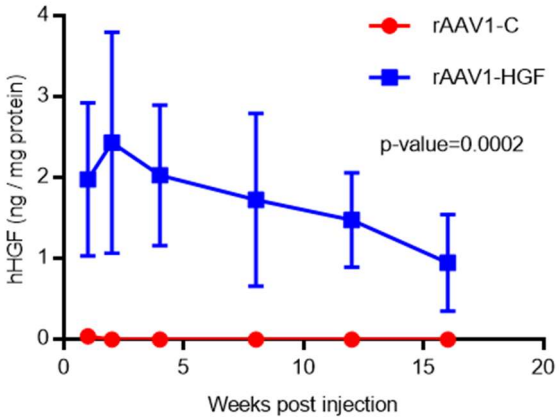

Figure III-6. Kinetics of HGF expression from rAAV1-HGF.

$5x10^9$ GC of rAAV1-HGF were intrathecally injected into 2-month-old C57BL/6 mice. The LSCs were collected 1, 2, 4, 8, 12, and 16 weeks after IT injection and subjected to ELISA for hHGF. For statistical analysis, two-way ANOVA was performed, followed by Sidak's post-hoc test. The p-value between the two groups was 0.0002. Values are represented as mean ± SEM.

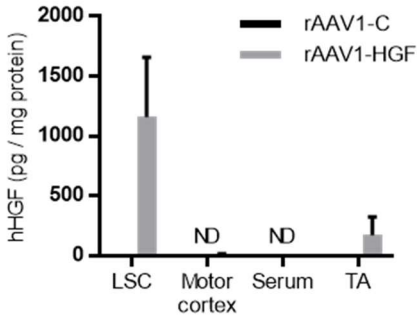

Figure III-7. ELISA for hHGF after IT injection of rAAV1-HGF.

C57BL/6 mice at P60 were intrathecally injected with $5x10^9$ GC of rAAV1-C or rAAV1-HGF. The LSCs, motor cortices, serum, and TA were collected 8 weeks after injection and subjected to ELISA for hHGF. Values are represented as mean ± SEM.

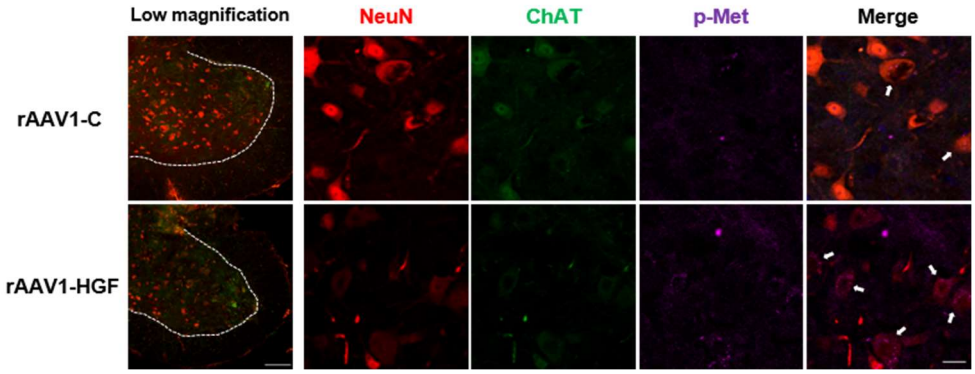

Figure III-8. IHC assay in the LSC after IT injection of rAAV1-HGF.

C57BL/6 mice at P60 were intrathecally injected with $5x10^9$ GC of rAAV1-C or rAAV1-HGF. One week later, LSCs were collected and subjected to IHC assay. Antibodies specific to ChAT (green) and NeuN (red) were used to label SMNs, together with those for p-Met (magenta). In low magnification panels, the boundary between white and grey matter is distinguished by dotted lines. In merge panels, p-Met-expressing SMNs are indicated by white arrows. Scale bar = 100 μm for low magnification panels and 20 μm for the others.

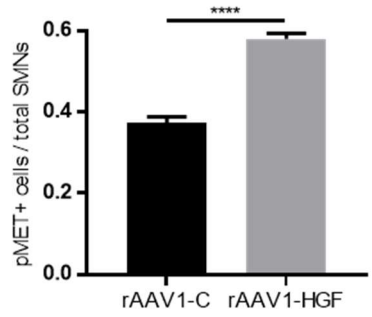

Figure III-9. Quantification of p-Met-expressing SMNs.

The proportion of SMNs expressing p-Met per total SMNs was measured and represented as a bar graph. For statistical analysis, Student's t-test was performed. $^{****}p < 0.0001$. Values are represented as mean ± SEM.

2.4. Effects of rAAV1-HGF in the sciatic nerve crush and SOD1-G93A transgenic mouse models

2.4.1. Effects of IT delivery of rAAV1-HGF in the sciatic nerve crush model

The effects of intrathecally delivered rAAV1-HGF on nerve damage were then checked in the sciatic nerve crush mouse model [74]. Crush injury was introduced in 2-month-old C57BL/6 mice, and $5x10^9$ GC of virus were intrathecally injected immediately. As shown in **Figure III-10, 11**, rAAV1-HGF significantly improved hindlimb strength and rotarod performance from 10 days after nerve crush, and these effects were maintained until the end of the experiment on day 28. These results suggested that rAAV1-HGF could promote functional recovery after sciatic nerve crush when delivered into the spinal cord. It is well established that when the sciatic nerve is injured, Wallerian degeneration occurs and axons regenerate again as time goes by [75]. Therefore, I used IHC to examine whether rAAV1-HGF had effects on nerve regeneration in the areas of the nerve damage. Five days after nerve injury, the sciatic nerve was collected, and labeled with SCG10, a marker for the regenerating axon [76]. When the length of the regenerated sciatic nerve was measured, rAAV1-C showed a 2.11 ± 0.09 mm increase from the damaged site, while in the rAAV1-HGF group, it was 37.91% higher at 2.91 ± 0.27 mm **(Figure III-12, 13)**.

The presynaptic terminal of the sciatic nerve forms NMJs with the postsynaptic end plate of the muscle to transmit the contractile signal to the muscle [74]. Therefore, TA muscle connected to the sciatic nerve was analyzed by IHC. In a normal state, the NMJ is pretzel-shaped and has well-preserved integrity. After nerve injury, however, the shape of the NMJ

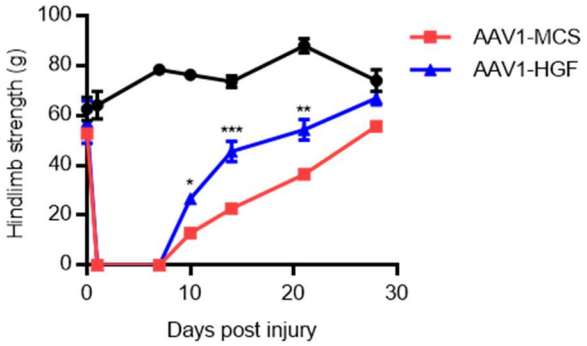

Figure III-10. Measurement of hindlimb strength after sciatic nerve crush.

Using 2-month-old C57BL/6 mice, sciatic nerve crush was induced, and $5x10^{11}$ GC of rAAV1-C or rAAV1-HGF were intrathecally injected into the LSC. Hindlimb strength was measured 1, 7, 10, 14, 21, and 28 days after nerve crush. Value at day 0 was measured before nerve crush. Value at day 0 was measured before nerve crush. For statistical analysis, two-way ANOVA was performed, followed by Tukey's post-hoc test. Values are represented as mean ± SEM. $^{*}p < 0.05$, $^{**}p < 0.005$, $^{***}p < 0.001$.

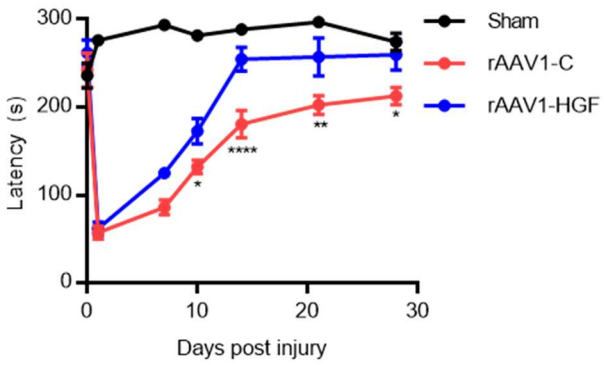

Figure III-11. Measurement of rotarod performance after sciatic nerve crush.

Using 2-month-old C57BL/6 mice, sciatic nerve crush was induced, and $5x10^{11}$ GC of rAAV1-C or rAAV1-HGF were intrathecally injected into the LSC. Mean latency to fall from the rotarod was measured 1, 7, 10, 14, 21, and 27 days after nerve crush. Value at day 0 was measured before nerve crush. For statistical analysis, two-way ANOVA was performed, followed by Tukey's post-hoc test. Values are represented as mean ± SEM. $^{*}p < 0.05$, $^{**}p < 0.005$, $^{***}p < 0.001$, $^{****}p < 0.0001$.

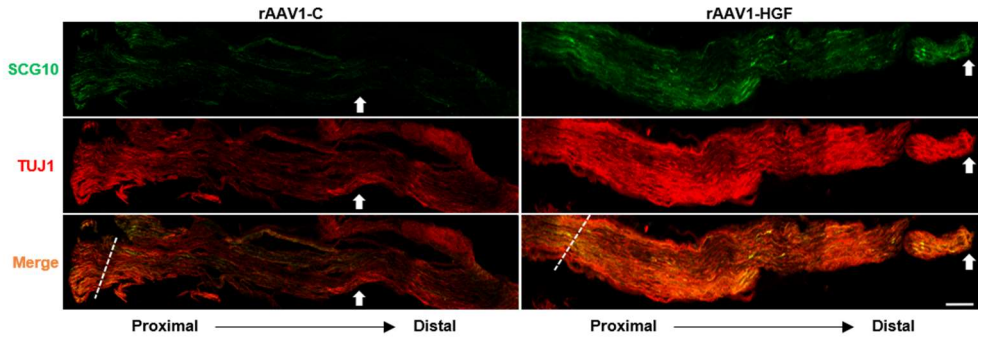

Figure III-12. Representative images of the sciatic nerves from mice treated with rAAV1-C or rAAV1-HGF after nerve crush.

Using 2-month-old C57BL/6 mice, sciatic nerve crush was induced, and $5x10^{11}$ GC of rAAV1-C or rAAV1-HGF were intrathecally injected into the LSC. For IHC assay, the sciatic nerves were collected 5 days after nerve crush. Antibodies specific to TUJ1 and SCG10 were used as markers for neurons and regenerating axons, respectively. Crush sites are indicated by dotted lines, and the tip of SCG10 signals is indicated by white arrows. Proximodistal direction is indicated by dotted lines. Scale bars = 200 μm.

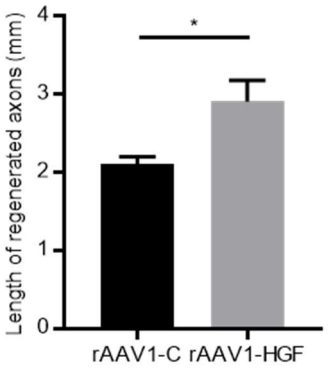

Figure III-13. Quantification of length of regenerated axons after sciatic nerve crush.

Using 2-month-old C57BL/6 mice, sciatic nerve crush was induced, and $5x10^{11}$ GC of rAAV1-C or rAAV1-HGF were intrathecally injected into the LSC. The sciatic nerves were collected 5 days after nerve crush, followed by IHC assay. Lengths of regenerated nerves were measured using Fiji software and represented as a bar graph. For statistical analysis, Student's t-test was performed. $^{*}p < 0.05$.

becomes abnormal and the degree of integrity decreases (**Figure III-14, 15**). Compared with the sham group to which the nerve injury was not introduced, the proportion of fully innervated NMJs in the rAAV1-C group was reduced 2.34-fold, and that of abnormally shaped NMJs was increased 7.75-fold. On the other hand, in the rAAV1-HGF group, the proportion of fully innervated NMJs increased by 69.7%, and that of denervated NMJs decreased 3.83-fold in comparison to the rAAV1-C group **(Figure III-16, 17, 18)**. The average α-BTX area was decreased by 41.75% in the rAAV1-C group compared to the sham group, but was increased by 56.76% in the rAAV1-HGF group. These results suggested that IT injection of rAAV1-HGF could promote the regeneration of neurons and re-establishment of NMJs possibly by acting on the cell body of motor neurons located in the spinal cord

2.4.2. Effects of IT delivery of rAAV1-HGF in the SOD1-G93A TG mouse model

Encouraged by the above results, the effects of rAAV1-HGF were also tested in the SOD1-G93A TG mouse model, the most commonly used animal model for ALS. First, it was investigated whether HGF proteins expressed from rAAV1-HGF could also increase the phosphorylation of Met in SOD1-G93A TG mice. $5x10^9$ GC of rAAV1-HGF were intrathecally injected to SOD1-G93A TG mice at P60, and the levels of Met phosphorylation were measured 40 days later using IHC **(Figure III-19)**. In non-TG mice, 35.24 ± 0.55% of SMNs were co-stained with p-Met. The number of p-Met-positive cells was lowered in TG mice injected with a control vector, rAAV1-C, to 29.98 ± 0.54%, but increased to 59.65 ± 1.35% in the rAAV1-HGF group **(Figure III-20)**. These findings suggested that the HGF

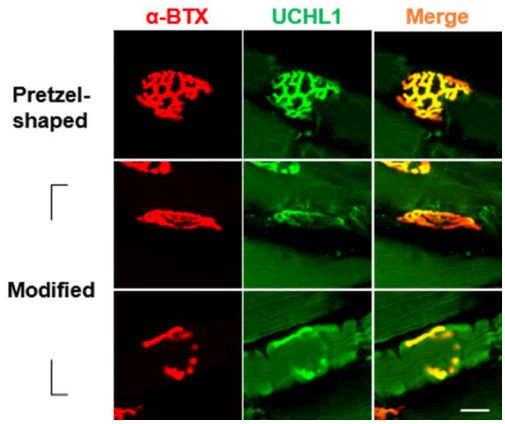

Figure III-14. Representative images of the shape of the NMJ.

Using 2-month-old C57BL/6 mice, sciatic nerve crush was induced, and $5x10^{11}$ GC of rAAV1-C or rAAV1-HGF were intrathecally injected into the LSC. For IHC assay, the TA was collected 5 days after nerve crush. An antibody specific to UCHL1 was used as a marker for presynaptic terminals, whereas that of α-bungarotoxin (α-BTX) was used for postsynaptic end plates [77]. The shapes of NMJs were analyzed to determine whether they were pretzel-shaped or distorted. Scale bar = 20 μm.

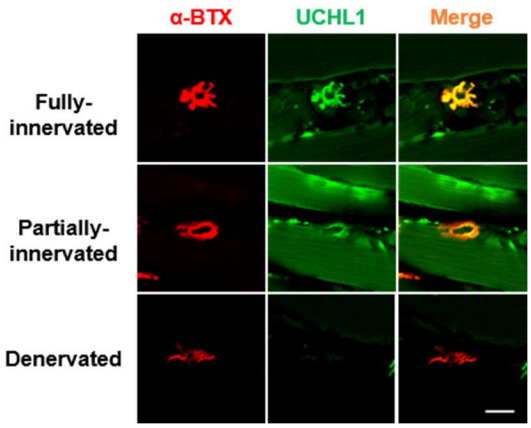

Figure III-15. Representative images of the integrity of the NMJ.

2-month-old C57BL/6 mice, sciatic nerve crush was induced, and $5x10^{11}$ GC of rAAV1-C or rAAV1-HGF were intrathecally injected into the LSC. For IHC assay, the TA was collected 5 days after nerve crush. An antibody specific to UCHL1 was used as a marker for presynaptic terminals, whereas that of α-bungarotoxin (α-BTX) was used for postsynaptic end plates. The integrity of NMJs was determined by measuring to what degree presynaptic terminals merged with postsynaptic end plates. Scale bar = 20 μm.

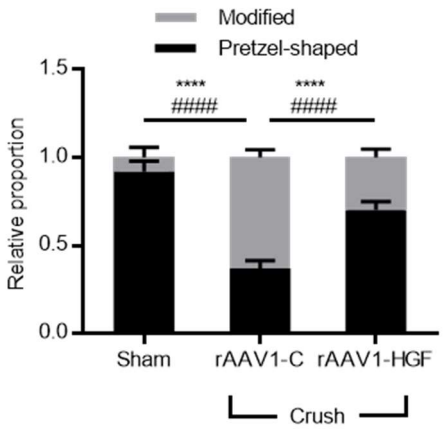

Figure III-16. Quantification of the shape of the NMJ.

After sciatic nerve crush, the shape of NMJs was measured. Values are represented as mean ± SEM. For statistical analysis, two-way ANOVA was performed, followed by Tukey's post-hoc test. $^{****}p < 0.0001$ for modified NMJ, $^{\#\#\#\#}p < 0.0001$ for pretzel-shaped NMJ.

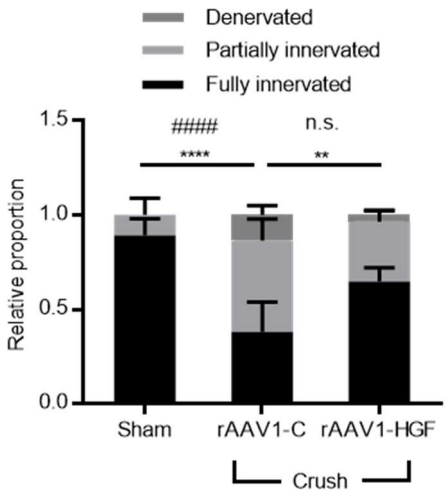

Figure III-17. Quantification of the integrity of the NMJ.

After sciatic nerve crush, the integrity of NMJs was measured. Values are represented as mean ± SEM. For statistical analysis, two-way ANOVA was performed, followed by Tukey's post-hoc test. In **Fig. 2h**, $^{**}p < 0.01$ and $^{****}p < 0.0001$ for fully innervated NMJ, $^{\#\#\#\#}p < 0.0001$ and *n.s.* > 0.05 partially innervated NMJ.

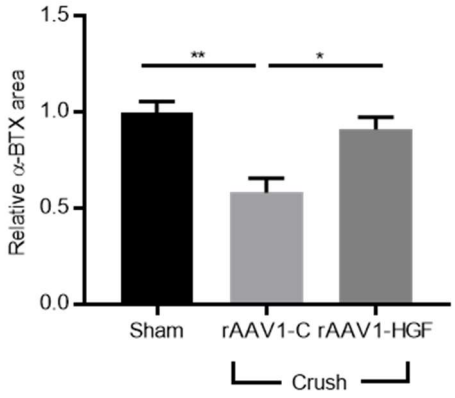

Figure III-18. Measurement of area stained with α-BTX.

After sciatic nerve crush, average α-BTX area was measured. Values are represented as mean ± SEM. For statistical analysis, one-way ANOVA was performed, followed by Tukey's post-hoc test. $^{*}p < 0.05$, $^{**}p < 0.005$.

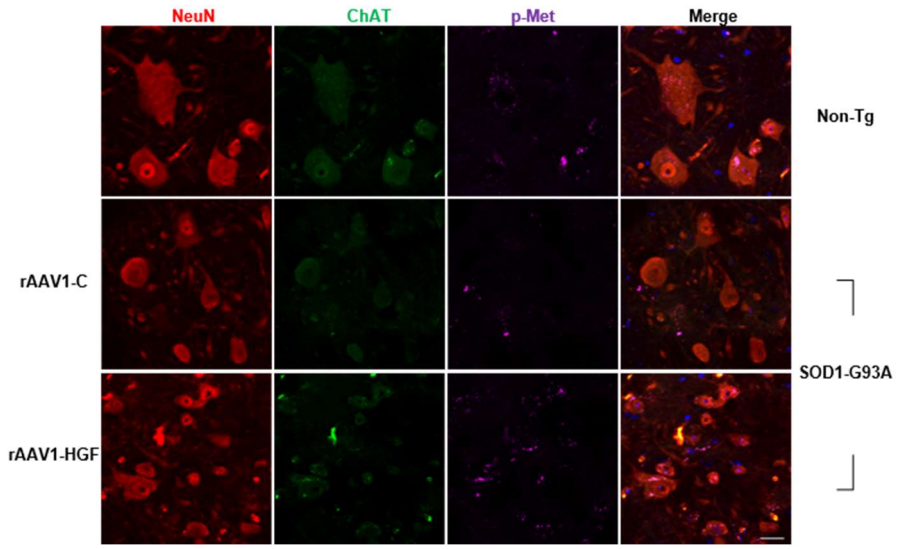

Figure III-19. Levels of phosphorylated Met after IT delivery of rAAV1-HGF.

Non-TG or TG mice at P60 were intrathecally injected with $5x10^9$ GC of rAAV1-C or rAAV1-HGF. The LSCs were collected at P100. Tissues were fixed and subjected to IHC assay. Antibodies specific to ChAT (green) and NeuN (red) were used to label SMNs, together with those for p-Met (magenta). Scale bar = 20 μm.

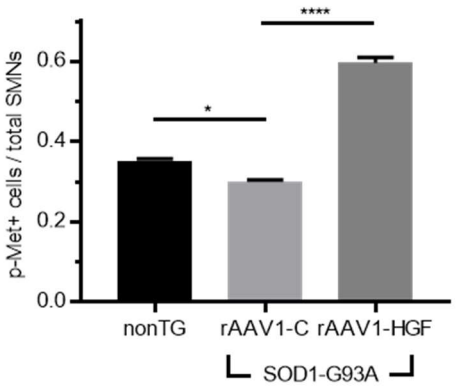

Figure III-20. The proportion of SMNs expressing p-Met.

Non-TG or TG mice at P60 were intrathecally injected with $5x10^9$ GC of rAAV1-C or rAAV1-HGF. The LSCs were collected at P100. Tissues were fixed and subjected to IHC assay. The proportion of SMNs expressing p-MET per total SMNs was measured and represented as a bar graph. Values are represented as mean ± SEM. $^{*}p < 0.05$, $^{****}p < 0.0001$.

proteins expressed from rAAV1-HGF could indeed increase the phosphorylation of Met in this mouse model.

To test whether rAAV1-HGF could exert any effect on disease progression of SOD1-G93A TG mice, body weight was measured and behavioral tests were performed once every week until P158 after injecting rAAV1-HGF into the LSC of TG mice at P60. IT delivery of rAAV1-HGF did not affect the rate of weight loss, but significant improvements were observed in rotarod, hanging wire, and grip strength tests **(Figure III-21, 22, 23, 24, and 25)**. In addition, survival rate was increased from 20% to 66.67% at P150, and median survival was also increased by 6.53% from 145.5 days to 155 days **(Figure III-26)**. These results suggested that IT delivery of rAAV1-HGF might slow disease progression and improve survival rate in this mouse model.

I tested whether IT injection of rAAV1-HGF could delay degeneration of SMNs in SOD1-G93A TG mice. $5x10^9$ GC of rAAV1-HGF were injected into the LSCs of SOD1-G93A TG mice at P60, and the LSCs were collected 40 days later (P100) followed by IHC. When compared to the non-TG group, the rAAV1-C group showed the number of SMNs in the ventral horn reduced 2.07-fold, the ratio of SMNs to total cells decreased by 58.65%, and the diameter of SMNs diminished by 39.83% **(Figure III-27)**. Although rAAV1-HGF did not increase the diameter of SMNs, the number of SMNs was increased 2.36-fold and the ratio of SMNs to total cells was increased by 67.11%, compared to the rAAV1-C **(Figure II-28, 29, 30)**.

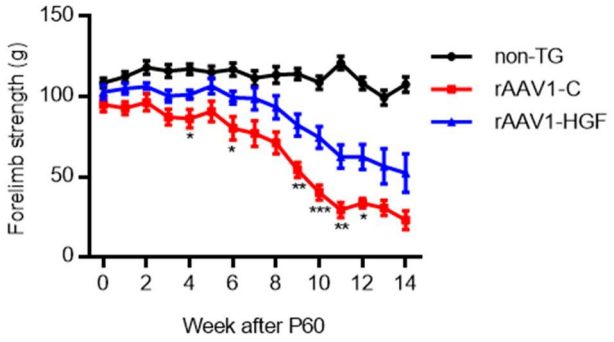

Figure III-21. The forelimb strength of SOD1-G93A mice after IT delivery of rAAV1-C or rAAV1-HGF.

SOD1-G93A TG mice at P60 were intrathecally injected with $5x10^{11}$ GC of rAAV1-C or rAAV1-HGF. The forelimb strength was measured once a week until P158. For statistical analysis, one-way ANOVA was performed followed by Tukey's post-hoc test at each time point. $^{*}p < 0.05$, $^{**}p < 0.01$, $^{***}p < 0.001$. Values are represented as mean ± SEM.

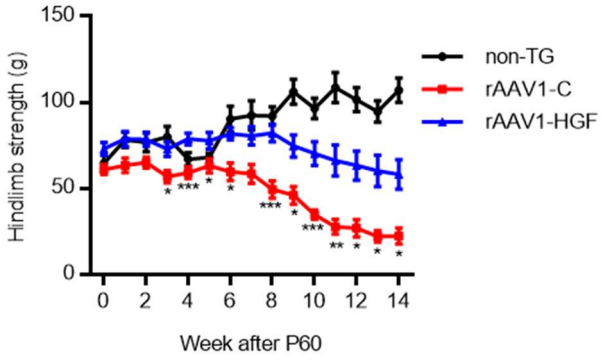

Figure III-22. The hindlimb strength of SOD1-G93A mice after IT delivery of rAAV1-C or rAAV1-HGF.

SOD1-G93A TG mice at P60 were intrathecally injected with $5x10^{11}$ GC of rAAV1-C or rAAV1-HGF. The hindlimb strength was measured once a week until P158. For statistical analysis, one-way ANOVA was performed followed by Tukey's post-hoc test at each time point. $^{*}p < 0.05$, $^{**}p < 0.01$, $^{***}p < 0.001$. Values are represented as mean ± SEM.

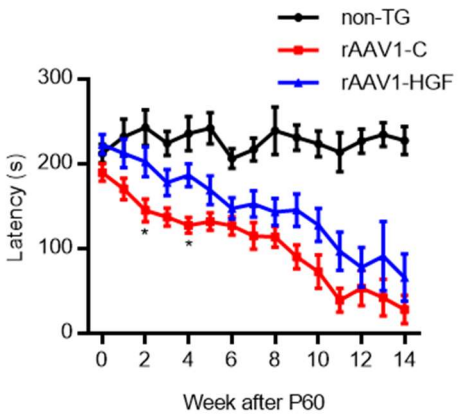

Figure III-23. Mean latency on rotarod after IT delivery of rAAV1-C or rAAV1-HGF in the SOD1-G93A mouse model.

SOD1-G93A TG mice at P60 were intrathecally injected with $5x10^{11}$ GC of rAAV1-C or rAAV1-HGF. Mean latency on the rotating rod was measured once a week until P158. For statistical analysis, one-way ANOVA was performed followed by Tukey's post-hoc test at each time point. $^{*}p < 0.05$. Values are represented as mean ± SEM.

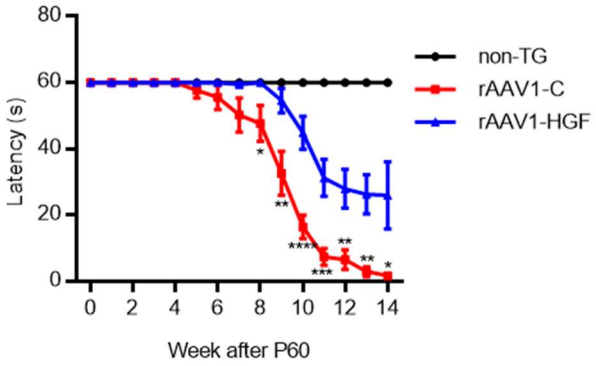

Figure III-24. Hanging wire test after IT delivery of rAAV1-C or rAAV1-HGF in the SOD1-G93A mouse model.

SOD1-G93A TG mice at P60 were intrathecally injected with $5x10^{11}$ GC of rAAV1-C or rAAV1-HGF. Hanging wire test was performed once a week until P158. For statistical analysis, one-way ANOVA was performed followed by Tukey's post-hoc test at each time point. $^{*}p < 0.05$, $^{**}p < 0.01$, $^{***}p < 0.001$, $^{****}p < 0.0001$. Values are represented as mean ± SEM.

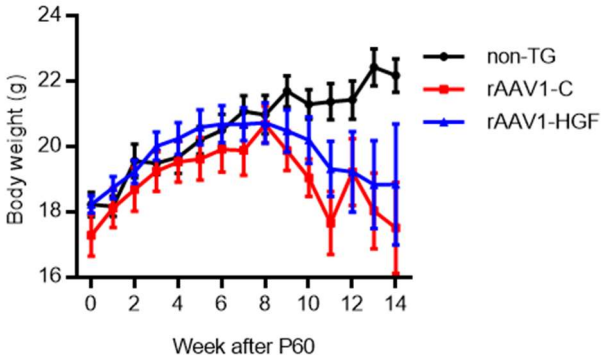

Figure III-25. The body weight of SOD1-G93A TG mice after IT delivery of rAAV1-C or rAAV1-HGF.

SOD1-G93A TG mice at P60 were intrathecally injected with $5x10^{11}$ GC of rAAV1-C or rAAV1-HGF. The body weight was measured once a week until P158. For statistical analysis, one-way ANOVA was performed followed by Tukey's post-hoc test at each time point. Values are represented as mean ± SEM.

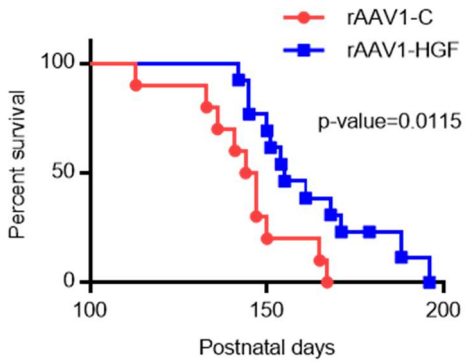

Figure III-26. Survival rate of SOD1-G93A TG mice after IT delivery of rAAV1-C or rAAV1-HGF.

SOD1-G93A TG mice at P60 were intrathecally injected with $5x10^{11}$ GC of rAAV1-C or rAAV1-HGF. Survival curve was drawn based on Mantel-Cox and Gehan-Breslow-Wilcoxon tests for comparing two groups. In the Gehan-Breslow-Wilcoxon test, p value was 0.0115. Median survival days were 145.5 for the rAAV1-C-treated group, and 155 for the rAAV1-HGF-treated group. For graphs, values are represented as mean ± SEM.

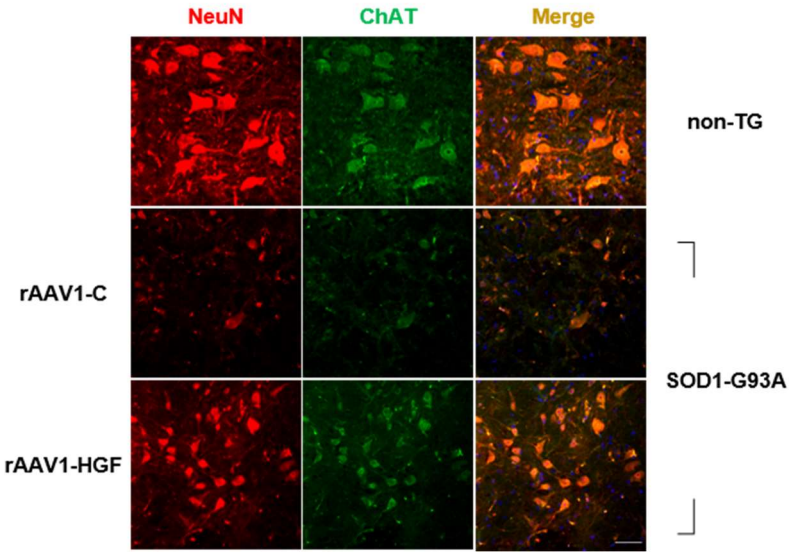

Figure III-27. Representative image of SMNs after IT delivery of rAAV1-C or rAAV1-HGF.

Non-TG or TG mice at P60 were intrathecally injected with rAAV1-C or rAAV1-HGF. The LSCs were collected at P100, followed by IHC assay. Antibodies specific to ChAT and NeuN were used to label SMNs. Scale bar: **a** = 50 μm.

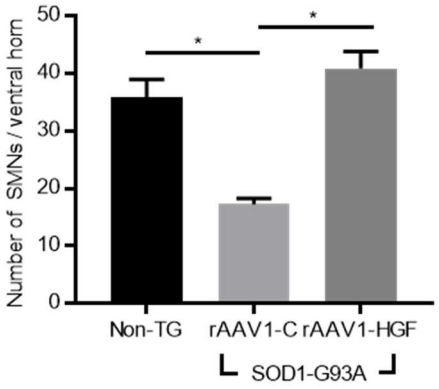

Figure III-28. Number of SMNs per ventral horn after IT delivery of rAAV1-C or rAAV1-HGF.

Non-TG or TG mice at P60 were intrathecally injected with rAAV1-C or rAAV1-HGF. The LSCs were collected at P100, followed by IHC assay. Number of SMNs per ventral horn was counted and represented as a bar graph. For statistical analysis, one-way ANOVA was performed, followed by Tukey's post-hoc test. Values are represented as mean ± SEM. $^{*}p < 0.05$.

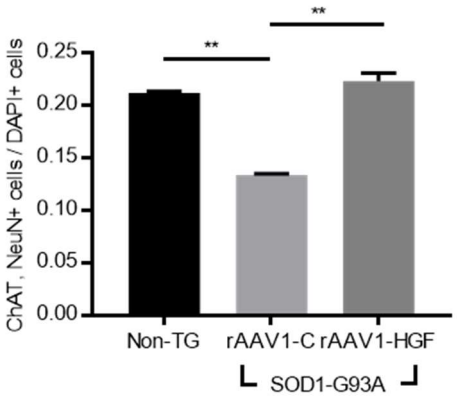

Figure III-29. Proportion of SMNs per DAPI-positive cells after IT delivery of rAAV1-C or rAAV1-HGF.

Non-TG or TG mice at P60 were intrathecally injected with rAAV1-C or rAAV1-HGF. The LSCs were collected at P100, followed by IHC assay. Proportion of SMNs per DAPI-positive cells was counted and represented as a bar graph. For statistical analysis, one-way ANOVA was performed, followed by Tukey's post-hoc test. Values are represented as mean ± SEM. $^{**}p < 0.005$.

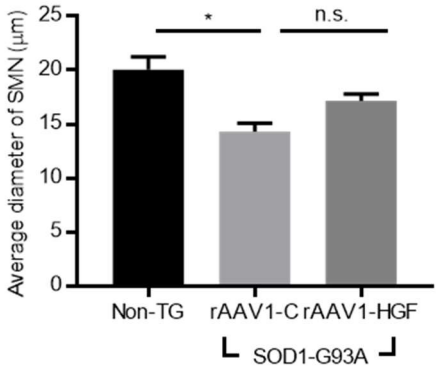

Figure III-30. Diameter of SMNs after IT delivery of rAAV1-C or rAAV1-HGF.

Non-TG or TG mice at P60 were intrathecally injected with rAAV1-C or rAAV1-HGF. The TA was collected at P100, followed by IHC assay. Diameter of SMNs were measured and represented as a bar graph. For statistical analysis, one-way ANOVA was performed, followed by Tukey's post-hoc test. Values are represented as mean ± SEM. $^{*}p < 0.05, n.s. > 0.05$.

It was also examined whether changes in SMNs by the rAAV1-HGF could lead to improvements in connected axon terminals and muscles. Similar to the experiments described above (**Figure III-14, 15, 16, 17, and 18**), the NMJ was observed and the weight of TA was measured. Compared to the non-TG group, in the rAAV1-C group, the proportion of fully innervated NMJs was decreased by 25.48%, the level of abnormal-shaped NMJs was increased 3.5-fold, and the weight of TA was decreased by 35.42%. When rAAV1-HGF was injected, however, the proportion of pretzel-shaped NMJs was increased by 32.58% (**Figure III-31, 32**), and the weight of TA, which was decreased by muscular atrophy in the rAAV1-C group, was increased by 38.42% (**Figure III-33**). No visible change was observed in the degree of NMJ integrity in the rAAV1-HGF group. These results indicated that IT delivery of rAAV1-HGF could promote the protection of peripheral nerves and NMJs as well as SMNs.

Although protein levels of HGF and Met have been shown to increase in SOD1-G93A TG mice, the level of biologically active forms of these proteins has not been well studied in the LSC at the symptomatic stage. It was found that the level of phosphorylated Met was slightly lower in SMNs of the ventral horn of SOD1-G93A TG mice at P100, indicating that the level of endogenously expressed HGF might not be sufficient to fully activate Met. When TG mice were intrathecally injected with rAAV1-HGF, however, the fraction of SMNs expressing phosphorylated Met approximately doubled, suggesting that exogenously added HGF could augment the activation of Met. Therefore, HGF appeared to produce cell-autonomous effects by directly affecting SMNs. HGF is also expected to generate non-autonomous effects by acting on glial cells. For example, it was reported that treatment of

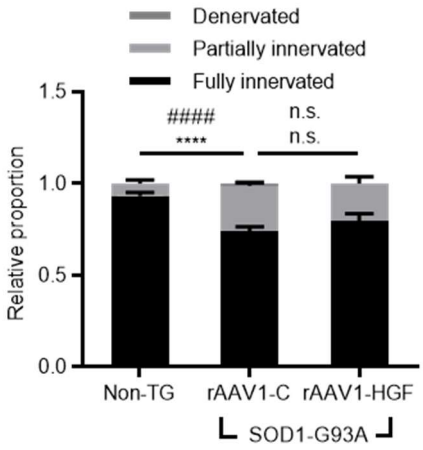

Figure III-31. The integrity of NMJs after IT delivery of rAAV1-C or rAAV1-HGF.

Non-TG or TG mice at P60 were intrathecally injected with rAAV1-C or rAAV1-HGF. The TA was collected at P100, followed by IHC assay. The integrity of NMJs was determined and represented as a bar graph. For statistical analysis, two-way ANOVA was performed, followed by Tukey's post-hoc test. $^{****}p < 0.0001$ for fully innervated NMJ and $^{\#\#\#\#}p < 0.0001$ for partially innervated NMJ. Values are represented as mean ± SEM.

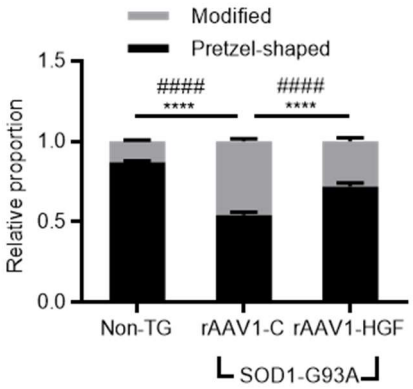

Figure III-32. The shape of NMJs after IT delivery of rAAV1-C or rAAV1-HGF.

Non-TG or TG mice at P60 were intrathecally injected with rAAV1-C or rAAV1-HGF. The TA was collected at P100, followed by IHC assay. The shape of NMJs was determined and represented as a bar graph. For statistical analysis, two-way ANOVA was performed, followed by Tukey's post-hoc test. $^{****}p < 0.0001$ for modified NMJ and $^{\#\#\#\#}p < 0.0001$ for pretzel-shaped NMJ. Values are represented as mean ± SEM.

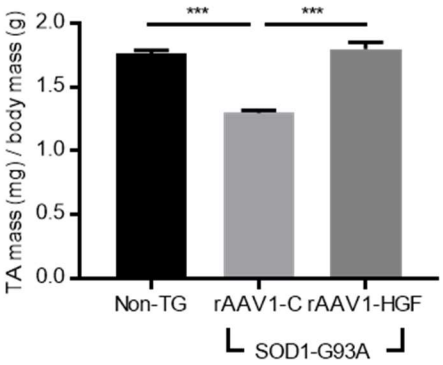

Figure III-33. Relative mass of the TA after IT delivery of rAAV1-C or rAAV1-HGF.

Non-TG or TG mice at P60 were intrathecally injected with rAAV1-C or rAAV1-HGF. The TA was collected at P100, followed by IHC assay. Relative mass of the TA was calculated using total body mass and represented as a bar graph. For statistical analysis, one-way ANOVA was performed, followed by Tukey's post-hoc test. $^{***}p < 0.001$. Values are represented as mean ± SEM.

primary astrocytes with HGF *in vitro* reduced the protein level of EAAT2, a glutamate transporter, and enhance the expression level of total Met in reactive astrocytes in the spinal cord [35, 36]. I also observed that treatment with rHGF could lower the levels of LPS-induced TNFα in the primary astrocyte culture system (data not shown). Together with the cell-autonomous effects described above, HGF has, when properly delivered to patients, the potential to generate powerful therapeutic effects by controlling two of the most important pathways in the pathogenesis of ALS and related motor neuron diseases.

2.5. Effects of HGF in the motor cortical culture

2.5.1. Effects of rHGF on axonal outgrowth of corticospinal motor neurons

The above data showed that IT delivery of rAAV1-HGF could improve motor functions and survival rates of SOD1-G93A TG mice, presumably by slowing down the degeneration of SMNs and restoring the morphology of NMJs. Since the interaction of HGF with lower motor neurons has been relatively well established compared to the interaction of HGF with upper motor neurons [78-80], we were interested in testing the possible involvement of upper motor neurons by using the motor cortical cultures system consisting of CSMNs and glial cells [65, 81].

The motor cortices were isolated from P3 non-TG or TG mice, and $2x10^4$ cells were cultured on a 24-well plate. Three days later, cells were fixed, followed by IHC analysis. CSMNs were labeled with UCHL1 and Ctip2, and Fiji software was used to measure the

axon length of CSMNs [82] **(Figure III-34)**.

Since CSMNs have previously been shown to produce HGF which may give experimental noise, the effects of endogenously expressed HGF were first tested using PHA665752, a chemical inhibitor of Met. When cells were treated with 1 μM of PHA665752 for 3 days, the axon length of CSMNs was reduced 3.42-fold in the non-TG group and 2.33-fold in the TG group **(Figure III-35)**. This result indicated that endogenously expressed HGF could positively affect the axonal outgrowth of CSMNs.

When 100 ng/ml of rHGF were added to the culture for 3 days, however, the axon length of CSMNs was increased by 48.61% in the non-TG group, and by 124.73% in the TG group **(Figure III-36)**. When PHA665752 was co-treated with rHGF, the HGF-mediated increase of CSMNs' axon length was inhibited by 127.7% in the non-TG group, and by 120.82% in the TG group **(Figure III-37)**. This is consistent with the data in **Figure III-43, 44** showing activation or inhibition of phosphorylation of the Met protein by HGF or PHA665752. These results suggested that activation of the HGF-Met signaling pathway might be involved in the promotion of axonal outgrowth of CSMNs.

2.5.2. Effects of inhibition of ERK, PI3K, and p38 on axonal outgrowth of CSMNs

Several signaling pathways have been shown to be turned on upon interaction between HGF and Met receptor. To identify the key pathway involved in the regulation of the HGF-mediated axonal outgrowth of CSMNs, $2x10^4$ cells were treated with specific chemical

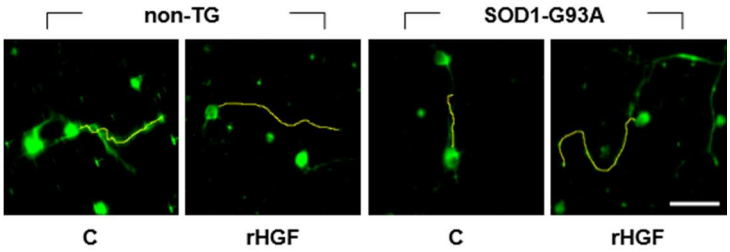

Figure III-34. Representative image of CSMNs derived from non-TG or SOD1-G93A TG mice.

SOD1-G93A TG mice were sacrificed at P3. After dissociating motor cortices, 20,000 cells were seeded on 24-well plates. Three days later, cells were fixed and subjected to immunocytochemistry (ICC) assay. Antibodies specific to UCHL1 (green) and Ctip2 (red, not shown) were used to label CSMNs. Serum-free media was used as a control medium (C). Cells were visualized with confocal laser scanning microscopy. The axon length of CSMNs was measured using Fiji software (yellow line). Scale bar: **a** = 50 μm.

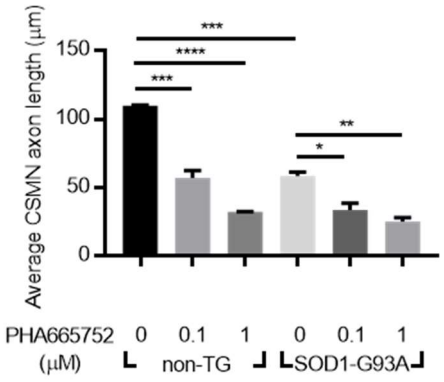

Figure III-35. The axon length of CSMNs after treatment with PHA665752 in the cortical culture.

SOD1-G93A TG mice were sacrificed at P3. After dissociating motor cortices, 20,000 cells were seeded on 24-well plates. Three days later, cells were fixed and subjected to immunocytochemistry (ICC) assay. The axon length of CSMNs was measured after treatment with PHA665752, an inhibitor for Met. Values are represented as mean ± SEM. For statistical analysis, one-way ANOVA was performed, followed by Tukey's post-hoc test. $^{*}p < 0.05$, $^{**}p < 0.01$, $^{***}p < 0.001$, $^{****}p < 0.0001$.

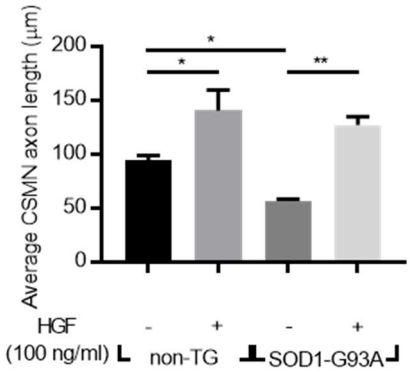

Figure III-36. The axon length of CSMNs after treatment with recombinant HGF protein in the cortical culture.

SOD1-G93A TG mice were sacrificed at P3. After dissociating motor cortices, 20,000 cells were seeded on 24-well plates. Three days later, cells were fixed and subjected to immunocytochemistry (ICC) assay. The axon length of CSMNs was measured after treatment with rHGF. Values are represented as mean ± SEM. For statistical analysis, one-way ANOVA was performed, followed by Tukey's post-hoc test. $^{*}p < 0.05$, $^{**}p < 0.01$.

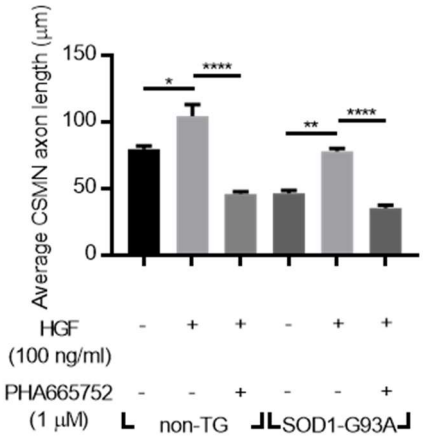

Figure III-37. The axon length of CSMNs after treatment with PHA665752 and rHGF in the cortical culture.

SOD1-G93A TG mice were sacrificed at P3. After dissociating motor cortices, 20,000 cells were seeded on 24-well plates. Three days later, cells were fixed and subjected to immunocytochemistry (ICC) assay. The axon length of CSMNs was measured after treatment with PHA665752 and rHGF. Values are represented as mean ± SEM. For statistical analysis, one-way ANOVA was performed, followed by Tukey's post-hoc test. $^{*}p < 0.05$, $^{**}p < 0.01$, $^{****}p < 0.0001$.

inhibitors for ERK (U0126), PI3K (LY294002), p38 (SB203580), and JNK (SP600125). When cells were treated with 3 different concentrations of respective inhibitors, the axon length of CSMNs was reduced in a dose-dependent manner by all agents except for SP600125 (**Figure III-38, 39, 40, and 41**). In all concentrations of chemical inhibitors used in this experiment, cytotoxic effects were not observed (**Figure III-42**). These results suggested that ERK, PI3K, and p38 might play roles in the HGF-mediated axonal outgrowth of CSMNs.

2.5.3. Effects of rHGF on ERK phosphorylation

It was tested whether HGF could activate ERK, PI3K, and p38 in the cortical culture. $3.2x10^6$ cells were treated with 100 ng/ml of rHGF, and 5 days later, total proteins were extracted, followed by Western blot analysis. As shown in **Figure III-43**, the level of phosphorylated ERK was increased by treatment with rHGF, while the levels of PI3K and p38 were not affected. The effect of rHGF was inhibited when cells were co-treated with 1 μM of PHA665752 or 10 μM of U0126 **(Figure III-44, 45**), suggesting that the HGF-Met pathway is involved in the phosphorylation of ERK in this cortical culture. It was tested whether inhibition of ERK could reduce the HGF-mediated increase of the axon length of CSMNs. As shown in **Figure III-46**, treatment with U0126 decreased the axon length of CSMNs 2.41-fold in the non-TG group and 2.03-fold in the TG group, indicating that HGF could promote axonal outgrowth of CSMNs by specifically up-regulating phosphorylation of ERK.

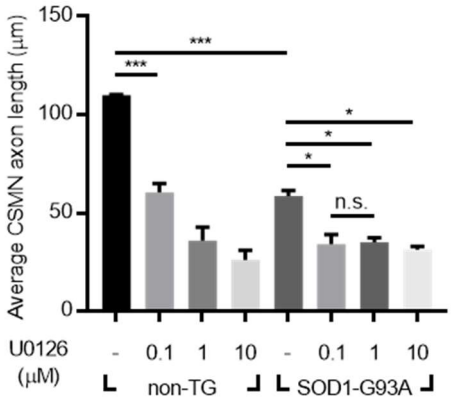

Figure III-38. The axon length of CSMNs after treatment with ERK inhibitor in the cortical culture.

SOD1-G93A TG mice were sacrificed at P3. After dissociating motor cortices, 20,000 cells were seeded on 24-well plates. Three days later, cells were fixed and subjected to immunocytochemistry (ICC) assay. The axon length of CSMNs was measured after treatment with U0126, an inhibitor for ERK. Values are represented as mean ± SEM. For statistical analysis, one-way ANOVA was performed, followed by Tukey's post-hoc test. $^{*}p < 0.05$, $^{***}p < 0.001$.

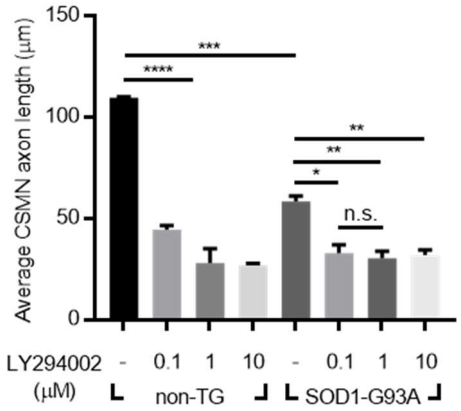

Figure III-39. The axon length of CSMNs after treatment with PI3K inhibitor in the cortical culture.

SOD1-G93A TG mice were sacrificed at P3. After dissociating motor cortices, 20,000 cells were seeded on 24-well plates. Three days later, cells were fixed and subjected to immunocytochemistry (ICC) assay. The axon length of CSMNs was measured after treatment with LY294002, an inhibitor for PI3K. Values are represented as mean ± SEM. For statistical analysis, one-way ANOVA was performed, followed by Tukey's post-hoc test. $^{*}p < 0.05$, $^{**}p < 0.01$, $^{***}p < 0.001$, $^{****}p < 0.0001$.

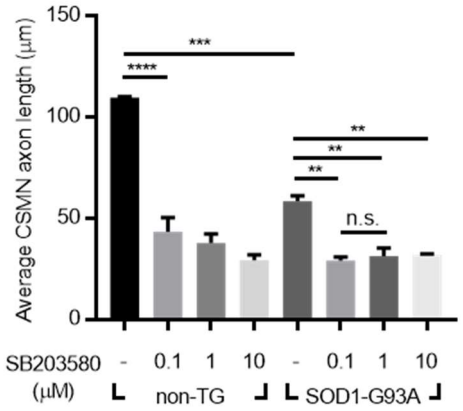

Figure III-40. The axon length of CSMNs after treatment with p38 inhibitor in the cortical culture.

SOD1-G93A TG mice were sacrificed at P3. After dissociating motor cortices, 20,000 cells were seeded on 24-well plates. Three days later, cells were fixed and subjected to immunocytochemistry (ICC) assay. The axon length of CSMNs was measured after treatment with SB203580, an inhibitor for p38. Values are represented as mean ± SEM. For statistical analysis, one-way ANOVA was performed, followed by Tukey's post-hoc test. $^{**}p < 0.01$, $^{***}p < 0.001$, $^{****}p < 0.0001$.

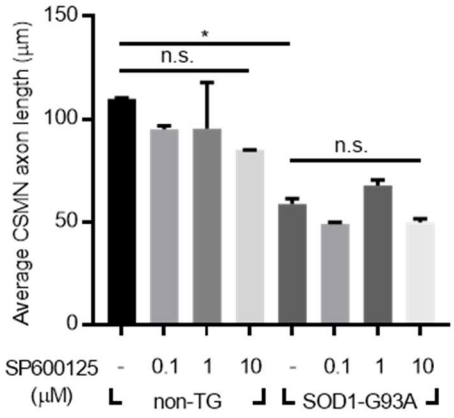

Figure III-41. The axon length of CSMNs after treatment with JNK inhibitor in the cortical culture.

SOD1-G93A TG mice were sacrificed at P3. After dissociating motor cortices, 20,000 cells were seeded on 24-well plates. Three days later, cells were fixed and subjected to immunocytochemistry (ICC) assay. The axon length of CSMNs was measured after treatment with SP600125, an inhibitor for JNK. Values are represented as mean ± SEM. For statistical analysis, one-way ANOVA was performed, followed by Tukey's post-hoc test. $^{*}p < 0.05$, *n.s.* > 0.05.

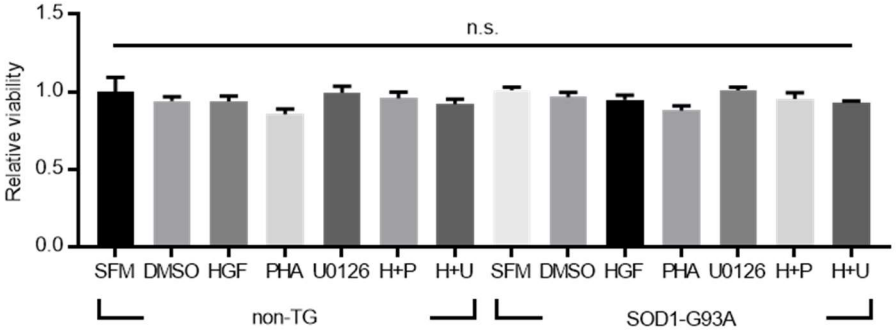

Figure III-42. Effects of rHGF or chemical inhibitors measured by WST1 assay in the motor cortical culture.

After dissociating motor cortices of P3 non-TG or TG mice, $1.6x10^5$ cells were seeded on PDL-coated 48-well cell plates in the presence of rHGF or respective inhibitors. Three days later, WST1 assay was performed. Cell viability was measured using a microplate reader and represented as a bar graph. Values are represented as mean ± SEM. *n.s.* > 0.05.

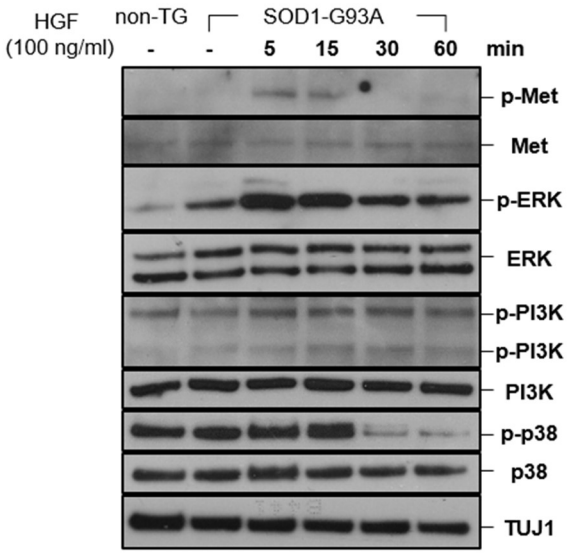

Figure III-43. Western blot analysis after treatment with rHGF in the cortical culture. Motor cortices from non-TG or TG mice at P3 were collected. After dissociation, cells were seeded on six-well plates with $3.2x10^6$ cells/well. Cells were treated with 100 ng/ml of rHGF, and 5 days later, total proteins were isolated, followed by Western blot analysis.

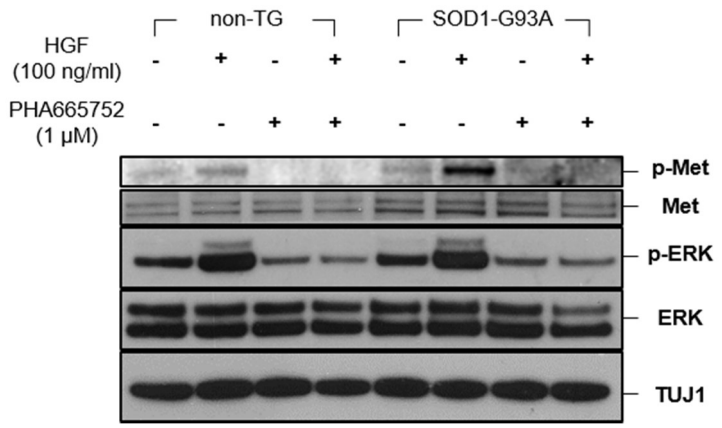

Figure III-44. Western blot analysis after treatment with PHA665752 and rHGF in the cortical culture.

Motor cortices from non-TG or TG mice at P3 were collected. After dissociation, cells were seeded on six-well plates with $3.2x10^6$ cells/well. Cells were treated with 100 ng/ml of rHGF and 1 μM of PHA665752, and 5 days later, total proteins were isolated, followed by Western blot analysis.

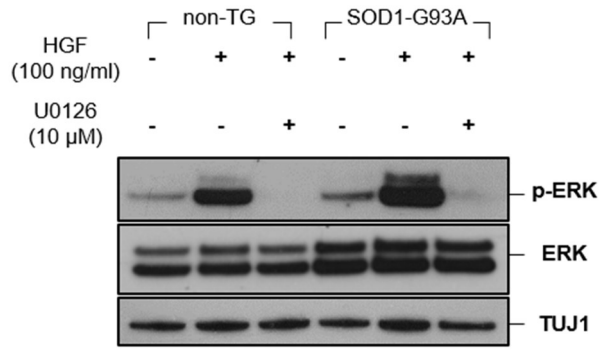

Figure III-45. Western blot analysis after treatment with U0126 and rHGF in the cortical culture.

Motor cortices from non-TG or TG mice at P3 were collected. After dissociation, cells were seeded on six-well plates with $3.2x10^6$ cells/well. Cells were treated with 100 ng/ml of rHGF and 10 μM of U0126, and 5 days later, total proteins were isolated, followed by Western blot analysis.

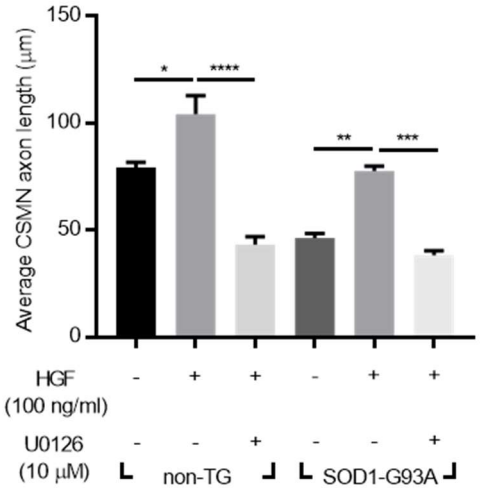

Figure III-46. The axon length of CSMNs after treatment with U0126 and rHGF in the cortical culture.

Motor cortices from non-TG or TG mice at P3 were collected. After dissociation, cells were seeded on six-well plates with $3.2x10^6$ cells/well. Cells were treated with 100 ng/ml of rHGF and 10 μM of PHA665752, and 5 days later, total proteins were isolated, followed by Western blot analysis. The axon length of CSMNs was measured and represented as a bar graph after co-treatment with rHGF and U0126. Values are represented as mean ± SEM. For statistical analysis, one-way ANOVA was performed, followed by Tukey's post-hoc test. $^{*}p < 0.05$, $^{**}p < 0.01$, $^{***}p < 0.001$, $^{****}p < 0.0001$.

To test whether the above *in vitro* results were reproducible *in vivo*, $5x10^9$ GC of viral vectors were intrathecally injected into SOD1-G93A TG mice at P60, and the LSC was analyzed for ERK. Compared with non-TG mice, the level of phosphorylated ERK was increased 2.04-fold in TG mice injected with a control vector, and was further enhanced 5.54-fold when injected with AAV vectors expressing HGF **(Figure III-47, 48)**. There was no difference in phosphorylation of other signaling molecules of the HGF-Met pathway, such as STAT3, cJUN, and GSK3β **(Figure III-49)**. These results indicated that ERK might indeed be an important factor of the HGF-mediated regeneration of motor neurons.

2.5.4. Effects of HGF-mediated ERK phosphorylation on levels of ROS

To get an overall picture of the effects of HGF on gene expression profile in CSMNs, cortical cells were treated with 100 ng/ml of rHGF, and total RNAs were extracted followed by microarray assay (**Figure III-50**). Among the 116 genes whose expression levels were changed more than 1.5-fold, 52 belonged to six major categories defined for fALS by Taylor et al., and 37 (71.15%) were involved in the control of protein quality and RNA metabolism [3]. Therefore, it was tested whether the HGF-Met-ERK signaling pathway could reduce hSOD1 protein aggregation and/or oxidative stress. Cortical cells were treated with rHGF, followed by IHC to examine the distribution of mutant hSOD1. When compared to the non-TG group containing no hSOD1 aggregates, the proportion of CSMNs in the TG group with hSOD1 aggregates was sharply increased to 0.4 ± 0.01 as shown in **Figure III-51, 52**. When treated with rHGF, however, this proportion was reduced to 0.06 ± 0.02, while it was

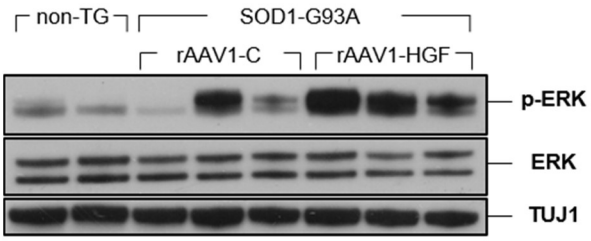

Figure III-47. Western blot analysis after IT delivery of rAAV1-C or rAAV1-HGF.

Non-TG or TG mice at P60 were intrathecally injected with rAAV1-C or rAAV1-HGF. The LSCs were collected, and total proteins were extracted at P100, followed by Western blot analysis.

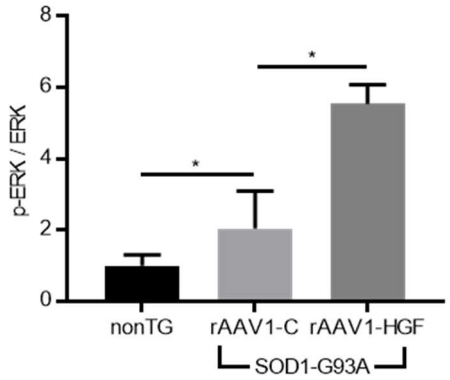

Figure III-48. Relative levels of phosphorylated ERK after IT delivery of rAAV1-C or rAAV1-HGF.

Non-TG or TG mice at P60 were intrathecally injected with rAAV1-C or rAAV1-HGF. The LSCs were collected, and total proteins were extracted at P100, followed by Western blot analysis. Relative levels of phosphorylated ERK were measured using Fiji software and represented as a bar graph. Values are represented as mean ± SEM. For statistical analysis, one-way ANOVA was performed, followed by Tukey's post-hoc test. $^{*}p < 0.05$.

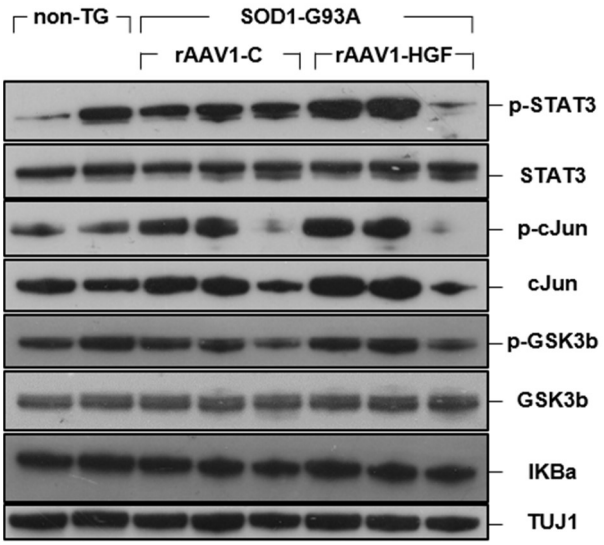

Figure III-49. Western blot analysis in the LSC after IT delivery of rAAV1-C or rAAV1-HGF.

Non-TG or TG mice at P60 were intrathecally injected with $5x10^9$ GC of rAAV1-C or rAAV1-HGF. The LSCs were collected at P100. Total proteins were extracted and subjected to Western blot analysis.

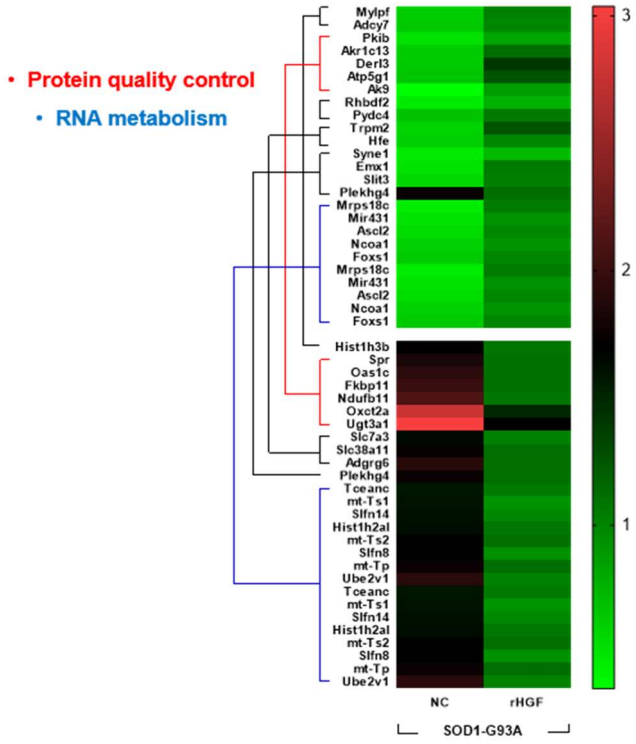

Figure III-50. Microarray analysis of motor cortical cells treated with rHGF.

Motor cortical cells were treated with 100 ng/ml of rHGF for 3 days, followed by microarray analysis using Affymetrix Genechip. SFM was used as a negative control (NC). After data extraction, RMA normalization was performed followed by DEG analysis. Differential expression was represented by color gradients. Genes were clustered based on 6 major categories defined by Taylor et al., as described in Results. Genes involved in protein quality control are labeled in red, while those related to RNA metabolism are labeled in blue. The rest of genes are labeled in black. The NC group is for non-TG NC vs. TG NC, whereas the rHGF group is for TG NC vs. TG rHGF.

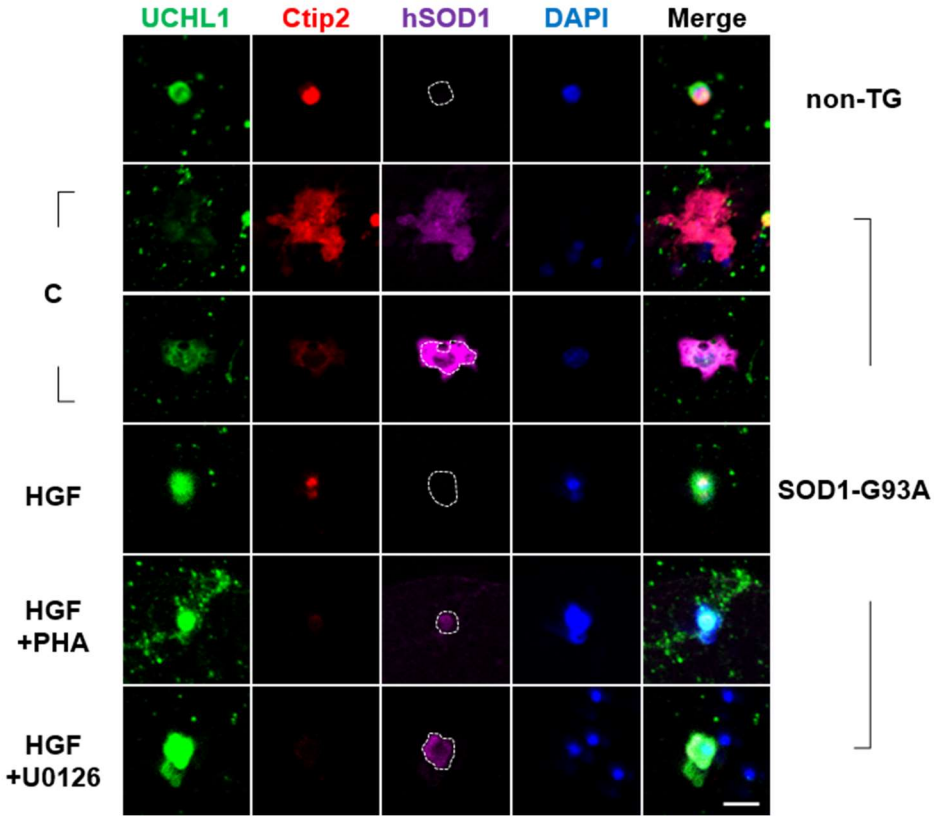

Figure III-51. Representative image of CSMNs after treatment with rHGF, PHA665752, and U0126 in the motor cortical culture.

SOD1-G93A TG mice were sacrificed at P3. After dissociating motor cortices, 20,000 cells were seeded on 24-well plates. Three days later, cells were fixed and subjected to immunocytochemistry (ICC) assay. Antibodies specific to UCHL1 and Ctip2 were used to label CSMNs, together with those for hSOD1 (magenta). C: Treated with SFM. In the hSOD1-stained panels, the cell boundaries of the CSMNs were outlined based on the UCHL1 signals, except for the panel in the second row, where the cell boundaries are ambiguous. Scale bar: **a** = 20 μm**.**

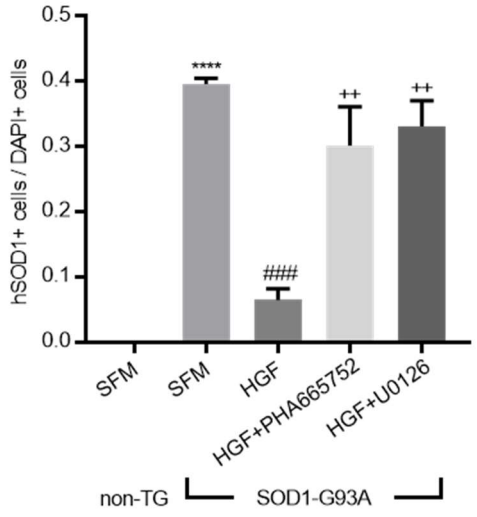

Figure III-52. Proportion of hSOD1-positive cells per DAPI-positive cells in the motor cortical culture.

SOD1-G93A TG mice were sacrificed at P3. After dissociating motor cortices, 20,000 cells were seeded on 24-well plates. Three days later, cells were fixed and subjected to immunocytochemistry (ICC) assay. Proportion of hSOD1-positive cells per DAPI-positive cells was counted and represented as a bar graph. For statistical analysis, one-way ANOVA was performed, followed by Tukey's post hoc test. $^{****}p < 0.0001$ for non-TG SFM vs. TG SFM, $^{###}p < 0.001$ for TG SFM vs. TG HGF, $^{++}p < 0.01$ for TG HGF vs. TG HGF + PHA665752 (or TG HGF + U0126).

increased to 0.3 ± 0.06 and 0.33 ± 0.04 by the addition of inhibitors for Met (PHA665752) or ERK (U0126), respectively (**Figure III-53**).

Since the aggregated form of mutant hSOD1 could increase oxidative stress, it was also tested whether the rHGF-mediated reduction of protein aggregation could alleviate oxidative stress by measuring hydrogen peroxide, peroxynitrite, hydroxyl radicals, nitric oxide, and peroxy radical in the cortical culture. Compared to the control group treated with SFM, treatment with rHGF decreased the level of oxidative stress by 34.22%, which was comparable to the effect (32.11%) of N-acetyl-L-cysteine (NAC), a well-known scavenger of oxygen free radical (**Figure III-53**). Such HGF-mediated decrease of oxidative stress was inhibited by 15.51% and 18.81% when rHGF was co-treated with PHA665752 and U0126, respectively (**Figure III-53**).

To test whether the axonal outgrowth of CSMNs could be promoted by alleviation of oxidative stress, the effect of rHGF was tested in the presence of pyocyanin, a ROS inducer. As shown in **Figure III-54**, the axon length of CSMNs was increased by 40.12% when treated with NAC. The effect of rHGF was almost 3-fold greater at 118.83%, which was inhibited by 32.1% in the presence of pyocyanin. Taken together, these results indicated that HGF-mediated induction of ERK phosphorylation plays an important role(s) in promoting the axonal outgrowth of CSMNs by mitigating protein aggregation and oxidative stress.

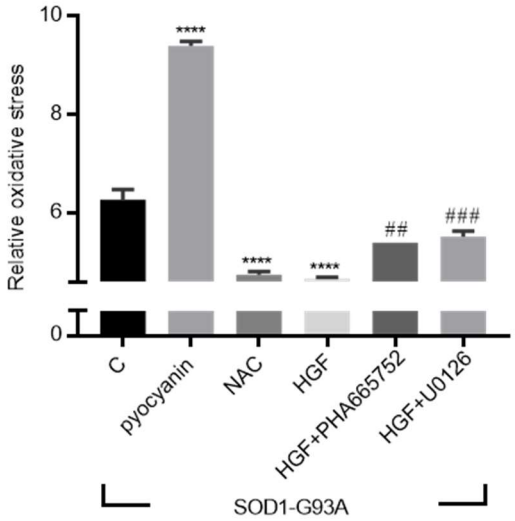

Figure III-53. Cellular ROS levels measured by a ROS detection kit in the motor cortical culture.

$6.4x10^4$ cells were seeded on 96-well plates. Cellular ROS levels were measured using a ROS detection kit and represented as a bar graph. Pyocyanin was used as an inducer of ROS, whereas NAC was employed as a scavenger of ROS. For statistical analysis, one-way ANOVA was performed, followed by Tukey's post-hoc test. $^{****}p < 0.0001$ for SFM vs. pyocyanin (or NAC or HGF), $^{\#\#}p < 0.01$ for HGF vs. HGF + PHA665752, $^{\#\#\#}p < 0.001$ for HGF vs. HGF + U0126.

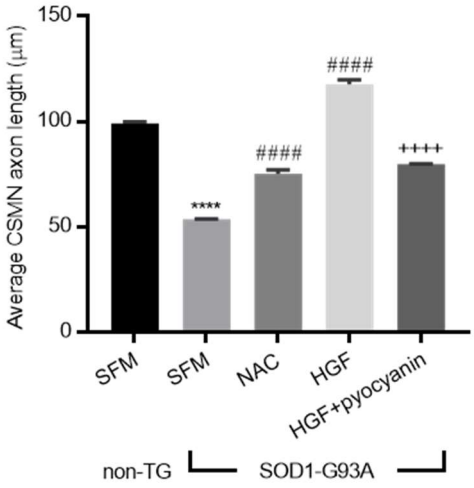

Figure III-54. The axon length of CSMNs after treatment with NAC, rHGF, and pyocyanin in the motor cortical culture.

SOD1-G93A TG mice were sacrificed at P3. After dissociating motor cortices, 20,000 cells were seeded on 24-well plates. Three days later, cells were fixed and subjected to immunocytochemistry (ICC) assay. The axon length of CSMNs was measured and represented as a bar graph. Values are represented as mean ± SEM. For statistical analysis, one-way ANOVA was performed, followed by Tukey's post-hoc test. $^{****}p < 0.0001$ for non-TG SFM vs. TG SFM, $^{\#\#\#\#}p < 0.0001$ for TG SFM vs. TG NAC (or TG HGF), $^{++++}p < 0.0001$ for TG HGF vs. TG HGF + pyocyanin.

3. Discussion

I investigated the effect of HGF-expressing rAAV in two mouse models—the sciatic nerve crush model and the SOD1-G93A TG model. Because different AAV serotypes may have different cell tropisms, I identified which of the AAV serotypes was most suitable for IT delivery. Based on the expression levels of HGF proteins in the lumbar spinal cord, AAV serotype 1 was chosen for IT delivery. When rAAV1-HGF was intrathecally injected into the lumbar spinal cord, the highest amounts of HGF proteins were detected 2 weeks after injection, and gradually declined until week 16. It is also interesting to note that IT delivery of rAAV1-HGF produced HGF proteins in the TA. As the majority of neurodegenerative diseases undergo concomitant atrophy of the skeletal muscles, rAAV1-HGF may potentially target both the skeletal muscle and spinal cord, which are important in the pathophysiology of a number of neurodegenerative diseases, including ALS. After selecting appropriate serotypes for IT injection methods and studying the expression kinetics *in vivo*, a recombinant AAV vector was introduced into the lumbar spinal cord, and tested for its effects.

A single administration of rAAV1-HGF into the lumbar spinal cord improved motor functions and NMJ structure in both mouse models. Of particular interest was the finding that IT injection of rAAV1-HGF could not only facilitate protection, but also delay the degeneration of motor neurons. In the nerve crush model, for example, the regenerative process takes place after Wallerian degeneration following nerve injury, and rAAV1-HGF was shown to promote the regeneration of the sciatic nerves and the recovery of the NMJ structure. In the SOD1-G93A TG mouse model, there is progressive degeneration of motor neurons and

muscle, and rAAV1-HGF could delay disease progression and the degeneration of SMNs. Therefore, rAAV1-HGF appears to perform dual activities in the pathogenesis of motor neuron degeneration that may result in additive effects.

For IT delivery, improvements in motor functions, NMJ morphology, and the protection of SMNs could have resulted from 3 sources: changes in SMNs, in upper motor neurons, or in a combination of both neurons. HGF is a known potent neurotrophic factor that can facilitate the proliferation, migration, differentiation, and survival of sensory neurons and motor neurons [83-86]. The interaction of HGF with lower motor neurons has been relatively well-characterized. For example, it has been reported that HGF could function as a survival factor for SMNs *in vitro* [78-80]. In addition, HGF has also been shown to induce remyelination of Schwann cells to promote the axonal outgrowth of peripheral neurons [57]. These findings suggested that HGF could directly and/or indirectly protect damaged lower motor neurons.

The molecular mechanisms of HGF's interaction with upper motor neurons have been poorly understood until now. In this study, therefore, I investigated the effects of HGF on upper motor neurons *in vitro*, using the primary motor cortical culture system consisting of CSMNs and glial cells. It was observed that HGF could facilitate the axonal outgrowth of CSMNs by controlling the phosphorylation of ERK (**Figure III-55**). When phenotypes of oxidative stress were analyzed based on microarray data, treatment of CSMNs with HGF proteins reduced the accumulation of mutant SOD1 proteins and levels of oxidative stress factors such as H_2O_2, $ONOO^-$, HO, NO, and ROO. All these effects were inhibited, however, when ERK phosphorylation was suppressed by U0126. These results suggested that upper

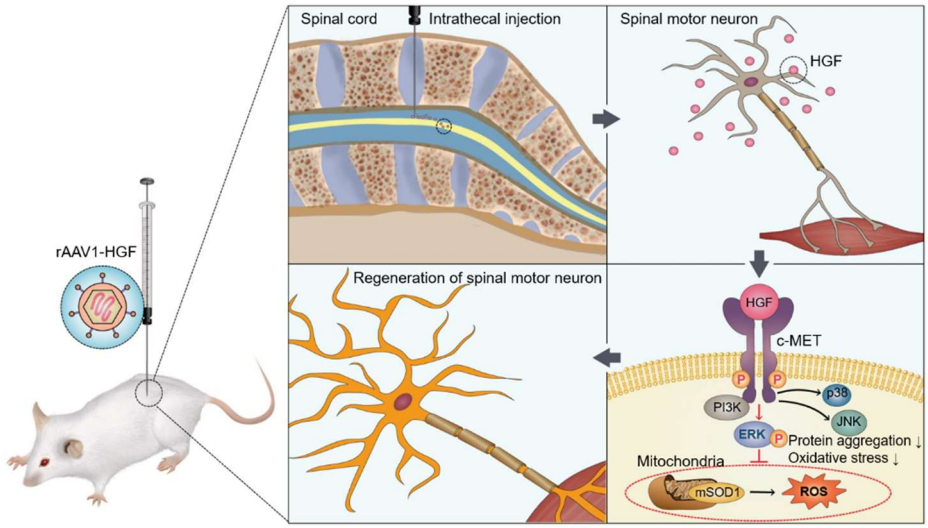

Figure. III-55. Summary of neuroprotective effects mediated by HGF.

When intrathecally injected into the subarachnoid space, rAAV1-HGF increases the phosphorylation of the Met receptor, subsequently inducing phosphorylation of ERK. As a consequence, the degree of protein aggregation and oxidative stress is lowered, eventually improving the conditions of SMNs.

motor neurons could also have played a role in the effects exerted by rAAV1-HGF, and that ERK might be a key signaling factor involved.

Chapter IV

Effects of intramuscularly delivered rAAV-HGF in the nerve crush and SOD1-G93A transgenic mouse models

1. Background

HGF is a multifunctional protein that can suppress liver cirrhosis, promote angiogenesis, and regulate the proliferation and differentiation of muscle satellite cells [18, 21, 87]. In addition, HGF is a neurotrophic factor that it can promote neurogenesis and neural induction, attenuate neuronal degeneration, and stimulate axon regrowth [83, 88-92]. When HGF binds to its receptor, Met, its intracellular domains involving Tyr1234/1235 of a catalytic region and Tyr1349/1356 of a multifunctional docking site are phosphorylated, activating multiple signaling pathways such as those of STAT3, ERK-JNK-p38, and PI3K-Akt, depending on cell types [23, 25, 29, 30].

Based on such physiological bioactivities, HGF has been tested for its therapeutic effects on a variety of diseases. The first diseases tested were ischemic diseases like critical limb ischemia (CLI) and coronary artery disease (CAD). These were followed by neurological diseases like diabetic peripheral neuropathy (DPN) and ALS [47-51, 93]. In all studies, a plasmid DNA containing the HGF sequence generated highly encouraging results without any significant adverse effects, consistent with data from various animal experiments. For example, there were signs of improvement in blood flow, neuropathic pain, and nerve regeneration in the respective disease models [45, 46, 53, 57, 58].

Among the many potential target indications of HGF, I investigated whether HGF could be used for several neuromuscular disorders as a neurotrophic factor capable of inducing the development, proliferation, and differentiation of neuronal cells [83, 86, 88-91]. The Met receptor is present in many cell types involved in this class of pathology: skeletal and

smooth muscle cells, neuronal cells, endothelial cells, and Schwan cells, among others [67]. In each cell type, the effects of HGF and relevant signaling pathways have been characterized. For example, the binding of HGF to the Met receptor activates the PI3K-Akt signaling pathway, promoting the migration of smooth muscle cells and maintaining the survival of motor neurons [94, 95]. In Schwann cells, HGF has also been shown to activate the ERK signaling pathway to promote the remyelination of injured nerves [57]. Additionally, by inhibiting the apoptotic death of neurons, HGF has been shown to prevent neuronal degeneration and promote axon regrowth [92]. Several studies have also shown that HGF can act as an axonal chemoattractant *in vitro*, promoting the survival of SMNs [78-80].

In addition to the effects exerted by IT delivery of rAAV1-HGF in two mouse models, it was also tested whether IM delivery of rAAV-HGF could generate therapeutic effects in the same models. The sciatic nerve crush model has been widely used when studying a variety of neurodegenerative diseases, since injured nerves undergo Wallerian degeneration followed by consecutive regenerative processes. Moreover, it has been well established that injury signals are transmitted from axons to the soma, resulting in the activation of regeneration-associated genes [96]. In the case of ALS, for example, the miRNA-206-HDAC4 cascade is important in the regeneration of the synapses of neuromuscular junctions, both in the sciatic nerve crush and SOD1-G93A TG mouse models [74].

About 20% of patients with fALS are known to develop mutations in SOD1, an enzyme that promotes the degradation of superoxide. This study used the SOD1-G93A TG mouse model, the most commonly used mouse model for ALS [55]. This model was

generated by overexpressing a mutant form of the SOD1 gene, in which the 93rd glycine (G) of the human SOD1 gene was changed to alanine (A). Excessive oxidative stress accumulates within the cell as a result, selectively killing motor neurons in the CNS. It has been reported that SOD1-G93A TG mice show phenotypes similar to ALS patients. For example, the blood-spinal cord barrier is damaged and the number of pericytes is reduced [97]. In an effort to treat ALS, the effects of a number of growth factors including BDNF, GDNF, IGF-1, VEGF, and G-CSF have been tested in the SOD1-G93A TG mouse model [98-102]. In the same context, the effects of IM delivery of rAAV-HGF were tested in these two mouse models for neuromuscular diseases—the sciatic nerve crush and SOD1-G93A TG mouse models.

2. Results

2.1. Determining the optimal AAV serotype for intramuscular injection

The goal of this study was to investigate the effect of relatively long-term stable gene expression of HGF in neuromuscular disease models. I first sought to identify a suitable AAV serotype for IM gene delivery. I compared the expression levels of hHGF proteins from 4 different serotypes, rAAV-1, -2, -5, and -6, after injecting $3.12x10^8$ GC of rAAV-HGF into the TA. The TA was collected 2 weeks later, followed by ELISA specific for hHGF. It was observed that rAAV6-HGF produced the highest amount of hHGF (252.91 ± 70.06 ng/mg) (**Figure IV-1**). Much lower levels of hHGF were detected in other serotypes, 63.29 ± 34.16 ng/mg for rAAV1-HGF, 0.95 ± 0.09 ng/mg for rAAV2-HGF, and 193.12 ± 40.34 ng/mg for rAAV5-HGF. The spinal cord is the hub where injury signals converge followed by

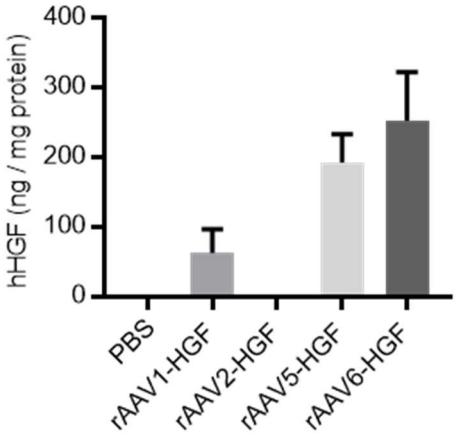

Figure IV-1. ELISA for hHGF after IM injection of rAAV-HGF.

$3.12x10^8$ GC of rAAV1, 2, 5, or 6-HGF were intramuscularly injected into C57BL/6 mice at postnatal day 60 (P60). The TA was collected and total proteins were isolated 2 weeks after injection, followed by ELISA specific for human HGF (hHGF).

subsequent transcriptional regulations [96, 103]. So it was checked which of the 4 different serotypes of rAAV could be retrogradely transported to the spinal cord when injected into the TA. Since it was difficult to detect hHGF with immunofluorescent assay, $4.12x10^8$ GC of each serotype of rAAV-GFP were injected into the TA, and 7 days later, the lumbar spinal cord was collected and subjected to IHC assay. As shown in **Figure IV-2**, mice injected with rAAV serotype 2 and 6 showed distinct GFP signals in the longitudinal section of the lumbar spinal cord, whereas other serotypes did not produce any positive signals. Combined with the data from IHC assay, rAAV serotype 6 not only moved to the spinal cord, but also produced the largest amount of hHGF proteins when intramuscularly introduced. rAAV6-HGF was therefore chosen for further experiments.

2.2. Kinetics of HGF expression from rAAV6-HGF

To examine time kinetics of HGF expression from rAAV6-HGF, $3.12x10^8$ GC of rAAV6-HGF were injected into the TA, and the TA was collected 1, 2, 4, 8, and 16 weeks later followed by ELISA specific for hHGF. The expression level of hHGF was 31.73 ± 8.5 ng/mg at week 1, thereafter gradually increasing to 45.65 ± 19.14 ng/mg at week 2, 97.18 ± 33.32 ng/mg at week 4, 143.84 ± 53.07 at week 8, and 184.3 ± 72.61 ng/mg at week 16 (**Figure IV-3**). Despite high levels and long-term expression of HGF in the muscle, hHGF proteins were not detectable in the serum (**Figure IV-4**).

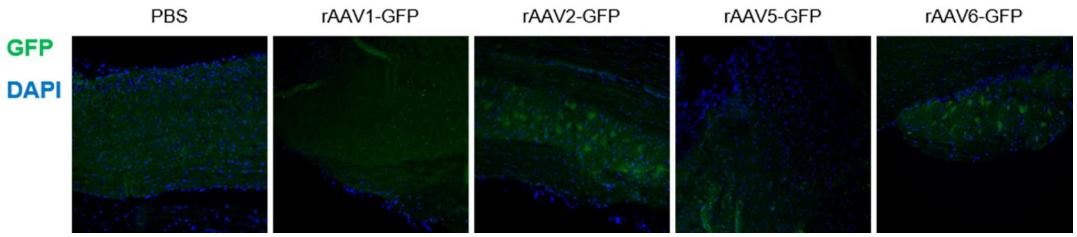

Figure IV-2. 2nd GFP expression in the lumbar spinal cord from different AAV serotypes.

At P60, $4.12x10^8$ GC of rAAV-GFP were injected into the TA of C57BL/6 mice. Seven days later, the lumbar spinal cord was collected followed by IHC using an antibody specific to GFP (green). Scale bar: 200 μm in (A).

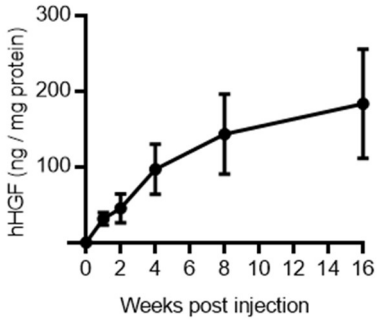

Figure IV-3. Kinetics of HGF expression from rAAV6-HGF.

$3.12x10^8$ GC of rAAV6-HGF were intramuscularly injected into 2-month-old C57BL/6 mice. The TA was collected 1, 2, 4, 8, and 16 weeks after IM injection and subjected to ELISA for hHGF. Values are represented as mean ± SEM.

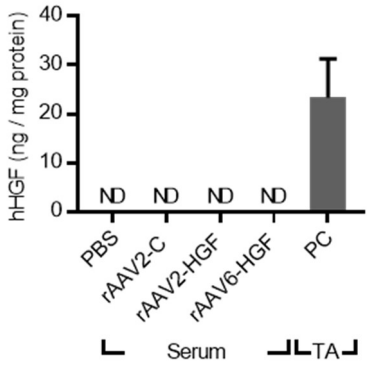

Figure IV-4. Levels of hHGF in the TA and serum.

$3.12x10^8$ GC of rAAV6-HGF were injected into the TA of C57BL/6 mice. Two weeks later, the TA and serum were collected followed by ELISA. Protein extracts from the TA of rAAV6-HGF-injected mice were used as a positive control, while rAAV-C lacking the HGF sequence was used as a negative control. ND: not detectable. Values are represented as mean ± SEM.

2.3. Effects of rAAV6-HGF in the sciatic nerve crush and SOD1-G93A transgenic mouse models

2.3.1. Effects of IM delivery of rAAV6-HGF in the sciatic nerve crush model

Effects of intramuscularly delivered rAAV6-HGF were first examined in the sciatic nerve crush mouse model. When peripheral nerves are injured, the skeletal muscles start to waste away, and atrophied muscles exhibit a decreased CSA [104-106]. Therefore, 2 weeks after the nerve injury, the CSA of the TA was measured using Fiji software following H&E staining (**Figure IV-5**). Compared with the sham group to which the injury was not induced, mean CSA was decreased by 57.12% from 2550.24 ± 99.67 μm^2 to 1093.63 ± 33.18 μm^2 when injected with rAAV-C, a control vector lacking the HGF sequence (**Figure IV-6**). The proportion of muscle fibers having low CSA was increased, while that of muscle fibers having high CSA was decreased (**Figure IV-5, 6**). When injected with rAAV6-HGF, however, the proportion of muscle fibers with CSA ranging from 500 μm^2 to 1500 μm^2 was decreased, while that of larger fibers (from 1500 μm^2 to 3000μm^2) was increased. Moreover, rAAV6-HGF increased mean CSA by 59.13%, compared to the control group (**Figure IV-7**). These results suggested that intramuscularly delivered rAAV-HGF could facilitate restoration of muscle histology.

It was also tested whether rAAV-HGF could promote regeneration of sensory and motor neurons following sciatic nerve injury, first by performing von Frey filament test. Two weeks after the nerve injury, the frequency of paw withdrawal in response to von Frey filaments was increased 7.67-fold from 5 ± 2.89% to 38.33 ± 4.01% in the control group

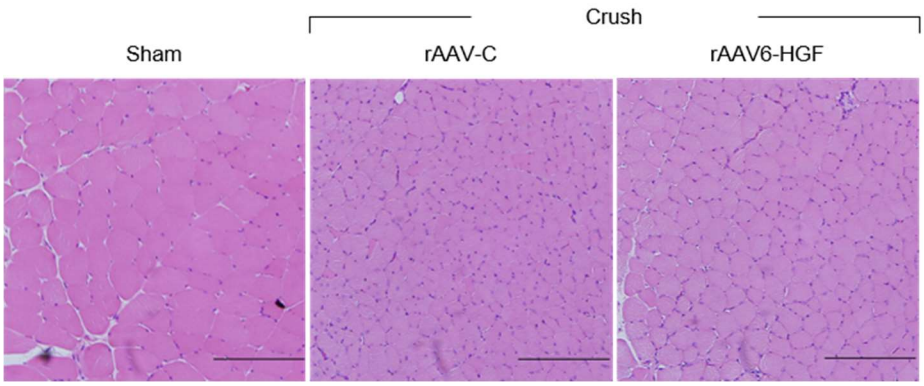

Figure IV-5. Representative image of the TA analyzed by H&E staining.

Nerve crush was introduced to C57BL/6 mice at P60, and $3.12x10^8$ GC of rAAV6-HGF were injected into the TA immediately after injury. The TA was collected 14 days after injection. Nerve injury was not induced in the sham group. Scale bar: 200 μm in (A).

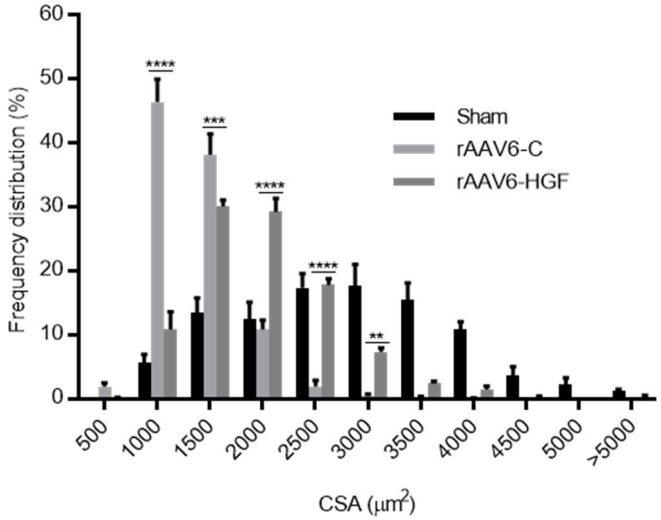

Figure IV-6. Distribution of different CSAs of the TA.

Nerve crush was introduced to C57BL/6 mice at P60, and 3.12×10^8 GC of rAAV6-HGF were injected into the TA immediately after injury. The TA was collected 14 days after injection. Nerve injury was not induced in the sham group. The size of muscle fibers on 500 μm^2 interval was determined, and then the percentage distribution was calculated. At least 300 individual muscle fibers were assessed for each mouse. For statistical analysis, two-way ANOVA was performed, followed by Tukey's post-hoc test. $^{**}p < 0.005$, $^{***}p < 0.001$, and $^{****}p < 0.0001$.

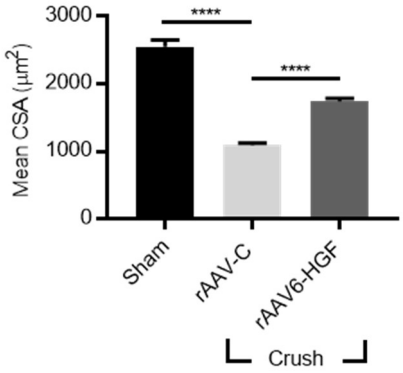

Figure IV-7. Mean CSA of the TA.

Nerve crush was introduced to C57BL/6 mice at P60, and $3.12x10^8$ GC of rAAV6-HGF were injected into the TA immediately after injury. The TA was collected 14 days after injection. Nerve injury was not induced in the sham group. The mean CSA was calculated. For statistical analysis, one-way ANOVA was performed, followed by Tukey's post-hoc test. $^{****}p < 0.0001$.

(**Figure IV-8**). When injected with rAAV6-HGF, however, it was decreased by 47.83% to 20 ± 5.16%, indicating that the degree of mechanical allodynia was lowered by IM injection of rAAV6-HGF.

Effects of rAAV6-HGF on regeneration of peripheral nerves were then evaluated using the neve pinch test. Seven days after the nerve injury, the length of regenerated axons was 1.38 ± 0.39 mm in the control group, while it was increased 2.3-fold to 3.17 ± 0.31 mm in the rAAV6-HGF group (**Figure IV-9**).

To test the motor functions, the rotarod test was performed for 14 days following the nerve injury. When the nerve injury was introduced, mean latency to fall off the rotating rod at day 3 was decreased 7.01- to 8.46-fold, when compared with the sham group (**Figure IV-10**). When rAAV6-HGF was intramuscularly injected, however, rotarod performance at day 14 was significantly increased 2.43-fold when compared to the control group. These results suggested that rAAV6-HGF could not only promote axonal regeneration, but also facilitate functional recovery of sensory and motor neurons.

2.3.2. Effects of IM delivery of rAAV6-HGF in the SOD1-G93A transgenic mouse model

Since rAAV6-HGF has been shown to effectively protect the motor neurons and the muscles in the nerve crush model, the effect of intramuscularly injected rAAV6-HGF was also tested in the SOD1-G93A TG mouse model, one of the most frequently used mouse models for ALS. To test if IM injection of rAAV6-HGF indeed produced reasonable amounts of

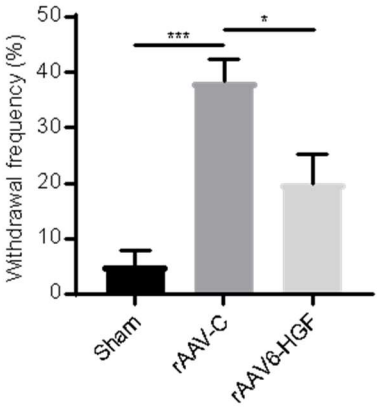

Figure IV-8. Withdrawal frequency of hind paw as measured by von Frey filament test after IM injection of rAAV6-HGF.

At P60, nerve crush was introduced to C57BL/6 mice, and 3.12×10^8 GC of rAAV6-HGF were injected into the TA immediately after injury. A von Frey filament test was performed using von Frey filaments 14 days after injection. For statistical analysis, one-way ANOVA was performed, followed by Tukey's post-hoc test. $^{*}p < 0.05$. $^{***}p < 0.001$.

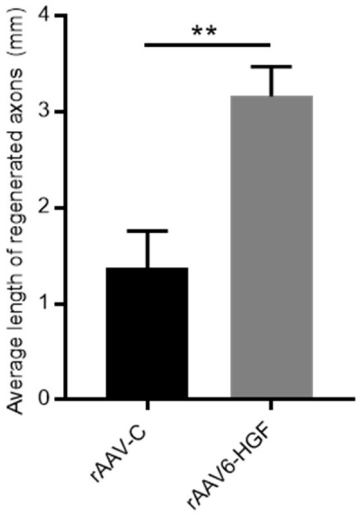

Figure IV-9. Response frequency in the nerve pinch test after IM injection of rAAV6-HGF.

At P60, nerve crush was introduced to C57BL/6 mice, and 3.12×10^8 GC of rAAV6-HGF were injected into the TA immediately after injury. The nerve pinch test was performed 14 days after injection. For statistical analysis, Student's t-test was performed. $^{**}p < 0.01$.

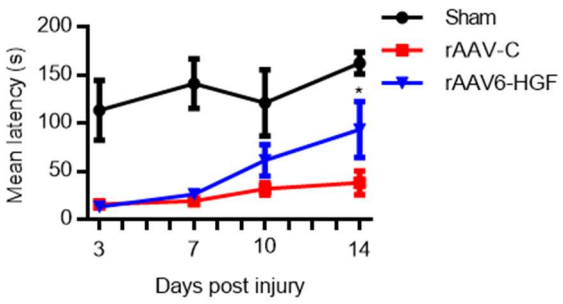

Figure IV-10. Mean latency to fall off the rotarod after IM injection of rAAV6-HGF.

At P60, nerve crush was introduced to C57BL/6 mice, and 3.12×10^8 GC of rAAV6-HGF were injected into the TA immediately after injury. The rotarod test was performed 3, 7, 10, and 14 days after injection. For statistical analysis, two-way ANOVA was performed, followed by Tukey's post-hoc test. $^{*}p < 0.05$ for rAAV-C vs. rAAV6-HGF.

hHGF proteins in this model, $3.12x10^8$ GC of rAAV6-HGF were injected into the TA of SOD1-G93A TG mice at postnatal day 90 (P90). At P120, 27.37 ± 11.17 ng/mg of hHGF were detectable in the TA of rAAV6-HGF-treated mice (**Figure IV-11**). This level is comparable to that obtained in wild type mice injected with rAAV6-HGF.

To test the effects of rAAV6-HGF, $3.12x10^8$ GC of rAAV6-HGF were injected into each of the 6 muscles including the TA, gastrocnemius (GC), and vastus lateralis (VL) of both legs, at P90. I then measured the body weight, limb strengths, neurological score, and survival rate for 67 days until P157, and the mass of the TA and GC at P120. IM injection of rAAV6-HGF did not have significant effects on the body weight and the limb strengths (**Figure IV-12, 13, and 14**). However, the mass of the TA and GC was significantly increased by 22.68% and 26.8%, respectively (**Figure IV-15, 16**). The increase in the neurological score was delayed in the rAAV6-HGF group, albeit not significantly (**Figure IV-17**). Most interestingly, mean survival rate at P142 was increased 4.38-fold in the rAAV6-HGF group, from 14.29% to 62.5%, when compared with the control group (**Figure IV-18**). These results suggested that intramuscularly delivered rAAV6-HGF might at least partially alleviate disease symptoms and increase the survival in this mouse model.

2.4. Regulation of genes involved in muscle atrophy by IM injection of rAAV6-HGF

Our data from both the nerve crush and SOD1-G93A TG mouse models indicated highly positive effects on muscle cells and subsequent motor functions. We previously reported that IM injection of HGF-expressing plasmid could alleviate neurogenic muscle

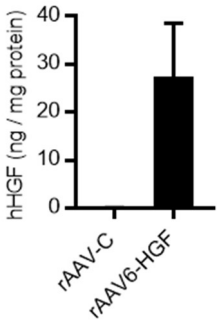

Figure IV-11. HGF expression from rAAV6-HGF in the SOD1-G93A TG mouse model.

$3.12x10^8$ GC of rAAV6-HGF were injected into the TA of SOD1-G93A TG mice at P90. The TA was collected at P120, followed by ELISA for hHGF. Values are represented as mean ± SEM.

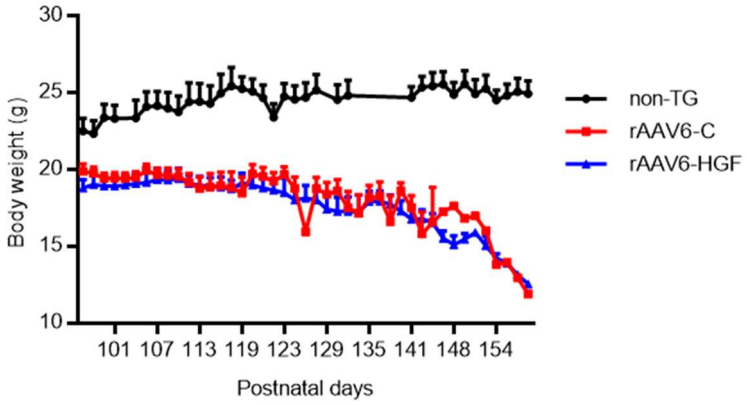

Figure IV-12. The body weight of SOD1-G93A TG mice after IM injection of rAAV6-HGF.

At P90, 3.12×10^8 GC of rAAV6-HGF were injected into 6 sites altogether (TA, GC, and VL of each leg). The body weight was measured until P157. Values are represented as mean ± SEM.

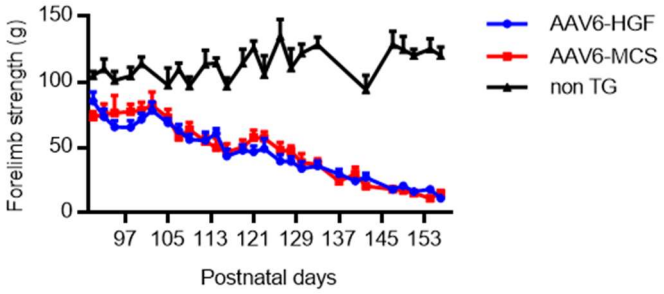

Figure IV-13. The forelimb strength of SOD1-G93A TG mice after IM injection of rAAV6-HGF.

At P90, 3.12×10^8 GC of rAAV6-HGF were injected into 6 sites altogether (TA, GC, and VL of each leg). The forelimb strength was measured until P157. Values are represented as mean ± SEM.

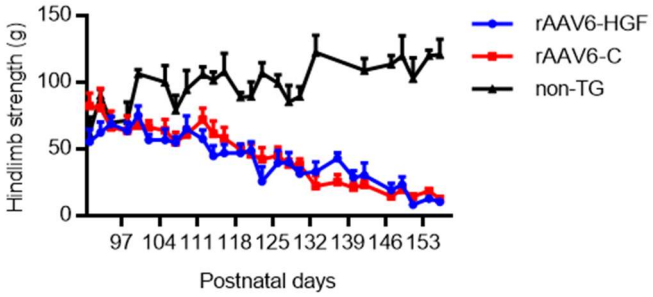

Figure IV-14. The hindlimb strength of SOD1-G93A TG mice after IM injection of rAAV6-HGF.

At P90, $3.12x10^8$ GC of rAAV6-HGF were injected into 6 sites altogether (TA, GC, and VL of each leg). The hindlimb strength was measured until P157. Values are represented as mean ± SEM.

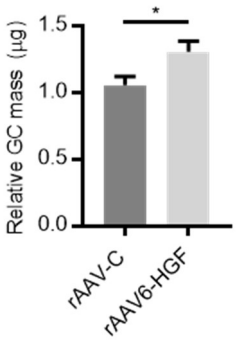

Figure IV-15. Relative mass of the GC of SOD1-G93A TG mice after IM injection of rAAV6-HGF.

At P90, 3.12×10^8 GC of rAAV6-HGF were injected into 6 sites altogether (TA, GC, and VL of each leg). At P120, the GC was isolated, followed by weight measurement. For statistical analysis, Student's t-tests were performed. $^*p < 0.05$. Values are represented as mean ± SEM.

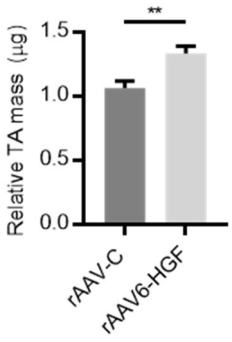

Figure IV-16. Relative mass of the TA of SOD1-G93A TG mice after IM injection of rAAV6-HGF.

At P90, 3.12×10^8 GC of rAAV6-HGF were injected into 6 sites altogether (TA, GC, and VL of each leg). At P120, the TA was isolated, followed by weight measurement. For statistical analysis, Student's t-tests were performed. $^{**}p < 0.005$. Values are represented as mean ± SEM.

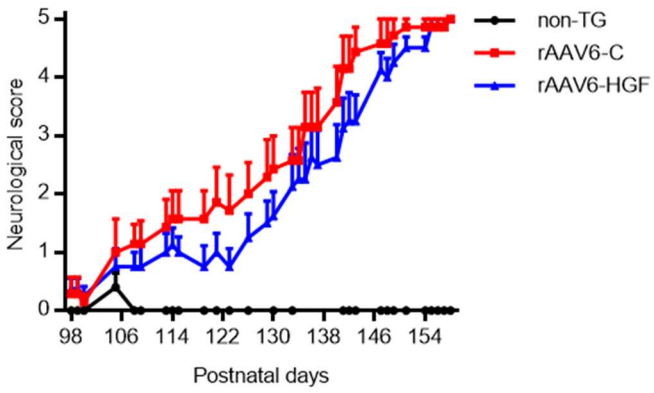

Figure IV-17. Mean neurological score of SOD1-G93A TG mice after IM injection of rAAV6-HGF.

At P90, $3.12x10^8$ GC of rAAV6-HGF were injected into 6 sites altogether (TA, GC, and VL of each leg). The neurological score was measured until P157. Values are represented as mean ± SEM.

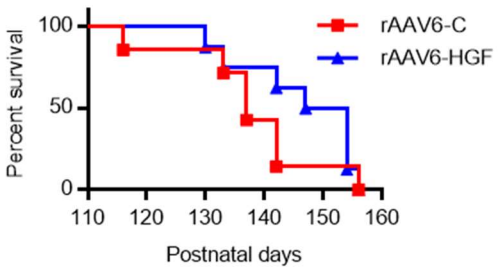

Figure IV-18. The survival rate of SOD1-G93A TG mice after IM injection of rAAV6-HGF.

At P90, $3.12x10^8$ GC of rAAV6-HGF were injected into 6 sites altogether (TA, GC, and VL of each leg). The survival rate was assessed based on Mantel-Cox and Gehan-Breslow-Wilcoxon tests. Median survival days were 137 for the rAAV-C group, and 150.5 for the rAAV6-HGF group.

atrophy by controlling the miR-206-HDAC4 cascade, eventually reducing the expression level of atrogenes, MuRF1 and atrogin-1, during the sub-acute stage after nerve injury [107]. Therefore, we investigated whether HGF produced from AAV could also improve muscle atrophy in the chronic stage after nerve injury by controlling the miR-206-HDAC4 pathway. RNA was prepared from the TA of nerve crushed mice at day 14 after injury followed by q-RTPCR [108]. It was found that the RNA levels of MuRF1 and atrogin-1 decreased, while those of miR-206, HDAC4, Myogenin, and MyoD remained unchanged, indicating miR-206 played little or no role (**Figure IV-19, 20**).

There is another pathway regulating the expression of MuRF1 and atrogin-1, in which FOXO1 and FOXO3 play critical roles [109]. It was found that the RNA level of FOXO1 increased 2.48-fold after nerve injury. When treated with rAAV6-HGF, the RNA level of FOXO1 decreased 2.34-fold compared to the rAAV-C group (**Figure IV-21**). A similar trend was also observed with the FOXO3 gene (**Figure IV-22**). These results suggested that HGF from rAAV could improve muscle atrophy by regulating the expression of the FOXO families.

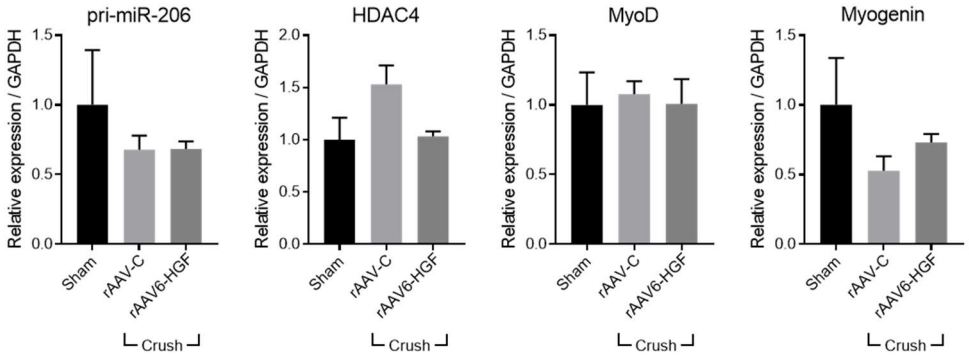

Figure IV-19. Effects of rAAV6-HGF on the expression of genes related to muscle atrophy in the nerve crush model.

C57BL/6 mice at P60 were intramuscularly injected with $3.12x10^8$ GC of rAAV6-HGF. Total RNA was prepared from the TA of nerve crushed mice followed by q-RTPCR. The relative expression levels of pri-miR-206, HDAC4, MyoD, and Myogenin are represented as bar graphs. Values are represented as mean ± SEM.

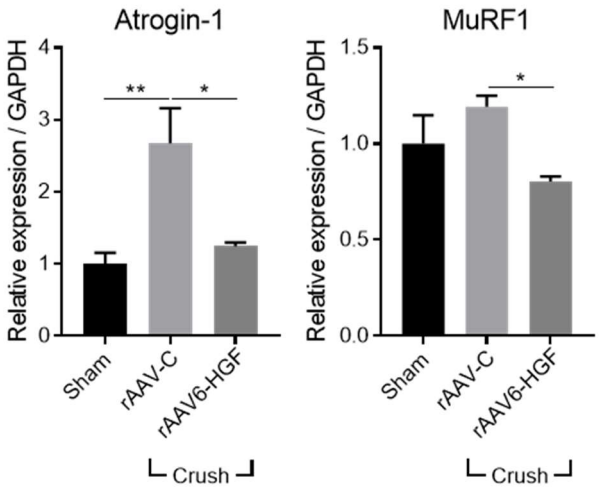

Figure IV-20. Effects of rAAV6-HGF on RNA expression of the TA in the nerve crush model.

C57BL/6 mice at P60 were intramuscularly injected with $3.12x10^8$ GC of rAAV6-HGF. The TA was collected, followed by q-RTPCR analysis. The relative RNA levels of MuRF1 and atrogin-1 are represented as bar graphs. For statistical analysis, one-way ANOVA was performed, followed by Tukey's post-hoc test. $^{*}p < 0.05$, $^{**}p < 0.01$, $^{***}p < 0.001$.

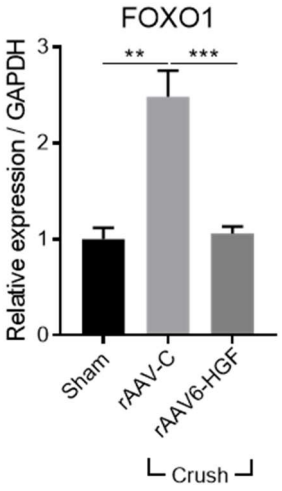

Figure IV-21. Effects of rAAV6-HGF on the level of FOXO1 of the TA in the nerve crush model.

C57BL/6 mice at P60 were intramuscularly injected with $3.12x10^8$ GC of rAAV6-HGF. The TA was collected, followed by q-RTPCR analysis. The relative RNA level of FOXO1 is represented as a bar graph. For statistical analysis, one-way ANOVA was performed, followed by Tukey's post-hoc test. $^{**}p < 0.01$, $^{***}p < 0.001$.

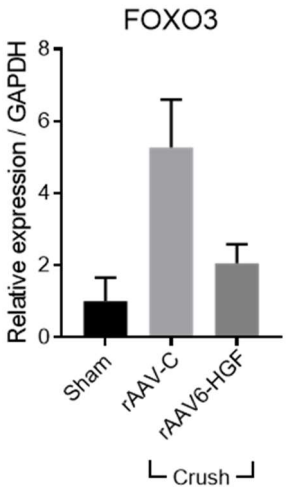

Figure IV-22. Effects of rAAV6-HGF on the level of FOXO3 of the TA in the nerve crush model.

C57BL/6 mice at P60 were intramuscularly injected with $3.12x10^8$ GC of rAAV6-HGF. The TA was collected, followed by q-RTPCR analysis. The relative RNA level of FOXO3 is represented as a bar graph.

3. Discussion

As in the case of IT gene delivery, I compared the expression levels of hHGF proteins from 4 different serotypes of rAAV-HGF after IM injection. Based on the expression levels of hHGF proteins in the TA, AAV serotype 6 was chosen for IM delivery. When rAAV6-HGF was intramuscularly injected, expression levels of HGF proteins continuously increased until 16 weeks after injection. Such an expression profile is particularly useful when applied to various neurodegenerative diseases that undergo progressive degeneration of the neuronal cells. Nevertheless, potential adverse effects exerted by the sustained expression of high levels of HGF proteins should be addressed in further studies.

When first tested in the nerve crush model, IM injection of rAAV6-HGF was able to lower the degree of nociceptive sensitization, improve muscle histology, and facilitate the recovery of motor performance. A variety of cell types respond to nerve injury and almost all key players contain the Met receptor, so the effects of rAAV6-HGF might have stemmed from several different sources. Firstly, HGF may have interacted with the Met receptors present in skeletal muscle cells to improve muscle integrity and motor functions. Based on this study and our previously published works, HGF expressed from rAAV6-HGF can improve the physical structure and functions of muscle, probably through two different pathways, one through the miR-206-HDAC4 cascade as previously reported by Choi et al. and the other via the FOXO signaling pathway as shown in this study, in which the expression of a variety of muscle atrogenes—including FOXO1, MuRF1, and atrogin-1 among others—are regulated by HGF [107]. It is worth noting that the HGF-mediated regulation of the FOXO signaling pathway

has been studied for endothelial cells, but never in the context of muscle and nerve injury.

Another possibility is that HGF may have interacted with neuronal cells. HGF could reach and interact with sensory neurons to promote axonal outgrowth, or NMJ to affect the motor neurons [74, 84]. Alternatively, HGF expressed from rAAV6-HGF might act on glial cells in the peripheral nervous system. It was reported that HGF could downregulate the expression of pain-related factors in the dorsal root ganglion, change the distribution pattern of activated microglia in the spinal cord, and reduce neuropathic pain [58]. In the nerve crush model, HGF was shown to interact with receptors in Schwann cells to promote remyelination and axon outgrowth [57]. Taken together, HGF expressed from intramuscularly delivered AAV has the potential to restore injured nerves and muscles by interacting with key cell types involved in the healing or repairing process.

In the SOD1-G93A TG mouse model, rAAV6-HGF did not improve body weight or limb strength, but did increase the weight of skeletal muscle and prolonged the mean survival rate from P137 to P150.5. These therapeutic effects likely resulted from HGF's effects on muscle cells and possibly motor neurons via NMJ, as discussed above. Overall, IM delivery of the HGF gene seems to be less effective than IT injection, but may be useful to relieve symptoms or slow down disease progression.

Chapter V

Concluding Remarks

In this thesis research, I explored the possibility of delivering the HGF gene by IT or IM injection of rAAV vector for neuromuscular diseases using the sciatic nerve crush and SOD1-G93A TG mouse models. For IT delivery, AAV serotype 1 was found to most effectively deliver and express the transgene in the ventral horn over the course of 16 weeks, with peak level achieved at 2 weeks post-injection. In the case of IM injection, rAAV6-HGF was the most efficient vehicle, and with this serotype, the expression level of hHGF continuously increased for 16 weeks post injection when the experiments had to be completed. Despite long-term, high-level expression of HGF in the muscle, however, hHGF was not detectable in the serum, consistent with previous publications [45-47, 49, 50].

Data from IT injection of rAAV1-HGF indicated that exogenous delivery of HGF might have regenerative potential and improve symptomatic motor performance in both crushed and SOD1-G93A TG mice. Of particular interest was the finding that IT injection of rAAV1-HGF could not only facilitate protection of but also delay the degeneration of motor neurons. It is known that protein levels of HGF and Met increase in the ventral horn of sALS patients at the early stage, while patients with motor neurons defective in HGF or Met are more susceptible to disease progression of ALS, being atrophied rapidly. A similar situation is observed in SOD1-G93A TG mice. Taken together, HGF can be a strong candidate that may be used for developing therapeutics for ALS.

Improvements in motor functions, NMJ morphology, and the protection of SMNs observed in this study could have resulted from 3 sources, as described in chapter III; changes in SMNs, in upper motor neurons, or in a combination of both neurons. Our data, together

with those from other investigators, suggested that HGF could not only protect damaged lower motor neurons, but also exert positive effects on upper motor neurons by facilitating the axonal outgrowth by controlling the phosphorylation of ERK as evidenced by results from CSMN experiments. Of course, it is also possible that HGF expressed from rAAV1-HGF could have affected both spinal and upper motor neurons.

IM delivery of rAAV expressing hHGF also generated highly encouraging results in two mouse models by improving neuromuscular integrity and functions. The effects of intramuscularly injected rAAV6-HGF could have several different sources; by interacting with the Met receptors present in skeletal muscle cells, neuronal cells, and/or glial cells in the peripheral nervous system. There are a bulk of data supporting the involvement of all 3 cell types. Our group has shown that HGF can improve the physical structure and functions of muscle, through two different pathways, one through the miR-206-HDAC4 cascade as previously reported by Choi et al. and the other via the FOXO signaling pathway described in this thesis. In addition, HGF can interact with sensory neurons to promote axonal outgrowth, or neuromuscular junction (NMJ) to affect motor neurons [74, 84]. Finally, HGF could downregulate the expression of CSF-1 in the dorsal root ganglion, and change the distribution pattern of activated microglia in the spinal cord as reported by Noh et al. [58].

One may argue that IT delivery of rAAV-HGF is much more effective than IM injection, so there is no use for the latter. However, IM delivery of HGF can be a very valuable tool for a number of neuromuscular diseases. It is a highly convenient delivery method that does not require any medical devices or invasive procedures. Since a vast majority of

neuromuscular diseases have unknown causes, IT injection of recombinant viral vectors, which is a relatively invasive procedure, may not be considered a primary choice until extensive pre-clinical studies have been completed for respective diseases. In the meantime, therefore, IM injection of HGF-expressing plasmid DNA or AAV can be used to improve related clinical symptoms, ultimately improving patients' enjoyment of daily activities.

In conclusion, data shown in this thesis suggested that exogenously added HGF, in the form of AAV, could improve behavioral defects, regenerate neurons, and even prolong survival in the case of SOD1-G93A TG mice when intrathecally or intramuscularly delivered. Taken together, it appears that rAAV expressing HGF may be developed as a novel therapeutic agent for various diseases in which upper and lower motor neuron degeneration is the major pathologic cause.

References

[1] M.C. Kiernan, S. Vucic, B.C. Cheah, M.R. Turner, A. Eisen, O. Hardiman, J.R. Burrell, M.C. Zoing, Amyotrophic lateral sclerosis, Lancet, 377 (2011) 942-955.

[2] O. Hardiman, L.H. van den Berg, M.C. Kiernan, Clinical diagnosis and management of amyotrophic lateral sclerosis, Nat Rev Neurol, 7 (2011) 639-649.

[3] J.P. Taylor, R.H. Brown, Jr., D.W. Cleveland, Decoding ALS: from genes to mechanism, Nature, 539 (2016) 197-206.

[4] C.A. Blizzard, K.A. Southam, E. Dawkins, K.E. Lewis, A.E. King, J.A. Clark, T.C. Dickson, Identifying the primary site of pathogenesis in amyotrophic lateral sclerosis - vulnerability of lower motor neurons to proximal excitotoxicity, Dis Model Mech, 8 (2015) 215-224.

[5] A. Al-Chalabi, O. Hardiman, The epidemiology of ALS: a conspiracy of genes, environment and time, Nat Rev Neurol, 9 (2013) 617-628.

[6] A.M. Haidet-Phillips, M.E. Hester, C.J. Miranda, K. Meyer, L. Braun, A. Frakes, S. Song, S. Likhite, M.J. Murtha, K.D. Foust, M. Rao, A. Eagle, A. Kammesheidt, A. Christensen, J.R. Mendell, A.H. Burghes, B.K. Kaspar, Astrocytes from familial and sporadic ALS patients are toxic to motor neurons, Nat Biotechnol, 29 (2011) 824-828.

[7] A. King, C. Troakes, B. Smith, M. Nolan, O. Curran, C. Vance, C.E. Shaw, S. Al-Sarraj, ALS-FUS pathology revisited: singleton FUS mutations and an unusual case with both a FUS and TARDBP mutation, Acta Neuropathol Commun, 3 (2015) 62.

[8] J. Gal, L. Kuang, K.R. Barnett, B.Z. Zhu, S.C. Shissler, K.V. Korotkov, L.J. Hayward, E.J. Kasarskis, H. Zhu, ALS mutant SOD1 interacts with G3BP1 and affects stress granule

dynamics, Acta Neuropathol, 132 (2016) 563-576.

[9] M. DeJesus-Hernandez, I.R. Mackenzie, B.F. Boeve, A.L. Boxer, M. Baker, N.J. Rutherford, A.M. Nicholson, N.A. Finch, H. Flynn, J. Adamson, N. Kouri, A. Wojtas, P. Sengdy, G.Y. Hsiung, A. Karydas, W.W. Seeley, K.A. Josephs, G. Coppola, D.H. Geschwind, Z.K. Wszolek, H. Feldman, D.S. Knopman, R.C. Petersen, B.L. Miller, D.W. Dickson, K.B. Boylan, N.R. Graff-Radford, R. Rademakers, Expanded GGGGCC hexanucleotide repeat in noncoding region of C9ORF72 causes chromosome 9p-linked FTD and ALS, Neuron, 72 (2011) 245-256.

[10] J.C. Schymick, K. Talbot, B.J. Traynor, Genetics of sporadic amyotrophic lateral sclerosis, Hum Mol Genet, 16 Spec No. 2 (2007) R233-242.

[11] A. Chio, J.C. Schymick, G. Restagno, S.W. Scholz, F. Lombardo, S.L. Lai, G. Mora, H.C. Fung, A. Britton, S. Arepalli, J.R. Gibbs, M. Nalls, S. Berger, L.C. Kwee, E.Z. Oddone, J. Ding, C. Crews, I. Rafferty, N. Washecka, D. Hernandez, L. Ferrucci, S. Bandinelli, J. Guralnik, F. Macciardi, F. Torri, S. Lupoli, S.J. Chanock, G. Thomas, D.J. Hunter, C. Gieger, H.E. Wichmann, A. Calvo, R. Mutani, S. Battistini, F. Giannini, C. Caponnetto, G.L. Mancardi, V. La Bella, F. Valentino, M.R. Monsurro, G. Tedeschi, K. Marinou, M. Sabatelli, A. Conte, J. Mandrioli, P. Sola, F. Salvi, I. Bartolomei, G. Siciliano, C. Carlesi, R.W. Orrell, K. Talbot, Z. Simmons, J. Connor, E.P. Pioro, T. Dunkley, D.A. Stephan, D. Kasperaviciute, E.M. Fisher, S. Jabonka, M. Sendtner, M. Beck, L. Bruijn, J. Rothstein, S. Schmidt, A. Singleton, J. Hardy, B.J. Traynor, A two-stage genome-wide association study of sporadic amyotrophic lateral sclerosis, Hum Mol Genet, 18 (2009) 1524-1532.

[12] N. Geevasinga, P. Menon, P.H. Ozdinler, M.C. Kiernan, S. Vucic, Pathophysiological and diagnostic implications of cortical dysfunction in ALS, Nat Rev Neurol, 12 (2016) 651-661.

[13] B.C. Cheah, S. Vucic, A.V. Krishnan, M.C. Kiernan, Riluzole, neuroprotection and amyotrophic lateral sclerosis, Curr Med Chem, 17 (2010) 1942-1199.

[14] J.D. Rothstein, Edaravone: A new drug approved for ALS, Cell, 171 (2017) 725.

[15] G. Bensimon, L. Lacomblez, V. Meininger, A controlled trial of riluzole in amyotrophic lateral sclerosis. ALS/Riluzole Study Group, N Engl J Med, 330 (1994) 585-591.

[16] T. Nakamura, K. Nawa, A. Ichihara, Partial purification and characterization of hepatocyte growth factor from serum of hepatectomized rats, Biochem Biophys Res Commun, 122 (1984) 1450-1459.

[17] Y. Ishiki, H. Ohnishi, Y. Muto, K. Matsumoto, T. Nakamura, Direct Evidence That Hepatocyte Growth-Factor Is a Hepatotrophic Factor for Liver-Regeneration and Has a Potent Antihepatitis Effect Invivo, Hepatology, 16 (1992) 1227-1235.

[18] Y. Matsuda, K. Matsumoto, T. Ichida, T. Nakamura, Hepatocyte growth factor suppresses the onset of liver cirrhosis and abrogates lethal hepatic dysfunction in rats, J Biochem, 118 (1995) 643-649.

[19] R. Montesano, K. Matsumoto, T. Nakamura, L. Orci, Identification of a Fibroblast-Derived Epithelial Morphogen as Hepatocyte Growth-Factor, Cell, 67 (1991) 901-908.

[20] Y. Sakakura, M. Kaibori, M. Oda, T. Okumura, A.H. Kwon, Y. Kamiyama, Recombinant human hepatocyte growth factor protects the liver against hepatic ischemia and reperfusion injury in rats, J Surg Res, 92 (2000) 261-266.

[21] E. Van Belle, B. Witzenbichler, D. Chen, M. Silver, L. Chang, R. Schwall, J.M. Isner,

Potentiated angiogenic effect of scatter factor/hepatocyte growth factor via induction of vascular endothelial growth factor: the case for paracrine amplification of angiogenesis, Circulation, 97 (1998) 381-390.

[22] K. Yamaura, K. Ito, K. Tsukioka, Y. Wada, A. Makiuchi, M. Sakaguchi, T. Akashima, M. Fujimori, Y. Sawa, R. Morishita, K. Matsumoto, T. Nakamura, J. Suzuki, J. Amano, M. Isobe, Suppression of acute and chronic rejection by hepatocyte growth factor in a murine model of cardiac transplantation: induction of tolerance and prevention of cardiac allograft vasculopathy, Circulation, 110 (2004) 1650-1657.

[23] L. Trusolino, A. Bertotti, P.M. Comoglio, MET signalling: principles and functions in development, organ regeneration and cancer, Nat Rev Mol Cell Biol, 11 (2010) 834-848.

[24] K. Mizuno, H. Inoue, M. Hagiya, S. Shimizu, T. Nose, Y. Shimohigashi, T. Nakamura, Hairpin loop and second kringle domain are essential sites for heparin binding and biological activity of hepatocyte growth factor, J Biol Chem, 269 (1994) 1131-1136.

[25] M. Kong-Beltran, J. Stamos, D. Wickramasinghe, The Sema domain of Met is necessary for receptor dimerization and activation, Cancer Cell, 6 (2004) 75-84.

[26] G. Kozlov, A. Perreault, J.D. Schrag, M. Park, M. Cygler, K. Gehring, I. Ekiel, Insights into function of PSI domains from structure of the Met receptor PSI domain, Biochem Biophys Res Commun, 321 (2004) 234-240.

[27] C. Basilico, A. Arnesano, M. Galluzzo, P.M. Comoglio, P. Michieli, A high affinity hepatocyte growth factor-binding site in the immunoglobulin-like region of Met, J Biol Chem, 283 (2008) 21267-21277.

[28] L. Arnold, J. Enders, S.M. Thomas, Activated HGF-c-Met Axis in Head and Neck Cancer, Cancers (Basel), 9 (2017).

[29] R. Paumelle, D. Tulasne, Z. Kherrouche, S. Plaza, C. Leroy, S. Reveneau, B. Vandenbunder, V. Fafeur, Hepatocyte growth factor/scatter factor activates the ETS1 transcription factor by a RAS-RAF-MEK-ERK signaling pathway, Oncogene, 21 (2002) 2309-2319.

[30] C. Ponzetto, A. Bardelli, Z. Zhen, F. Maina, P. dalla Zonca, S. Giordano, A. Graziani, G. Panayotou, P.M. Comoglio, A multifunctional docking site mediates signaling and transformation by the hepatocyte growth factor/scatter factor receptor family, Cell, 77 (1994) 261-271.

[31] L. Naldini, E. Vigna, R. Ferracini, P. Longati, L. Gandino, M. Prat, P.M. Comoglio, The tyrosine kinase encoded by the MET proto-oncogene is activated by autophosphorylation, Mol Cell Biol, 11 (1991) 1793-1803.

[32] R. Ferracini, P. Longati, L. Naldini, E. Vigna, P.M. Comoglio, Identification of the major autophosphorylation site of the Met/hepatocyte growth factor receptor tyrosine kinase, J Biol Chem, 266 (1991) 19558-19564.

[33] R. Onozato, T. Kosaka, H. Kuwano, Y. Sekido, Y. Yatabe, T. Mitsudomi, Activation of MET by gene amplification or by splice mutations deleting the juxtamembrane domain in primary resected lung cancers, J Thorac Oncol, 4 (2009) 5-11.

[34] T. Nakamura, K. Sakai, T. Nakamura, K. Matsumoto, Hepatocyte growth factor twenty years on: Much more than a growth factor, J Gastroenterol Hepatol, 26 Suppl 1 (2011) 188-

202.

[35] S. Kato, H. Funakoshi, T. Nakamura, M. Kato, I. Nakano, A. Hirano, E. Ohama, Expression of hepatocyte growth factor and c-Met in the anterior horn cells of the spinal cord in the patients with amyotrophic lateral sclerosis (ALS): immunohistochemical studies on sporadic ALS and familial ALS with superoxide dismutase 1 gene mutation, Acta Neuropathol, 106 (2003) 112-120.

[36] W. Sun, H. Funakoshi, T. Nakamura, Overexpression of HGF retards disease progression and prolongs life span in a transgenic mouse model of ALS, J Neurosci, 22 (2002) 6537-6548.

[37] S. Daya, K.I. Berns, Gene Therapy Using Adeno-Associated Virus Vectors, Clin Microbiol Rev, 21 (2008) 583-593.

[38] C. Zincarelli, S. Soltys, G. Rengo, J.E. Rabinowitz, Analysis of AAV serotypes 1-9 mediated gene expression and tropism in mice after systemic injection, Mol Ther, 16 (2008) 1073-1080.

[39] M.F. Naso, B. Tomkowicz, W.L. Perry, 3rd, W.R. Strohl, Adeno-Associated Virus (AAV) as a Vector for Gene Therapy, BioDrugs, 31 (2017) 317-334.

[40] B. Hauck, L. Chen, W. Xiao, Generation and characterization of chimeric recombinant AAV vectors, Mol Ther, 7 (2003) 419-425.

[41] H.S. Loring, M.K. ElMallah, T.R. Flotte, Development of rAAV2-CFTR: History of the First rAAV Vector Product to be Used in Humans, Hum Gene Ther Methods, 27 (2016) 49-58.

[42] M. Hocquemiller, L. Giersch, M. Audrain, S. Parker, N. Cartier, Adeno-Associated Virus-

Based Gene Therapy for CNS Diseases, Hum Gene Ther, 27 (2016) 478-496.

[43] F. Cecchi, D.C. Rabe, D.P. Bottaro, Targeting the HGF/Met signaling pathway in cancer therapy, Expert Opin Ther Targets, 16 (2012) 553-572.

[44] H. Zhou, M.J. Mazzulla, J.D. Kaufman, S.J. Stahl, P.T. Wingfield, J.S. Rubin, D.P. Bottaro, R.A. Byrd, The solution structure of the N-terminal domain of hepatocyte growth factor reveals a potential heparin-binding site, Structure, 6 (1998) 109-116.

[45] W.B. Pyun, W. Hahn, D.S. Kim, W.S. Yoo, S.D. Lee, J.H. Won, B.S. Rho, Z.Y. Park, J.M. Kim, S. Kim, Naked DNA expressing two isoforms of hepatocyte growth factor induces collateral artery augmentation in a rabbit model of limb ischemia, Gene Ther, 17 (2010) 1442-1452.

[46] W. Hahn, W.B. Pyun, D.S. Kim, W.S. Yoo, S.D. Lee, J.H. Won, G.J. Shin, J.M. Kim, S. Kim, Enhanced cardioprotective effects by coexpression of two isoforms of hepatocyte growth factor from naked plasmid DNA in a rat ischemic heart disease model, J Gene Med, 13 (2011) 549-555.

[47] T.D. Henry, A.T. Hirsch, J. Goldman, Y.L. Wang, D.L. Lips, W.D. McMillan, S. Duval, T.A. Biggs, H.H. Keo, Safety of a non-viral plasmid-encoding dual isoforms of hepatocyte growth factor in critical limb ischemia patients: a phase I study, Gene Ther, 18 (2011) 788-794.

[48] S. Ajroud-Driss, M. Christiansen, J.A. Allen, J.A. Kessler, Phase 1/2 Open-label Dose-escalation Study of Plasmid DNA Expressing Two Isoforms of Hepatocyte Growth Factor in Patients With Painful Diabetic Peripheral Neuropathy, Molecular Therapy, 21 (2013) 1279-1286.

[49] J.A. Kessler, A.G. Smith, B.S. Cha, S.H. Choi, J. Wymer, A. Shaibani, S. Ajroud-Driss, A. Vinik, V.D.-I.S. Group, Double-blind, placebo-controlled study of HGF gene therapy in diabetic neuropathy, Ann Clin Transl Neurol, 2 (2015) 465-478.

[50] R.L. Sufit, S. Ajroud-Driss, P. Casey, J.A. Kessler, Open label study to assess the safety of VM202 in subjects with amyotrophic lateral sclerosis, Amyotroph Lat Scl Fr, 18 (2017) 269-278.

[51] M.R. Kibbe, A.T. Hirsch, F.O. Mendelsohn, M.G. Davies, H. Pham, J. Saucedo, W. Marston, W.B. Pyun, S.K. Min, B.G. Peterson, A. Comerota, D. Choi, J. Ballard, R.A. Bartow, D.W. Losordo, W. Sherman, V. Driver, E.C. Perin, Safety and efficacy of plasmid DNA expressing two isoforms of hepatocyte growth factor in patients with critical limb ischemia, Gene Ther, 23 (2016) 399.

[52] S.H. Lee, S. Kim, N. Lee, J. Lee, S.S. Yu, J.H. Kim, S. Kim, Intrathecal delivery of recombinant AAV1 encoding hepatocyte growth factor improves motor functions and protects neuromuscular system in the nerve crush and SOD1-G93A transgenic mouse models, Acta Neuropathologica Communications, 7 (2019) 14.

[53] K.R. Cho, J.S. Choi, W. Hahn, D.S. Kim, J.S. Park, D.S. Lee, K.B. Kim, Therapeutic angiogenesis using naked DNA expressing two isoforms of the hepatocyte growth factor in a porcine acute myocardial infarction model, Eur J Cardiothorac Surg, 34 (2008) 857-863.

[54] M.E. Gurney, Motor-Neuron Degeneration in Mice That Express a Human Cu,Zn Superoxide-Dismutase Mutation (Vol 264, Pg 1772, 1994), Science, 269 (1995) 149-149.

[55] P.H. Tu, P. Raju, K.A. Robinson, M.E. Gurney, J.Q. Trojanowski, V.M. Lee, Transgenic

mice carrying a human mutant superoxide dismutase transgene develop neuronal cytoskeletal pathology resembling human amyotrophic lateral sclerosis lesions, Proc Natl Acad Sci U S A, 93 (1996) 3155-3160.

[56] C.M. Wooley, R.B. Sher, A. Kale, W.N. Frankel, G.A. Cox, K.L. Seburn, Gait analysis detects early changes in transgenic SOD1(G93A) mice, Muscle Nerve, 32 (2005) 43-50.

[57] K.R. Ko, J. Lee, D. Lee, B. Nho, S. Kim, Hepatocyte Growth Factor (HGF) Promotes Peripheral Nerve Regeneration by Activating Repair Schwann Cells, Sci Rep, 8 (2018) 8316.

[58] B. Nho, J. Lee, J. Lee, K.R. Ko, S.J. Lee, S. Kim, Effective control of neuropathic pain by transient expression of hepatocyte growth factor in a mouse chronic constriction injury model, FASEB J, 32 (2018) 5119-5131.

[59] J.M. Inloes, K.L. Hsu, M.M. Dix, A. Viader, K. Masuda, T. Takei, M.R. Wood, B.F. Cravatt, The hereditary spastic paraplegia-related enzyme DDHD2 is a principal brain triglyceride lipase, Proc Natl Acad Sci U S A, 111 (2014) 14924-14929.

[60] R. Kumar, C.R. Hunt, A. Gupta, S. Nannepaga, R.K. Pandita, J.W. Shay, R. Bachoo, T. Ludwig, D.K. Burns, T.K. Pandita, Purkinje cell-specific males absent on the first (mMof) gene deletion results in an ataxia-telangiectasia-like neurological phenotype and backward walking in mice, Proc Natl Acad Sci U S A, 108 (2011) 3636-3641.

[61] H. Shiotsuki, K. Yoshimi, Y. Shimo, M. Funayama, Y. Takamatsu, K. Ikeda, R. Takahashi, S. Kitazawa, N. Hattori, A rotarod test for evaluation of motor skill learning, J Neurosci Methods, 189 (2010) 180-185.

[62] R. Furlan, C. Cuomo, G. Martino, Animal models of multiple sclerosis, Methods Mol

Biol, 549 (2009) 157-173.

[63] T. Tatlisumak, R.A. Carano, K. Takano, T.J. Opgenorth, C.H. Sotak, M. Fisher, A novel endothelin antagonist, A-127722, attenuates ischemic lesion size in rats with temporary middle cerebral artery occlusion: a diffusion and perfusion MRI study, Stroke, 29 (1998) 850-857; discussion 857-858.

[64] X. Xu, K.W. Chua, C.C. Chua, C.F. Liu, R.C. Hamdy, B.H. Chua, Synergistic protective effects of humanin and necrostatin-1 on hypoxia and ischemia/reperfusion injury, Brain Res, 1355 (2010) 189-194.

[65] J.H. Jara, B. Genc, G.A. Cox, M.C. Bohn, R.P. Roos, J.D. Macklis, E. Ulupinar, P.H. Ozdinler, Corticospinal Motor Neurons Are Susceptible to Increased ER Stress and Display Profound Degeneration in the Absence of UCHL1 Function, Cereb Cortex, 25 (2015) 4259-4272.

[66] G.M. Alexander, K.L. Erwin, N. Byers, J.S. Deitch, B.J. Augelli, E.P. Blankenhorn, T.D. Heiman-Patterson, Effect of transgene copy number on survival in the G93A SOD1 transgenic mouse model of ALS, Mol Brain Res, 130 (2004) 7-15.

[67] M. Uhlen, L. Fagerberg, B.M. Hallstrom, C. Lindskog, P. Oksvold, A. Mardinoglu, A. Sivertsson, C. Kampf, E. Sjostedt, A. Asplund, I. Olsson, K. Edlund, E. Lundberg, S. Navani, C.A. Szigyarto, J. Odeberg, D. Djureinovic, J.O. Takanen, S. Hober, T. Alm, P.H. Edqvist, H. Berling, H. Tegel, J. Mulder, J. Rockberg, P. Nilsson, J.M. Schwenk, M. Hamsten, K. von Feilitzen, M. Forsberg, L. Persson, F. Johansson, M. Zwahlen, G. von Heijne, J. Nielsen, F. Ponten, Proteomics. Tissue-based map of the human proteome, Science, 347 (2015) 1260419.

[68] J.C. Dodge, A.M. Haidet, W. Yang, M.A. Passini, M. Hester, J. Clarke, E.M. Roskelley, C.M. Treleaven, L. Rizo, H. Martin, S.H. Kim, R. Kaspar, T.V. Taksir, D.A. Griffiths, S.H. Cheng, L.S. Shihabuddin, B.K. Kaspar, Delivery of AAV-IGF-1 to the CNS extends survival in ALS mice through modification of aberrant glial cell activity, Mol Ther, 16 (2008) 1056-1064.

[69] J.C. Dodge, C.M. Treleaven, J.A. Fidler, M. Hester, A. Haidet, C. Handy, M. Rao, A. Eagle, J.C. Matthews, T.V. Taksir, S.H. Cheng, L.S. Shihabuddin, B.K. Kaspar, AAV4-mediated expression of IGF-1 and VEGF within cellular components of the ventricular system improves survival outcome in familial ALS mice, Mol Ther, 18 (2010) 2075-2084.

[70] A. Henriques, C. Pitzer, T. Dittgen, M. Klugmann, L. Dupuis, A. Schneider, CNS-targeted viral delivery of G-CSF in an animal model for ALS: improved efficacy and preservation of the neuromuscular unit, Mol Ther, 19 (2011) 284-292.

[71] Y.Q. Gu, J. Zhang, L.R. Guo, S.J. Cui, X.F. Li, D.Y. Ding, J.M. Kim, S.H. Ho, W. Hahn, S. Kim, A phase I clinical study of naked DNA expressing two isoforms of hepatocyte growth factor to treat patients with critical limb ischemia, J Gene Med, 13 (2011) 602-610.

[72] H. Buning, L. Perabo, O. Coutelle, S. Quadt-Humme, M. Hallek, Recent developments in adeno-associated virus vector technology, J Gene Med, 10 (2008) 717-733.

[73] K. McEown, Y. Takata, Y. Cherasse, N. Nagata, K. Aritake, M. Lazarus, Chemogenetic inhibition of the medial prefrontal cortex reverses the effects of REM sleep loss on sucrose consumption, Elife, 5 (2016).

[74] A.H. Williams, G. Valdez, V. Moresi, X. Qi, J. McAnally, J.L. Elliott, R. Bassel-Duby, J.R.

Sanes, E.N. Olson, MicroRNA-206 delays ALS progression and promotes regeneration of neuromuscular synapses in mice, Science, 326 (2009) 1549-1554.

[75] J.E. Shin, Y.C. Cho, B. Beirowski, J. Milbrandt, V. Cavalli, A. DiAntonio, Dual Leucine Zipper Kinase Is Required for Retrograde Injury Signaling and Axonal Regeneration, Neuron, 74 (2012) 1015-1022.

[76] J.E. Shin, S. Geisler, A. DiAntonio, Dynamic regulation of SCG10 in regenerating axons after injury, Exp Neurol, 252 (2014) 1-11.

[77] B. Genc, J.H. Jara, M.C. Schultz, M. Manuel, M.J. Stanford, M. Gautam, J.L. Klessner, G. Sekerkova, D.B. Heller, G.A. Cox, C.J. Heckman, C.J. DiDonato, P.H. Ozdinler, Absence of UCHL 1 function leads to selective motor neuropathy, Ann Clin Transl Neurol, 3 (2016) 331-345.

[78] A. Ebens, K. Brose, E.D. Leonardo, M.G. Hanson, Jr., F. Bladt, C. Birchmeier, B.A. Barres, M. Tessier-Lavigne, Hepatocyte growth factor/scatter factor is an axonal chemoattractant and a neurotrophic factor for spinal motor neurons, Neuron, 17 (1996) 1157-1172.

[79] V. Wong, D.J. Glass, R. Arriaga, G.D. Yancopoulos, R.M. Lindsay, G. Conn, Hepatocyte growth factor promotes motor neuron survival and synergizes with ciliary neurotrophic factor, J Biol Chem, 272 (1997) 5187-5191.

[80] Y. Yamamoto, J. Livet, R.A. Pollock, A. Garces, V. Arce, O. deLapeyriere, C.E. Henderson, Hepatocyte growth factor (HGF/SF) is a muscle-derived survival factor for a subpopulation of embryonic motoneurons, Development, 124 (1997) 2903-2913.

[81] P.H. Ozdinler, J.D. Macklis, IGF-I specifically enhances axon outgrowth of corticospinal motor neurons, Nat Neurosci, 9 (2006) 1371-1381.

[82] M.V. Yasvoina, B. Genc, J.H. Jara, P.L. Sheets, K.A. Quinlan, A. Milosevic, G.M. Shepherd, C.J. Heckman, P.H. Ozdinler, eGFP expression under UCHL1 promoter genetically labels corticospinal motor neurons and a subpopulation of degeneration-resistant spinal motor neurons in an ALS mouse model, J Neurosci, 33 (2013) 7890-7904.

[83] K. Kadoyama, H. Funakoshi, W. Ohya, T. Nakamura, Hepatocyte growth factor (HGF) attenuates gliosis and motoneuronal degeneration in the brainstem motor nuclei of a transgenic mouse model of ALS, Neurosci Res, 59 (2007) 446-456.

[84] F. Maina, M.C. Hilton, C. Ponzetto, A.M. Davies, R. Klein, Met receptor signaling is required for sensory nerve development and HGF promotes axonal growth and survival of sensory neurons, Gene Dev, 11 (1997) 3341-3350.

[85] F. Maina, R. Klein, Hepatocyte growth factor, a versatile signal for developing neurons, Nat Neurosci, 2 (1999) 213-217.

[86] Y. Okura, H. Arimoto, N. Tanuma, K. Matsumoto, T. Nakamura, T. Yamashima, T. Miyazawa, Y. Matsumoto, Analysis of neurotrophic effects of hepatocyte growth factor in the adult hypoglossal nerve axotomy model, Eur J Neurosci, 11 (1999) 4139-4144.

[87] R. Gal-Levi, Y. Leshem, S. Aoki, T. Nakamura, O. Halevy, Hepatocyte growth factor plays a dual role in regulating skeletal muscle satellite cell proliferation and differentiation, Biochim Biophys Acta, 1402 (1998) 39-51.

[88] T. Miyazawa, K. Matsumoto, H. Ohmichi, H. Katoh, T. Yamashima, T. Nakamura,

Protection of hippocampal neurons from ischemia-induced delayed neuronal death by hepatocyte growth factor: A novel neurotrophic factor, J Cerebr Blood F Met, 18 (1998) 345-348.

[89] J. Shang, K. Deguchi, Y. Ohta, N. Liu, X. Zhang, F. Tian, T. Yamashita, Y. Ikeda, T. Matsuura, H. Funakoshi, T. Nakamura, K. Abe, Strong neurogenesis, angiogenesis, synaptogenesis, and antifibrosis of hepatocyte growth factor in rats brain after transient middle cerebral artery occlusion, J Neurosci Res, 89 (2011) 86-95.

[90] A. Streit, C.D. Stern, C. Thery, G.W. Ireland, S. Aparicio, M.J. Sharpe, E. Gherardi, A role for HGF/SF in neural induction and its expression in Hensen's node during gastrulation, Development, 121 (1995) 813-824.

[91] A. Streit, S. Sockanathan, L. Perez, M. Rex, P.J. Scotting, P.T. Sharpe, R. Lovell-Badge, C.D. Stern, Preventing the loss of competence for neural induction: HGF/SF, L5 and Sox-2, Development, 124 (1997) 1191-1202.

[92] T. Nakamura, S. Mizuno, The discovery of hepatocyte growth factor (HGF) and its significance for cell biology, life sciences and clinical medicine, Proc Jpn Acad Ser B Phys Biol Sci, 86 (2010) 588-610.

[93] R. Morishita, H. Makino, M. Aoki, N. Hashiya, K. Yamasaki, J. Azuma, Y. Taniyama, Y. Sawa, Y. Kaneda, T. Ogihara, Phase I/IIa clinical trial of therapeutic angiogenesis using hepatocyte growth factor gene transfer to treat critical limb ischemia, Arterioscler Thromb Vasc Biol, 31 (2011) 713-720.

[94] S.J. Koo, S.L. Pfaff, Fine-tuning motor neuron properties: signaling from the periphery,

Neuron, 35 (2002) 823-826.

[95] T.E. Taher, P.W. Derksen, O.J. de Boer, M. Spaargaren, P. Teeling, A.C. van der Wal, S.T. Pals, Hepatocyte growth factor triggers signaling cascades mediating vascular smooth muscle cell migration, Biochem Biophys Res Commun, 298 (2002) 80-86.

[96] I. Rishal, M. Fainzilber, Axon-soma communication in neuronal injury, Nat Rev Neurosci, 15 (2014) 32-42.

[97] E.A. Winkler, J.D. Sengillo, J.S. Sullivan, J.S. Henkel, S.H. Appel, B.V. Zlokovic, Blood-spinal cord barrier breakdown and pericyte reductions in amyotrophic lateral sclerosis, Acta Neuropathol, 125 (2013) 111-120.

[98] S. Park, H.T. Kim, S. Yun, I.S. Kim, J. Lee, I.S. Lee, K.I. Park, Growth factor-expressing human neural progenitor cell grafts protect motor neurons but do not ameliorate motor performance and survival in ALS mice, Exp Mol Med, 41 (2009) 487-500.

[99] M.H. Mohajeri, D.A. Figlewicz, M.C. Bohn, Intramuscular grafts of myoblasts genetically modified to secrete glial cell line-derived neurotrophic factor prevent motoneuron loss and disease progression in a mouse model of familial amyotrophic lateral sclerosis, Hum Gene Ther, 10 (1999) 1853-1866.

[100] B.K. Kaspar, J. Llado, N. Sherkat, J.D. Rothstein, F.H. Gage, Retrograde viral delivery of IGF-1 prolongs survival in a mouse ALS model, Science, 301 (2003) 839-842.

[101] M. Azzouz, G.S. Ralph, E. Storkebaum, L.E. Walmsley, K.A. Mitrophanous, S.M. Kingsman, P. Carmeliet, N.D. Mazarakis, VEGF delivery with retrogradely transported lentivector prolongs survival in a mouse ALS model, Nature, 429 (2004) 413-417.

[102] A. Henriques, C. Pitzer, A. Schneider, Neurotrophic growth factors for the treatment of amyotrophic lateral sclerosis: where do we stand?, Front Neurosci, 4 (2010) 32.

[103] R.T. Ambron, E.T. Walters, Priming events and retrograde injury signals. A new perspective on the cellular and molecular biology of nerve regeneration, Mol Neurobiol, 13 (1996) 61-79.

[104] D. Gigo-Benato, T.L. Russo, S. Geuna, N.R. Domingues, T.F. Salvini, N.A. Parizotto, Electrical stimulation impairs early functional recovery and accentuates skeletal muscle atrophy after sciatic nerve crush injury in rats, Muscle Nerve, 41 (2010) 685-693.

[105] A. Bonetto, D.C. Andersson, D.L. Waning, Assessment of muscle mass and strength in mice, Bonekey Rep, 4 (2015) 732.

[106] L. Gan, M. Qian, K. Shi, G. Chen, Y. Gu, W. Du, G. Zhu, Restorative effect and mechanism of mecobalamin on sciatic nerve crush injury in mice, Neural Regen Res, 9 (2014) 1979-1984.

[107] W. Choi, J. Lee, J. Lee, K.R. Ko, S. Kim, Hepatocyte Growth Factor Regulates the miR-206-HDAC4 Cascade to Control Neurogenic Muscle Atrophy following Surgical Denervation in Mice, Mol Ther Nucleic Acids, 12 (2018) 568-577.

[108] S. Yi, H. Zhang, L. Gong, J. Wu, G. Zha, S. Zhou, X. Gu, B. Yu, Deep Sequencing and Bioinformatic Analysis of Lesioned Sciatic Nerves after Crush Injury, Plos One, 10 (2015) e0143491.

[109] M. Sandri, C. Sandri, A. Gilbert, C. Skurk, E. Calabria, A. Picard, K. Walsh, S. Schiaffino, S.H. Lecker, A.L. Goldberg, Foxo transcription factors induce the atrophy-related

ubiquitin ligase atrogin-1 and cause skeletal muscle atrophy, Cell, 117 (2004) 399-412.

국문초록

근위축성 측삭 경화증 (ALS)은 운동 신경의 퇴행으로 인해 근력 약화, 마비, 그리고 결과적으로 호흡 부전이 유발되는 치명적인 신경근 질환이다. ALS 에 대한 치료법을 개발하기 위해 다양한 화학 물질, 재조합 단백질, 그리고 유전자 치료법이 개발되었지만, 현재까지 FDA 의 승인을 받은 약물은 riluzole 과 edaravone 으로 단 두 개뿐이다. 그러나 그들의 치료 효과는 상대적으로 낮으며, 여전히 이 절망적인 질병의 의학적 해결책에 대한 높은 요구가 존재한다.

이 연구에서는 간세포 성장 인자 (HGF)의 전달이 신경근 장애가 있는 두 마우스 모델인 좌골 신경 손상 모델과 SOD1-G93A 형질전환 모델에서 유익한 효과를 줄 수 있는지 조사했다. HGF 는 세포 증식, 혈관 신생, 그리고 신경 발생과 같은 다양한 세포 활성을 매개하는 것으로 알려진 신경 영양성 (neurotrophic) 인자이다. HGF 단백질의 장기 발현을 유도하기 위해 HGF 유전자를 포함한 재조합 아데노 관련 바이러스 (rAAV-HGF)를 이용하였다. HGF 단백질의 발현 수준과 분포에 기초하여 AAV 혈청형 6 을 근육 주사용으로, AAV 혈청형 1 을 척수 강내 주사용으로 선별하였다.

rAAV-HGF 의 효과는 먼저 좌골 신경 손상 모델에서 조사되었다. 근육으로 전달된 rAAV6-HGF 는 기계적 이질통 (mechanical allodynia)의 정도를 줄이고 경골 전방근 (TA)에서 근육 섬유의 단면적 (CSA)를 증가 시켰으며 운동 기능을 향상시켰다. 또한 근육에 주사한 rAAV6-HGF 는 ALS 에 가장 일반적으로

사용되는 마우스 모델인 SOD1-G93A 형질전환 모델에서 질병 증상을 완화시켰다. 한편, rAAV1-HGF 의 척수 강내 주사는 마우스의 뒷다리 힘과 로타로드 (rotarod) 성능을 향상 시켰으며, 조직학적 분석을 통해 재생된 말초 신경의 길이가 증가하고 신경근 접합부 (NMJ)의 구조가 회복된 것을 관찰하였다. 또한 rAAV1-HGF 가 마우스의 운동 기능을 향상시키고 생존율을 증가시킬 뿐만 아니라, 척수 운동 뉴런 (SMN)의 수를 증가시키고 NMJ 의 모양을 복원시킬 수 있음이 관찰되었다.

시험 관내 (*in vitro*) 운동 피질 배양 (motor cortical culture) 실험에서 나타난 바와 같이 재조합 HGF 단백질 (rHGF)의 처리는 피질척수 운동 뉴런 (CSMN)의 축삭 길이를 증가시켰다. ERK 에 대한 억제제를 처리했을 때 축삭 신장 (axon elongation), 단백질 응집, 그리고 산화 스트레스에 대한 HGF 의 영향이 억제되었는데, 이는 ERK 의 인산화가 운동 신경의 보호에 중요한 역할을 할 수 있음을 의미한다.

종합하면 HGF 유전자는 ALS 에 대한 치료제를 개발하기 위한 좋은 시작점으로 보이며, 특히 재조합 AAV 벡터는 유용한 유전자 전달 수단이 될 수 있을 것이다.

핵심어: 근위축성 측삭 경화증, 아데노 관련 바이러스, 간세포 성장 인자, 피질척수 운동 뉴런, 산화 스트레스

학번: 2015-22640